USAFA-TR-90-14

(2)

A NUMERICAL MODEL OF LASER-INDUCED FLUORESCENCE IN A HYDROGEN PLASMA

MAJOR MARC R. HALLADA

DEPT OF PHYSICS

MARCH 1991

FINAL REPORT

DEAN OF THE FACULTY

UNITED STATES AIR FORCE ACADEMY

COLORADO 80840

USAFA-TR-90-14

Technical Review by Dr. Tom Henshaw
Frank J. Seiler Research Laboratory
USAFA Academy, Colorado 80840

Technical Review by Capt Greg Finney
Department of Physics
USAF Academy, Colorado 80840

Editorial Review by Lt Col Donald C. Anderson
Department of English
USAF Academy, Colorado 80840

This research report entitled "A Numerical Model of Laser-Induced Flourescence In a Hydrogen Plasma" is presented as a competent treatment of the subject, worthy of publication. The United States Air Force Academy vouches for the quality of the research, without necessarily endorsing the opinions and conclusions of the author.

This report has been cleared for open publication and public release by the appropriate Office of Information in accordance with AFM 190-1, AFR 12-30, and AFR 80-3. This report may have unlimited distribution.

Robert K. Morrow Jr.

ROBERT K. MORROW JR., Lt Col, USAF
Director of Research

6 MAR 91
Dated

REPORT DOCUMENTATION PAGE

Form Approved
OMB No. 0704-0188

1. AGENCY USE ONLY (Leave blank)	2. REPORT DATE	3. REPORT TYPE AND DATES COVERED
	10 March 1991	Final

4. TITLE AND SUBTITLE
A Numerical Model of Laser-Induced Flourescence In A Hydrogen Plasma

5. FUNDING NUMBERS

6. AUTHOR(S)
Marc R. Hallada

7. PERFORMING ORGANIZATION NAME(S) AND ADDRESS(ES)
Department of Physics
United States Air Force Academy
USAF Academy CO 80840-5701

8. PERFORMING ORGANIZATION REPORT NUMBER
USAFA-TR-90-14

9. SPONSORING/MONITORING AGENCY NAME(S) AND ADDRESS(ES)
AFIT/CI
Wright-Patterson AFB OH 45433

10. SPONSORING/MONITORING AGENCY REPORT NUMBER

11. SUPPLEMENTARY NOTES
calculations performed at Lawrence Livermore National Laboratory

12a. DISTRIBUTION/AVAILABILITY STATEMENT
Approved for public release; distribution unlimited.

12b. DISTRIBUTION CODE

13. ABSTRACT (Maximum 200 words)
Discrepancies between observed and predicted level populations before and during laser-induced fluorescence in a hydrogen plasma are partially resolved using improved numerical models. Using a rate equation model, it is found that the H^- ion and the molecular species H_2, H_2^+, and H_3^+ play important roles in such plasmas. The dissociative recombination of H_2^+ and H_3^+ preferentially populate the $\eta = 3$ and $\eta = 2$ atomic hydrogen levels, respectively. Vibrationally excited H_2 produces H^- via dissociative attachment, while the mutual neutralization of H^- and H^+ populates the $\eta = 3$ level. The initial z-pinch appears to cause electrons and ions to stream directly to the walls, where they remain attached for several hundred microseconds. This reduces the plasma density by over 50% and causes ambipolar diffusion to overshadow recombination in the electron density decay. With these additional species and processes, many of the experimental observables, both before and during laser illumination, are reproduced. The agreement with experiment is further improved by a kinetics equation model which confirms the importance of radiation trapping and its role in producing a hot, non-Maxwellian bump in the electron distribution in the vicinity of 10 eV.

14. SUBJECT TERMS
Dissociative Attachment; Non-Maxwellian;
Mutual Neutralization;
Radiation Trapping

15. NUMBER OF PAGES
199

16. PRICE CODE

17. SECURITY CLASSIFICATION OF REPORT	18. SECURITY CLASSIFICATION OF THIS PAGE	19. SECURITY CLASSIFICATION OF ABSTRACT	20. LIMITATION OF ABSTRACT
UNCLASSIFIED	UNCLASSIFIED	UNCLASSIFIED	

Acknowledgments

First, I thank the members of my Doctoral Committee, Dr. Richard W. Lee, Dr. William L. Morgan, Dr. John S. DeGroot and Dr. Douglas W. McColm for their patience and confidence in me. I am expecially grateful to Dick Lee for giving me good advice, for providing me all the computational capabilities I needed to complete this project, and for prodding me along when I needed it most.

I also thank the members of the Physics Department at the United States Air Force Academy for their support. Dr. (Colonel) James H. Head and Dr. (Lieutenant Colonel) Richard Durham were especially helpful and encouraging. In addition, I thank Dr. (Captain) Perry R. Malcolm for graciously allowing me to monopolize his computer so that I could typeset this document with TEX.

And finally, I thank those who have sacrificed more than any others in helping to accomplish this task. I dedicate this work to them – to my family – to my patient and loving wife Cheryl – and to our children Christopher, Joshua, Francis, and Therese – who have brightened our lives and taught us what is really important – to act justly, to love tenderly, and to walk humbly with our God.

Contents

List of Figures

List of Tables

Chapter 1

Introduction

The study of plasmas which are not in LTE (Local Thermodynamic Equilibrium) requires an accurate knowledge of the collisional population and depopulation rates for individual atomic and molecular levels. Such non-LTE plasmas, in which the radiation emitted by the plasma as the result of various de-excitation and recombination reactions is not in equilibrium with the particles in the plasma, are found frequently in the laboratory and in astrophysical situations. In order to understand these non-LTE plasmas, accurate rate coefficients and cross-sections for the processes occurring in the plasmas must be available.

There are two general approaches for obtaining these rate coefficients. The first approach involves the experimental measurement of reaction cross-sections using particles with specific energies. The other approach is to directly measure the rate for a particular process occuring in the plasma of interest. Although the second approach is easily accomplished in neutral gases using a technique known as laser-induced fluorescence (LIF), plasmas present several difficulties. With the advent of high-powered, tuneable lasers these difficulties were presumbably overcome and it was shown theoretically by Burgess and Skinner (1974) that LIF could be used to measure the *in situ* plasma rates out of both the upper and lower levels of a given transition. However, the subsequent experimental validation of this theoretical technique (Burgess, *et al*, 1978) using a "simple" hydrogen plasma produced more questions than answers. In fact, the experimental results obtained called into question the validity of plasma models which had been long applied to both laboratory and astrophysical plasmas. The present

work attempts to resolve these discrepancies between theory and experiment by expanding and refining the simplistic plasma models which had been used. Before describing this expanded model, however, it is important to understand the sequence of experimental and theoretical work which led to the present theoretical model.

Bibliography

Burgess D D and Skinner C H 1974 *J. Phys. B: At. Mol. Phys.* **7** L297–301

Burgess D D, Kolbe G, and Ward J M 1978 *J. Phys. B: At. Mol. Phys.* **11** 2765–2778

Chapter 2

Survey of Previous Work

2.1 The Measurement of Atomic and Molecular Rates in Plasmas

The desire for accurate rate coefficients for the processes occuring in plasmas was temporarily satisfied using measured reaction cross-sections for particles with specific energies. For example, electron collision cross-sections could be obtained experimentally using atomic beams and fixed-energy electrons. These energy-dependent cross-sections could then be used to calculate the rate (1/sec) for such a process in a plasma with a given electron speed distribution, $f(v)$. For example, for electron collisional excitation of an atom from level i to level j, the calculated rate would be:

$$R_{ij} = n_e \int_{v_0}^{\infty} f(v)\sigma_{ij}(v)dv$$

where n_e is the total electron density, $f(v)$ is the electron speed distribution, v_0 is the threshold speed for the process, and $\sigma_{ij}(v)$ is the velocity-dependent cross-section for the process.

However, the actual rate for a process occuring in a plasma is greatly affected by the plasma itself - by internal electromagnetic fields, by shielding of positive ions by electrons, and by various waves in the plasma, to name just a few. Thus, to understand a particular plasma it is much more desirable to measure the rates directly in that plasma so that the *in situ* effects are accounted for.

The traditional technique of performing such a measurement is to use a short excitation pulse from a laser to selectively pump a certain atomic or molecular level. After the pumping has ceased, the excited state relaxes, the fluorescence radiation is observed, and the rate of its decay is measured. Depending upon the density of the gas, the measured rate could be due to collisional or radiative de-excitation, or both. This (short pump pulse) type of laser-induced fluorescence (LIF) has long been used in the measurement of rates and the determination of level structures in neutral gases. (Measures, 1968) In the case where background radiation does not mask the fluorescence signal, the optical depth of the gas to the fluorescence signal is large (*i.e.* the probability that a fluorescence photon will escape from the gas without being re-absorbed is large), and the collisional rates in these neutral gases are low (so that the fluorescing state is not collisionally quenched before the fluorescence can be observed), the pump lasers do not have to be of very high powers or have very short pulse lengths.

In a plasma, however, the situation is drastically different. The presence of large numbers of mobile electrons make the collisional de-excitation rates relatively rapid, necessitating very short excitation pulses. Also, the high levels of plasma background radiation require higher power pump lasers in order to allow the fluorescence radiation to be detected. In addition, the excited states of each species have larger populations, relative to the ground state, greatly reducing the optical depth for the fluorescence signal. Thus, the low optical depth of plasmas requires high power pump lasers if the fluorescence signal is to be detected. Consequently, while LIF has long been used to measure rates in neutral gases (since tuneable dye lasers with powers of watts or milliwatts are all that is required in these cases), it has been only relatively recently that sufficient laser powers have been available for LIF to be used successfully in plasmas. But even when such tuneable lasers became available in the mid 70s, the rapid relaxation of excited plasma states (via electron collisions) required inconveniently-short pump pulses so that the fluorescence could be observed before the state was collisionally quenched. Fortunately, a new approach to the short-pulse dilemma was not long in coming.

2.2 Long-Pulse LIF

An alternative technique for measuring *in situ* plasma rates was proposed and initially demonstrated by Burgess and Skinner in 1974. Their method relied on the use of a **long** laser excitation pulse. (The use of long excitation pulses had been addressed previously by Measures, *et al.* in 1968, but it was only in the context of local plasma diagnostics. See Appendix A.) In addition, the laser used had to be of sufficient power to "saturate" the transition, *i.e.* to populate the states in the ratio of their statistical degeneracies. The resulting variation in the observed fluorescence, while the laser remained on, was then used to deduce the *in situ* rates for various plasma processes.

As described in Appendix B, the fluorescence may theoretically occur in two possible forms. In most cases of experimental interest, after the initiation of the pump laser pulse, the observed fluorescence increases rapidly to a maximum and then decays exponentially to a steady-state plateau, all while the pump laser continues to saturate the transition. Then, as the pump laser intensity decreases to zero, the observed fluorescence decreases from the plateau intensity to the pre-laser intensity. This predicted fluorescence pattern was, in fact, observed qualitatively by Burgess and Skinner, as shown in Figure 2.1, for LIF in a Helium plasma. (Burgess and Skinner, 1974) As shown in Appendix B, measurements of the intensities of the fluorescence spike and plateau (relative to the background intensity) and of the exponential decay rate allow the determination of several atomic parameters: the ratio of the initial populations of the upper and lower levels, the total rate into both levels, and the rates out of **each** level.

Thus, Burgess and Skinner's long-pulse technique improved upon the traditional short pulse method by allowing the determination of decay rates from the **lower** level also and by removing the effect of decays from the upper level to the lower level. If applied to a low-density plasma, this technique could be used to determine the *in situ* (effective) spontaneous emission coefficient for an ultraviolet transition using easily available tuneable dye lasers, which operate at visible wavelengths. The effective spontaneous emission coefficient can be greatly altered by the "trapping" of radiation by the plasma. For example, if all of the spontaneous radiation emitted in a certain transition of a species in the plasma is re-absorbed by other atoms or molecules in the plasma before it can leave the plasma, the radiation

is said to be completely "trapped" and the effective Einstein A coefficient would vanish. That is, the species would behave as if it did not spontaneously emit radiation in this transition at all. Conversely, this technique could also allow the determination of collisional de-excitation rates from first-excited states in high density plasmas. By comparison, spectroscopic methods can usually yield only **spontaneous** transition rates. (Burgess and Skinner, 1974)

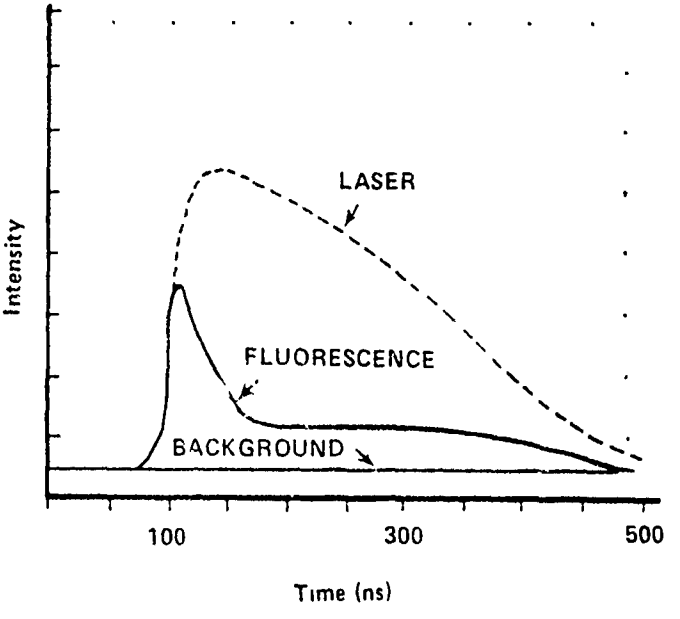

Figure 2.1: LIF in a He plasma

2.3 Attempted Validation of Long Pulse LIF Technique

The long pulse LIF technique proposed by Burgess and Skinner held great promise of filling the many gaps in our understanding of atomic and molecular processes occurring in plasmas. However, a subsequent experiment by Burgess, Kolbe, and Ward in 1978, using a "simple" hydrogen plasma, produced more questions than answers. In this experiment, molecular hydrogen in a pyrex cylinder was ionized using a z-pinch gas discharge and then allowed to recombine. The authors assumed that during the time span of their experiment (the "recombination" phase of the plasma) the only significant species present were hydrogen atoms, protons, and electrons. In addition, it was assumed that the plasma was in steady state with respect to the electron concentration and temperature (n_e and T_e) and the ground state concentration of atomic hydrogen ($n_{H(1)}$). They maintained that any additional processes due to H_2 or H_2^+ were unlikely, or, at most, inconsequential. (Burgess, *et al.*, 1978) However, with these assumptions, and using accepted values for the electron collisional excitation and de-excitation rates (Johnson, 1972), the atomic hydrogen level populations predicted by Burgess and Skinner's theoretical model were found to be in substantial disagreement with the experimentally-observed populations. The authors concluded that their assumption of a simple (atomic hydrogen only) plasma in equilibrium was valid, but that the excitation and de-excitation rates which they used were too large by a factor of at least five. Further, they suggested that the observed decay of the $n = 2$ level of hydrogen, upon termination of the laser excitation, was primarily due to collisional de-excitations to the $n = 1$ level and not due to excitations to upper levels at all. (Burgess, *et al.*, 1978)

The failure of such simple theoretical models is not unexpected, however, whenever detailed experimental probes (such as LIF) reveal a level of detail not previously known. The solution to such a dilemma is to refine both experimental techniques and theoretical models. The first step in this process was taken by Brugess and his collaborators in 1980. (Burgess, *et al.*, 1980)

2.4 Comparison between Rate Equation Model and LIF Experiments

A more detailed investigation of LIF in this "simple" hydrogen plasma was therefore begun in hopes of resolving the questions raised by the "validation" experiment. This investigation included a long series of LIF experiments in which the plasma parameters and hydrogen level populations were carefully measured using a variety of methods. (See Appendix C for a description of these experiments.) In addition, a multi-level collisional-radiative (CR) numerical model of the plasma was constructed and compared with the experimental results. In keeping with the assumptions of the previous investigators (Burgess, Kolbe, and Ward, 1978), this model assumed that the plasma was in steady state (with respect to n_e, T_e, and $n_{H(1)}$) and that the only species present were atomic hydrogen, protons, and electrons. Because of the care with which they did their experiments, the comparison between their experimental results and the predictions of their numerical rate-equation model, which was published in 1980 (Burgess, Myerscough, Skinner, and Ward, 1980) was even more discouraging than the previous "validation" experiment. Their CR model failed by "large margins" to predict the observed behavior of the plasma both with and without laser illumination. This failure was particularly significant because, as stated by the authors, the plasma conditions being modeled were "not dissimilar to those in astrophysical situations where such models have been widely applied." (Burgess, *et al.*, 1980)

The collisonal-radiative (CR) model of Burgess, *et al.* was incorrect in four areas. First, their model showed a "remarkable discrepancy" in predicting the initial (prior of laser illumination) population of the $n = 2$ level of hydrogen. This descrepancy was greatest at the higher temperatures and electron densities considered in the experiment, for which the CR model predicted an $n = 2$ population more than an order of magnitude less than the measured population. Second, the CR model predicted a relaxation rate from the LIF peak (see Appendix B) which was much faster than the measured rate. Third, the CR model predicted an LIF plateau (see Appendix B) which was much lower than the observed long-term enhancement in the laser induced fluorescence. Fourth, the laser intensity actually required to "saturate" the fluorescing transition (*i.e.* to put the upper and

lower level populations in the ratio of their statistical weights) was much lower than the CR model predicted. (Burgess, *et al.*, 1980)

Burgess and his collaborators concluded that these four discrepancies between their experiment and their numerical model were the result of errors in the model in two categories: neglected processes and miscalculated rates for some of the processes that were considered. They maintained that the observed slow relaxation from the LIF peak and the elevated level of the plateau required the effective electron collisional rates in the plasma to be significantly lower than the collisonal rates given by Johnson (Johnson, 1972), which they used in their model. On the other hand, they concluded that the observed high initial population of the $n = 2$ level could not be explained simply by lower collisional rates, but that one or more additional, unaccounted for, processes must be populating the $n = 2$ level. They also held that the observed plateau enhancement could be explained by either decreased collisional rates or additional processes into the $n = 2$ level, or both. (Burgess, *et al.*, 1980)

In an attempt to justify these decreased rates and identify additional processes, Burgess and his collaborators made several suggestions. They suggested that decreased electron-collisional rates could be the result of Debye shielding of the long-range e^-–H potential, which would, in turn, modify the excitation cross-section near threshold. Alternatively, they proposed that super-elastic collisions of electrons with "overpopulated" excited levels in atomic hydrogen could lead to the production of a non-Maxwellian electron distribution. They pointed out that if the distribution of electrons in the plasma was enhanced at lower energies, the effective electron-collisional rates would be decreased, as seemingly required by the experimental results. Although Burgess and his collaborators were able to suggest some reasons to justify lower collisional rates, they were much less successful identifying additional processes into the $n = 2$ level. Even though they admitted that such additional processes were not hard to envision (perhaps involving H_2 or H_2^+), they maintained that the rates for all such processes appeared to be negligible. (Burgess, *et al.*, 1980)

2.5 Plasma Effects on Collision Rates in Hydrogen

Several of the suggestions made by Burgess and his colleagues were investigated by another group and reported in 1983. (Lee, Morgan, Whitten, and Kolbe, 1983) Using the experimental results obtained by the previous group, Lee and his collaborators calculated the effects of plasma screening, a non-Maxwellian electron energy distribution, and radiation field pumping.

Lee and his group claimed that plasma screening effects on inelastic electron-ion collision cross-sections were negligible. They justified their position by comparing the Debye length in the experimental plasma, which was over 1000 Å, with the maximum Debye length for which such screening could significantly alter the collision cross-sections. Lee, *et al.*, cited screened Coulomb potential calculations by several groups to place an upper limit of 30 Å on the Debye length required for such screening to be significant. Thus, the plasma under investigation appeared to be too tenuous for Debye screening to alter the collision cross-sections.

However, Lee and his collaborators did find that although the electron distribution was initially Maxwellian, it became significantly non-Maxwellian as the plasma cooled and recombined. In particular, the observed time history of the level populations indicated that, as the plasma cooled, the electron distribution developed a large "bump" at approximately 10 eV. (See Figure 2.2) In an attempt to explain the growth of this bump, Lee, *et al.*, observed that as the plasma cooled and the ground state atomic hydrogen population increased, the optical depth of the plasma for Lyman-alpha (Ly_α) radiation increased. Further, they argued that as the optical depth increased, the efficiency of the radiation trapping was increased and the effective Einstein A coefficient, for spontaneous transitions from the $n = 2$ level to the $n = 1$ level, vanished. Consequently, the rate into the $n = 2$ level was increased. Superelastic collisions of electrons with atoms in the now "overpopulated" $n = 2$ level would thereby increase the rate of production of "hot" electrons. Although electron-electron collisions would normally quickly thermalize these hot electrons and distribute their energy uniformly throughout the distribution, Lee, *et al.*, maintained that this thermalization rate would be rapidly reduced as the plasma cooled and

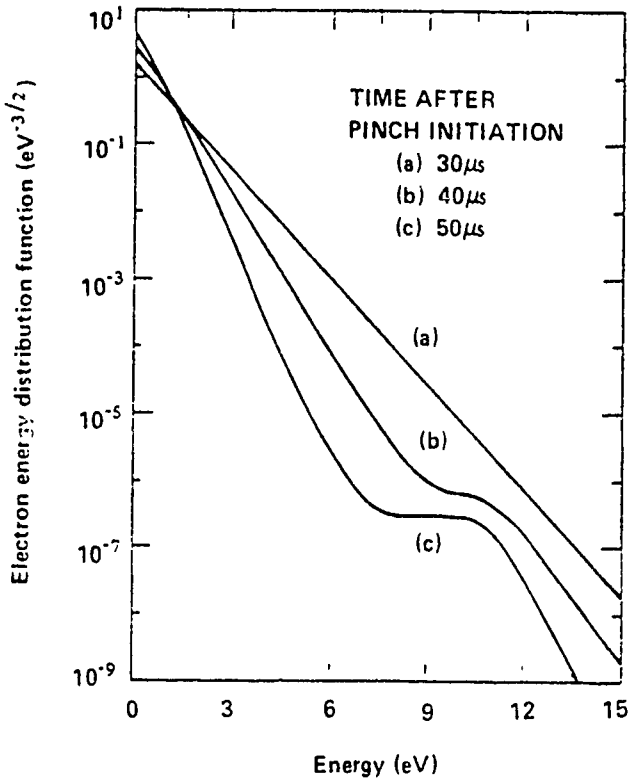

Figure 2.2: Growth of Non-Maxwellian Component

recombined and the electron density thereby declined. Thus, they predicted that a greater **fraction** of the electrons would become "hot" as the plasma evolved, as the hydrogen level populations in the Burgess, *et al.*, (1980) experiment seemed to indicate.

Although the work of Lee, *et al.*, answered several of the questions raised by the Burgess, *et al.*, experiment, it also raised two new issues. First, in an attempt to simulate the temporal evolution of the plasma's recombination phase using the measured electron temperatures, they found that the recombination rates used in their model were much slower than the experimental results seemed to indicate. That is, the experimentally-measured electron density decreased much more rapidly than their numerical model predicted. Second, since they showed that radiation trapping and the resulting production of hot electrons were indeed significant, it was suggested that in order for any model of this "simple" hydrogen plasma to give reasonable results it would have to be made much more sophisticated. In particular, they proposed that the Maxwellian rate equations be replaced by kinetic equations for electrons in a number of small energy ranges. In addition, it was asserted that the simple "escape factor" approach to radiation trapping (see Appendix F) was inappropriate for the plasma being modeled because of the extreme departure of the measured level populations from their theoretical LTE values. Consequently, they maintained that it was necessary to do the radiative transfer explicitly for the Ly_α radiation, the presumed progenitor of the hot electrons.

2.6 Investigation of Wall Effects on the Atomic Hydrogen Concentration

In each of the analyses by Burgess and his collaborators, the concentration of hydrogen atoms and ions was calculated under the assumption that the molecular hydrogen used to fill the discharge was completely dissociated by the z-pinch and remained so during the recombination phase. However, experiments done by Newton and Sexton in 1969 and Jones in 1981, with similar plasmas, called this method of determining the atomic hydrogen concentration into question. Jones presented evidence, based on measured electron densities and the observation of H_α and H_β emission by the plasma when an auxillary discharge was passed through the plasma, that the concentration of hydrogen atoms and ions in the recombination phase of certain plasmas was considerably less than the "fill" concentration. (The "fill" concentration is the atomic hydrogen concentration calculated by assuming that the molecular hydrogen used to fill the discharge is completely dissociated and that none of it is lost.)

A partially ionized plasma normally decays first by recombination,

$$\frac{\partial n}{\partial t} \sim -n^2 ,$$

when the charge density is high, and later decays by diffusion,

$$\frac{\partial n}{\partial t} \sim -n ,$$

after the charge density has reached a lower value. Thus, the electron density normally decays reciprocally with time at first,

$$n \sim \frac{1}{\alpha t} ,$$

and later decays exponentially with time,

$$n \sim e^{-t} .$$

In certain z-pinch plasmas, however, Newton and Sexton (1969) found that the electron decay was always exponential, even at early times. In an attempt to explain these observations, they noted that in these z-pinch

plasmas, sufficient energy was delivered to the plasma to both dissociate the molecular hydrogen and completely ionize the resulting atomic hydrogen also. Newton and Sexton (1969) claimed that when this much energy is delivered to a z-pinch plasma, the ions and electrons expand directly to the walls without any neutral background atoms to control their "conventional" diffusion. Thus, with a much lower number of charged particles in the plasma, recombination is not the dominant process early in the recombination phase. In fact, they found that the decay was exponential, as in diffusive decay, even at early times. (However, for energies **lower** than that required for such complete ionization, the initial electron decay was primarily controlled by **recombination**. Thus, for energies sufficient to completely dissociate and ionize the hydrogen, the electrons and ions appeared to expand directly to the walls and a large fraction of these positive hydrogen ions remained "attached" to the (quartz) walls "for at least some hundreds of microseconds", making them unavailable for recombination with plasma electrons. Consequently, the electron decay was primarily diffusive and Jones (1982) determined that up to 40 % of the hydrogen was "missing" from the plasma for several hundred microseconds.

The z-pinch hydrogen plasma used by Burgess and his collaborators (Burgess, *et al.*, 1980 and Nightingale and Burgess, 1983) appeared to follow this same behavior. As described by Newton and Sexton (1969), the energy density which must be supplied to the plasma to fully ionize it may be approximated as:

$$w_{id} = n_H \cdot \left(\epsilon_{iH} + \frac{1}{2} \cdot \epsilon_{dH_2} + g\right),$$

where ϵ_{iH} is the ionization evergy of atomic hydrogen, ϵ_{dH_2} is the dissociation energy of molecular hydrogen, and g is a factor which takes into account the radiative loss of energy during the ionization process. (According to McWhirter and Hearn (1963), this g factor is approximately unity for such z-pinches.) Thus, at a fill pressure of .45 Torr, as used by Burgess, *et al.* in their experiments, the energy density required for complete dissociation and ionization of the hydrogen is about 73 mJ/cm^3. Using the description of the discharge apparatus and the pinch parameters given by Burgess, *et al.*, (1980) and Kolbe (1985), the energy actually dissipated in the hydrogen plasma was estimated to be about 82 mJ/cm^3. (See Appendix D.) Comparing this estimate of the energy density applied to the Burgess plasma

with that required for complete dissociation and ionization, 73 mJ/cm^3, it appears that this plasma was indeed fully ionized, that these ions probably expanded freely to the walls, and that a significant fraction of them were subsequently unavailable (for hundreds of microseconds) for recombination with electrons. (See Appendix E.) The time history of the electron densities measured by Burgess, *et al.* was, in fact, nearly (within 2%) exponential, as would be the case if the wall attachment mechanism proposed by Newton and Sexton (1969) and used by Jones (1982) were valid. This exponential electron decay was also observed in subsequent z-pinch experiments by Nightingale and Burgess (1983). However, using a technique with a much greater temporal resolution, they observed large oscillations in the electron density for times within 80 μs of the initial pinch. These oscillations were thought to be due to a propagating cylindrical acoustic pulse following the pinch.

This interplay of diffusion and recombination in determining the electron density in an afterglow hydrogen plasma was also investigated theoretically by Long and Newton (1971). They treated the plasma as three interpenetrating fluids (protons, electrons, and neutral atoms) in an infinitely long, cylindrical vessel with cold walls. Including the effects of collisional ionization and recombination, radiative energy losses, thermal conduction and diffusion, and (temperature dependent) ambipolar diffusion of the electrons and ions, Long and Newton obtained radial and temporal distributions of the plasma temperature and species concentrations. Their model also assumed that the ions and electrons which diffused to the walls recombined there and returned to the plasma as cold (300 °K) neutral atoms. Beginning with a spatially uniform distribution of each species, they first observed a rapid expansion of the plasma as the outer regions were cooled by wall contact. By 20 μs, the radial electron density profile had become similar to the zero order Bessel function,though somewhat steeper near the wall, presumbably because the ambipolar diffusion coefficient in their model was allowed to vary with the radial decrease in the plasma temperature. Their model also exhibited the rapid growth (within 10 μs) of a dense layer of neutral atoms close to the wall. At later times ($\sim$ 75 μs), the cool atoms in this wall sheath (approximately 0.5 cm thick) re-entered the plasma by diffusion, contributing to the reduction of the model's plasma temperature on axis.

Jones, using a discharge system similar to those of Burgess and of New-

ton and Sexton, with energies claimed to be sufficient to fully ionize the hydrogen, estimated that as much as 40% of the total fill concentration of hydrogen was attached to the walls early in the plasma's (so-called) recombination phase. (Jones,1982) In addition, using measured (average) recombination coefficients for hydrogen atoms on pyrex surfaces (Wood and Wise, 1958), Jones placed an upper limit of 10% on the resulting fraction of molecular hydrogen in the plasma by 100 μs after initiation of the pinch. However, as described in Appendix E, the recombination coefficients given by Wood and Wise are not entirely appropriate in modeling the desorption of hydrogen from the walls of a z-pinch discharge tube. Specifically, the wall concentration of adsorbed hydrogen atoms may be much greater than the equilibrium value assumed in their analysis. As a result, the recombination probabilities (coefficients) given by Wood and Wise may underestimate actual values when applied to experiments of the type performed by Burgess, *et al.* (1980).

Although Jones appeared to indicate that 10% was a rather insignificant concentration of molecular hydrogen, the influence of this seemingly small concentration may be greater than he expected. It was suggested by Wood and Wise (1961) that the molecular hydrogen in such discharges may be highly excited, vibrationally and/or electronically, as a result of the surface recombination which is responsible for much of it. This excitation can have a significant effect on a hydrogen plasma because, as noted in other sections of this investigation, such excitations can greatly increase the rates for specific processes. The production of such excited molecules as the result of surface recombination has actually been observed, by Reeves, *et al.* (1960), for nitrogen atoms incident on nickel, cobalt, and silver surfaces. Reeves and his collaborators concluded that the nitrogen atoms incident on these surfaces recombined with adsorbed oxygen atoms, producing electronically excited NO molecules which then returned to the plasma.

In summary, the discharge chamber walls in z-pinch plasmas (and in the experiments of Burgess, *et al.*, in particular) may affect the plasma in several ways. First, the walls may cause a drastic reduction in the number of atoms available to the plasma for several hundred microseconds after the pinch, altering the rates for both microscopic and macroscopic processes in the plasma. Second, these atoms at the walls may serve as a source of significant numbers of electronically and vibrationally excited molecules, which could also impact the rates for a number of processes occurring in the

plasma. Finally, the walls can produce a significant short-term cylindrical oscillation in both the neutral and electron densities.

2.7 Continuum Absorption and Level Populations

The absorptivity and level populations of a plasma similar to that used in the original experiments by Burgess, *et al.* (1980) was studied both experimentally and theoretically by Nightingale and Burgess in 1983. Investigating the opacity at frequencies near that for the H_α transition, they found anomalously large values for the hydrogen continuum absorption between 6400Å and 6545Å. The measured absorption was approximately an order of magnitude greater than that predicted by a 20-level collisional-radiative model. In addition, the measured $n = 2$ level population was, for late times, lower than the predicted values by up to a factor of three.

In an attempt to explain the high absorptivity, Nightingale and Burgess (1983) noted that molecular hydrogen has transitions between high electronically-excited molecular levels which span the entire frequency range investigated. They therefore suggested that the molecular hydrogen concentrations may actually be much higher than had been previously predicted. In addition, noting that the cross-section for bound-free absorption by H^- ions is relatively large in this frequency range, they also suggested that the H^- concentration in the plasma may also be much larger than was previously thought.

Although Nightingale and Burgess argued that these unexpectedly high concentrations of H_2 and H^- could be the source of the plasma's anomalous absorptivity, they could envision no mechanism by which these species could appreciably alter the hydrogen level populations. Using accepted rates for the processes of collisional ionization,

$$e^- + H_2 \Longrightarrow H(1s) + H(2s) + e^- \ ,$$

dissociative recombination,

$$e^- + H_2^+ \Longrightarrow H(1s) + H(2s) \ ,$$

and mutual neutralization,

$$H^+ + H^- \Longrightarrow H(1s) + H(2s) \ ,$$

they determined that completely unrealistic concentrations of H_2, H_2^+, and H^- would be required in order for these processes to compete with rates into

the $n = 2$ level from higher-lying atomic hydrogen levels. (In these reaction equations, e^- represents electrons, $H(i)$ represents atomic hydrogen in the ith electronic state, H^+ represents protons, H^- represents atomic hydrogen with an additional bound electron, H_2 represents molecular hydrogen, and H_2^+ represents molecular hydrogen with only one bound electron.) They maintained that the collisional-radiative model's underestimate of the experimentally measured level populations early in the recombination phase could possibly be the result of inflated collisional rates into the $n = 2$ level. However, they also found that these reduced rates do not decrease the calculated level populations to the values they observed at later times. As Nightingale and Burgess concluded: "... the existence of these large discrepancies in a well-diagnosed plasma which should have relaxed to a quasi-stationary condition in which all processes should be well understood, and under conditions closely similar to those of astrophysical interest, is both surprising and disturbing ..." (Nightingale and Burgess, 1983)

2.8 The Role of H^- Ions in Low-Pressure Hydrogen Plasmas

Both collisional-radiative models used by Burgess and his collaborators (Burgess, *et al.*, 1980; and Nightingale and Burgess, 1983) neglected all processes involving H^- ions. They claimed that, at the plasma temperatures of interest, the only H^- process which could be significant in populating the $n = 2$ or higher levels was that of mutual neutralization:

$$H^- + H^+ \Longleftrightarrow H(1s) + H(i) ,$$

where $H(i)$ represents the ith electronic state of atomic hydrogen. However, using an LTE estimate of the H^- concentration and accepted rates for this process, they concluded that even this process would be insignificant compared to the electron collisional rates between excited atomic hydrogen states and/or the continuum.

In view of the large fractions of H^- ions observed in other low-pressure hydrogen plasmas (Nicolopoulou, *et al.*, 1977; and Bacal and Hamilton, 1979) and the determination by Nightingale and Burgess that the H^- population must be far larger than they had predicted, W. M. Jones decided that a more direct check of the importance of mutual neutralization should be accomplished. (Jones,1985) In order to do this, Jones monitored the H_α emission of a hydrogen plasma while axially irradiating it with a ruby laser (with a photon energy of 1.8 eV), which is known to be an efficient means of destroying H^- ions. (Bacal, *et al.*, 1979) During the laser pulse, a definite decrease in the H_α emission was observed. This implied that the $n = 3$ atomic hydrogen concentration had indeed been decreased by the decline in H^- brought about by the laser pulse. Thus, it appeared that mutual neutralization does indeed play an important role in populating the $n = 3$ level.

In order to determine what fraction of the $n = 3$ level population was due to mutual neutralization, Jones first had to determine how effective the ruby laser pulse was in depleting the H^- population. Using the rate coefficients for mutual neutralization calculated by Bates and Lewis (1955) and cross-sections for electron collision detachment measured by Walton *et al.* (1971), Jones determined the total loss rate for H^- ions in the absence of laser irradiation. (The theoretical rate coefficients of Bates and Lewis are

in good agreement with recent experimental measurements (Szücs,*et al.*, 1984) and with a more detailed theoretical treatment (Fussen and Kubach, 1986).) Since this rate was almost two orders of magnitude less than the rate he estimated for photodetachment by the laser, Jones concluded that the laser would completely destroy any H^- ions in the irradiated volume. Consequently, with the observed laser-initiated dip in the H_α emission (and thus the $n = 3$ population) to about 67% of its initial value, Jones estimated that as much as 35% of the $n = 3$ population could be attributed to the process of mutual neutralization.

With the direct connection between the H^- and $n = 3$ state concentrations provided by this process of mutual neutralization, any change in the H^- concentration would have an impact on the hydrogen level populations within 10 ns. Consequently, Jones suggested that a correct model of a recombination-phase hydrogen plasma must incorporate the process of mutual neutralization and any other processes which may be significant in altering the H^- population. Such processes include those of photodetachment

$$h\nu + H^- \Longrightarrow H(i) + e^- ,$$

electron collisional detachment/three-body (electron) collisional ionization

$$e^- + H^- \Longleftrightarrow H(i) + e^- + e^- ,$$

and associative detachment/dissociative attachment

$$H(i) + H^- \Longleftrightarrow H_2(v*) + e^- ,$$

where $H_2(v*)$ represents an excited vibrational level of molecular hydrogen.

Recent experimental work (Bacal, *et al.*, 1981) on low pressure (5×10^{-3} to 5×10^{-2} Torr) hydrogen discharges has suggested that dissociative attachment of thermal electrons to highly vibrationally-excited ($v > 4$) hydrogen molecules is the most probable source of the large H^- concentrations observed in these plasmas.

$$H_2(v*) + e^- \Longrightarrow H^- + H$$

Theoretical models of somewhat higher density hydrogen plasmas ($n_H = 4 \times 10^{14}$ 1/cm^3), produced by electron-beam bombardment, indicated that

a principal source of this vibrational excitation is through singlet excitation by energetic electrons.

$$e^- + H_2(X^1\Sigma_g, v'' = 0) \Longrightarrow e^- + H_2(B^1\Sigma_u, C^1\Pi_u)$$

$$H_2(B^1\Sigma_u, C^1\Pi_u) \Longrightarrow H_2(X^1\Sigma_g, v'') + h\nu$$

In addition, Bacal, *et al.* (1981) pointed out that the process for forming H_3^+ (which is, by far, the dominant positive ion species in these plasmas) leaves a "substantial fraction" of the H_3^+ with internal energies in excess of 2 eV. This energy could then be transferred to H_2 by wall collisions or by proton transfer.

$$H_3^+(v*) + e^-(wall) \Longrightarrow H_2(v*) + H$$

$$H_3^+(v*) + H_2(v = 0) \Longrightarrow H_2(v*) + H_3^+$$

Previous models (Hiskes,1982) of the production of H^- in plasmas produced by electron beams considered that energetic electrons were primarily responsible for the large populations of vibrationally-excited molecular hydrogen. However, more recent models (Hiskes and Karo, 1989) have indicated the additional importance of surface interactions in the production of H^-. In addition to the production of vibrationally excited H_2 (and the subsequent production of H^- by dissociative attachment) as the result of the impact of molecular hydrogen ions (especially H_3^+), Hiskes and Karo proposed that H^- is formed directly, from the atomic hydrogen dissociation products rebounding from the surface and from the dissociation of H_2^- near the surface.

The vibrationally-excited molecular hydrogen population is modified by thermal electron – molecule, molecule – molecule, and molecule – wall interactions. Considering $H_2(v*)$ production by electron collisional excitation and losses by molecular and wall collisions, Hiskes, *et al.* (1982), obtained theoretical vibrational population distributions with "plateaus" between $v'' = 4$ and $v'' = 10$. These predictions by Hiskes were partially confirmed by an experimental investigation (Graham, 1984) in which vibrational level populations (up to $v = 3$) were measured. From these measured populations, an estimate for the rate of production of molecular hydrogen with $v > 4$ was made. Using theoretical dissociative attachment rates (Wadehra and Bardsley, 1979; and Wadehra, 1979) for vibrational levels $v'' = 1 - 9$

and rotational state J=0, Graham (1984) showed that the estimated production rate for $H_2(v > 4)$ molecules was sufficient to produce the observed concentrations of H^-. More recently, (Eenshuistra, *et al.*, 1989) extended the experimental measurement of the vibrational level populations of H_2 up to $v'' = 5$, further confirming the plateau predictions of Hiskes. In addition, Hiskes (1982) noted that although $H_2(v*)$ collisions with the walls can somewhat quench the vibrational motion, such collisions are also very effective in populating high rotational levels. Further, he stated that such rotational excitation had been shown theoretically and experimentally to increase dissociative attachment rates by factors of from 5 to 100. Thus, a complete explanation of the observed concentrations of H^- ions in low pressure discharges would appear to require a knowledge of the distribution of rotational levels for each $H_2(v^*)$ molecule, along with the associated dissociative attachment rates.

2.9 The Roles of H_2 and H_2^+ in Low Pressure Hydrogen Plasmas

Although Burgess, *et al.* (1980) claimed that any processes involving H_2 or H_2^+ would be inconsequential, subsequent experiments by Nightingale and Burgess (1983) caused them to conclude that the molecular hydrogen concentration was much larger than had been thought. With a greater concentration of molecular hydrogen and the growth in the fraction of "hot" ($\approx$ 10 eV) electrons as the plasma recombines (Lee, *et al.*, 1983), a number of previously-neglected processes might actually be quite significant. For example, electronic excitation of H_2 (as the result of collisions with hot electrons or as the result of wall recombinations) to the singlet B and C states, followed by their radiative decay, could be an important source of vibrationally-excited $H_2(X, v*)$ molecules. The population of these vibrationally-excited molecules could be significant because it is now generally accepted that dissociative attachment of electrons to $H_2(X, v*)$ is the most important process for producing H^- in low pressure hydrogen plasmas. (Hiskes, 1987) This H^-, in turn, is thought to play an important role in populating the lower electronic levels in atomic hydrogen. (Jones, 1985) In addition, electronic excitation of H_2 to the triplet a and c (metastable) states could make the "quenching" of atomic hydrogen by these states, as described by Catherinot, *et al.* (1978), more feasible than Hiskes, *et al.*, (1979) claimed.

The hottest of the non-Maxwellian electrons may even be able to directly ionize the molecular hydrogen and produce significant concentrations of H_2^+. However, it should be noted that H_2^+ is rarely observed in low-pressure ($\approx$ .5 Torr) hydrogen plasmas because of the rapid rate ($\approx 1.2 \times 10^{-9}$ cm^3/sec at .1 eV) at which it reacts with neutral hydrogen molecules. (Hiskes, *et al.*, 1979)

$$H_2^+(v*) + H_2(v = 0) \Longrightarrow H_3^+(v**) + H$$

Since the rate for ionization of H_2 is approximately 6.0×10^{-9} cm^3/sec for Maxwellian electrons with a temperature of 10 eV, the enhanced population of hot electrons in the z-pinch plasma of Burgess, *et al.*, (1980) could increase the percentage of H_2^+ in the plasma. With higher concentrations of H_2^+, a number of other processes would become significant. These addi-

tional processes would include: electron-impact dissociation,

$$e^- + H_2^+(v) \Longrightarrow e^- + H^+ + H(1s) ,$$

with a rate of 1.7×10^{-8} cm^3/sec at 1 eV, and dissociative recombination,

$$e^- + H_2^+(v) \Longrightarrow H(1s) + H(n) , n \geq 2 ,$$

with a rate of 5.5×10^{-8} cm^3/sec at 1 eV, and increasing with decreasing electron energy. In addition, higher concentrations of H_2^+ could make dissociative recombination more significant. According to the dissociative recombination rates given by Janev, *et al.*, (1987), the $n = 3$ level would be populated twice as fast as the $n = 4$ level and over four times as fast as the $n = 2$ level of atomic hydrogen. Thus, dissociative recombination of H_2^+ could have a significant impact on the atomic hydrogen concentration, and on the $n = 3$ level population in particular.

2.10 The Role of H_3^+ in Low Pressure Hydrogen Plasmas

The dominant positive ion in low pressure ($\approx$ .5 Torr) hydrogen plasmas is often found to be H_3^+. (Ortenburger, *et al.*, 1960 and Bacal, *et al.*, 1981) Consequently, a model of such a plasma should include the most important processes involving this positive ion.

As mentioned in the section dealing with the production of H^-, H_3^+ may be partially responsible for the production of significant concentrations of vibrationally-excited H_2. The process by which H_3^+ is formed often leaves this ion with an internal energy in excess of 2 eV. This energy can then be transformed into vibrational excitation of neutral hydrogen molecules by wall collisions or by proton transfers.

$$H_3^+(v*) + e^-(wall) \Longrightarrow H_2(v*) + H$$

$$H_3^+(v*) + H_2(v=0) \Longrightarrow H_2(v*) + H_3^+$$

Follow-on dissociative attachment of electrons to these vibrationally-excited $H_2(v*)$ molecules would greatly increase the H^- population. Then, mutual neutralization of the H^- formed, with H^+, H_2^+, or H_3^+, would provide an additional source for populating the atomic hydrogen levels.

In addition, dissociative recombination of plasma electrons with H_3^+ would directly feed the $n = 2$ level and also increase the population of vibrationally-excited H_2.

$$e^- + H_3^+ \Longrightarrow \begin{cases} H + H + H & \text{(a)} \\ H_2(v \geq 4) + H(n=2) & \text{(b)} \end{cases} \qquad (2.1)$$

The branching to channels (a) and (b), measured by Mitchell, *et al.* (1983), favors the formation of H + H + H by about 2.5:1.0 in the energy range from 0.1 to 1.0 eV. However, above 1.0 eV, theoretical calculations by Kulander and Guest (1979) predict that the dominant channel is $H_2(v \geq 6)$ + H(n = 2). Thus, with the growth in the fraction of "hot" ($\approx$ 10 eV) electrons as the plasma recombines (Lee, *et al.*, 1983), dissociative recombination of H_3^+ would become a significant means of populating the $n = 2$ level of atomic hydrogen.

2.11 Summary of Previous Work

- Discrepancies Between Burgess Experiment and Atomic Rate Equation Models
  - Population of $n = 2$ state in unperturbed plasma is much less than that predicted by theory (for times late in the recombination phase)
  - Relaxation rate from LIF peak is much slower than that predicted by theory
  - LIF plateau is much higher than that predicted by theory
  - Laser intensity required to saturate the transition is much lower than that predicted by theory
- Possible Causes of These Discrepancies
  - A significant fraction of the electrons in the plasma become "hot" as the plasma recombines
  - Radiation trapping of all emissions (not just Lyman_α) may be important
  - H^- may be present in greater concentrations than previously thought due to dissociative attachment of $H_2(v*)$
  - Walls of plasma containment vessel may significantly alter the plasma
    - up to 40% of the hydrogen may be absent from the plasma for several hundred microseconds
    - recombination of atomic hydrogen at the walls could serve as a source of electronically and vibrationally excited molecular hydrogen, which could comprise up to 10% of the plasma
    - cylindrical acoustic oscillations may cause significant short-term fluctations in the electron and neutral densities
  - H_3^+ may be an important source of atomic hydrogen in the $n = 2$ state and of vibrationally excited molecular hydrogen
  - H^- may be an important source of atomic hydrogen in the $n = 2$ and $n = 3$ (especially) states due to mutual neutralization

Bibliography

Bacal M, Bruneteau A M, Graham W G, Hamilton G W, and Nachman M 1981 *J. Appl. Phys.* **52** 1247–54

Bacal M, Hamilton G W, Bruneteau A M, and Doucet H J 1979 *Rev. Sci. Instrum.* **50** 719–21

Bates D R and Lewis J T 1955 *Proc. Phys. Soc. A* **68** 173

Burgess D D and Skinner C H 1974 *J. Phys. B: At. Mol. Phys.* **7** L297–301

Burgess D D, Kolbe G, and Ward J M 1978 *J. Phys. B: At. Mol. Phys.* **11** 2765–2778

Burgess D D, Myerscough V P, Skinner C H, and Ward J M 1980 *J. Phys. B: At. Mol. Phys.* **13** 1675–1701

Chen F F 1984 *Introduction to Plasma Physics and Controlled Fusion, 2nd edition, Vol 1* (New York: Plenum Press) 167-8

Fussen D and Kubach C 1986 *J. Phys. B: At. Mol. Phys.* **19** L31–34

Graham W G 1984 *J. Phys. D* **17** 2225–2231

Hiskes J R 1987 *Comments on At. and Mol. Phys.* **19** 2

Hiskes J R, Bacal M, and Hamilton G W 1979 *Lawrence Livermore National Laboratory, CA* **UCID**–18031

Hiskes J R, Karo A M, Bacal M, Bruneteau A M, and Graham W G 1982

J. Appl. Phys. **53** 3469

Jones W M 1982 *Plasma Physics* **24** 361–368

Jones W M 1985 *J. Phys. B: At. Mol. Phys.* **18** 2105–2109

Kolbe G 1985 *PhD Thesis* Imperial College of Science and Technology London, England

Kulander K C and Guest M F 1979 *J. Phys. B: At. Mol. Phys.* L501

Lee R W, Morgan W L, Whitten B L, and Kolbe G 1983 *Lawrence Livermore National Laboratory, CA* **UCRL**–88714

Long J W and Newton A A 1971 *Numerical Simulation of Hydrogen Afterglows Proceedings, 10th Int'l Conf. on Phenomena in Ionized Gases, Oxford, Ed. R N Franklin*

McWhirter R W P and Hearn A G 1963 *Proc. Phys. Soc.* **82** 641–54

Measures R M 1968 *J. Appl. Phys.* **39** 5232–5245

Mitchell J B A, Forand J L, Ng C T, Lerac D P, Mitchell R E, Mul P M, Claeys W, Sen A, and McGowan J Wm 1983 *Phys. Rev. Lett.* **51** 885

Newton A A and Sexton M C 1969 *J. Phys. B: At. Mol. Phys.* **2** 1069–1074

Nicolopoulou E, Bacal M, and Doucet H J *J. Physique* **38** 1399–404

Nightingale M P S and Burgess D D 1983 *J. Phys. B: At. Mol. Phys.* **16** 4101–4115

Ortenburger I B, Hertzberg M, and Ogg R A 1960 *J. Chem. Phys.* **33** 579–583

Peart B, Bennett M A, and Dolder K 1985 *J. Phys. B: At. Mol. Phys.* **17** 1613–1622

Reeves R R, Mannella G, and Harteck P 1960 *J. Chem. Phys.* **32** 946–947

Szücs S, Karemera M, Terao M, and Brouillard F 1984 *J. Phys. B: At. Mol. Phys.* **17** 1613–1622

Wadehra J M 1979 *Appl. Phys. Lett.* **35** 917

Wadehra J M, and Bardsley J N 1979 *Phys. Rev. A* **20** 1398

Walton D S, Peart B, and Dolder K T 1971 *J. Phys. B: At. Mol. Phys.* **4** 1343–8

Wood B J and Wise H 1958 *J. Chem. Phys.* **29** 1416

Wood B J and Wise H 1958 *J. Chem. Phys.* **65** 1976–83

Wood B J and Wise H 1958 *J. Chem. Phys.* **66** 1049–53

Chapter 3

Numerical Models of Hydrogen Plasmas

3.1 Processes Included and Assumptions

In order to correctly interpret the magnitude and temporal behavior of the LIF observed in a hydrogen plasma, the behavior of the neutral hydrogen level populations before, during, and after laser illumination must be understood. However, in order to understand their behavior during and after laser illumination, the initial, unperturbed level populations must first be accounted for. Previous models (Burgess, *et al.*, 1980; Koopman, *et al.*, 1978; and Gohil and Burgess, 1983) have all assumed that the molecular hydrogen initially present is completely dissociated when the plasma is formed. In addition, no loss processes from the plasma were considered, so that the total concentration of atomic hydrogen in the plasma was assumed to be constant at a value determined by the initial fill pressure in the gas discharges used. The plasma was also assumed to be neutral, with no significant concentrations of ions other than H^+. Consequently, the H^+ concentration was taken to be equal to the electron concentration. Thus, previous theoretical models considered only electron collisional processes between bound atomic states and between bound atomic states and the continuum, spontaneous emission and photoexcitation between bound atomic states, and radiative and collisional recombination transitions from the continuum to bound atomic states.

The more recent models have all made use of the electron collisional ex-

citation and ionization rates given by Johnson (1972) for atomic hydrogen. Rates for the inverses of these processes, collisional de-excitation and collisional (three-body) recombination, were calculated by invoking detailed balance. For the radiative processes of spontaneous and stimulated emission and radiative recombination, the rates given by Seaton (1959) were usually used. (See Appendix F.) With the high neutral hydrogen densities assumed in these plasma models, photoexcitation rates were included by using escape factors to adjust the corresponding spontaneous emission rates. For example, with a high concentration of ground state atomic hydrogen, photons emitted by spontaneous transitions to the ground state would be nearly completely trapped due to the large optical depth of the Lyman$_\alpha$ transition. Thus, the spontaneous emission rates for the Lyman series were often set to zero in these numerical models. (See Appendix F.)

If the plasma is also subjected to laser illumination, laser-induced processes must also be accounted for. Burgess, *et al.*, (1980) estimated the effects of various laser-induced processes, including photoexcitation, stimulated emission, photoionization from the $n = 3$ level of atomic hydrogen, stimulated recombination, and laser-induced collisions involving virtual intermediate states. They concluded that the most significant of these processes were laser photoexcitation and its inverse process of stimulated emission. The other processes were found to be slower by several orders of magnitude, with photoionization from the $n = 3$ level being the most significant of these.

3.2 Rate Equation Models

With or without such laser-induced processes, an **exact** description of the level populations in a hydrogen plasma requires the solution of an infinite set of coupled differential equations. Of necessity, then, a numerical model of such a plasma must truncate this set of equations at some level, p. Since the higher-lying levels of atomic hydrogen are usually strongly coupled (because of the high collision rates), their populations are approximately given by their LTE (Saha-Boltzmann) values. Thus, the number of atomic hydrogen levels explicitly included in such a model may be limited to some integral number, p, above which the level populations are approximately in LTE. Previous investigators often chose the value for p such that the

population of that level stayed within some small fraction of a percent of its LTE value throughout the time period being modeled. Burgess *et al.* (1980) found that values for p of 8 or higher were sufficient to fulfill this requirement. A number of such LTE levels were often included in previous numerical models to ensure their convergence. The maximum LTE level, $p*$, used in these models was typically between 20 and 25 (Koopman, *et al.*, 1978), although Gohil and Burgess (1983) used a value of 50 for $p*$. In each case, the populations of these LTE levels ($p < i \leq p*$) were assumed to depend solely upon the electron temperature and number density. Making use of these assumptions, the otherwise infinite set of coupled differential equations was reduced to a more manageable size in the rate equation models used by previous investigators.

For each level explicitly included in these standard collisional-radiative models, the population N_i of the ith atomic hydrogen level, in a plasma which is not laser irradiated, was described by a set of rate equations similar to those given by Gohil and Burgess (1983):

$$\begin{aligned}\frac{dN_i}{dt} = & \sum_{j=i+1}^{p} N_j A_{ji} + n_e\left[\sum_{\substack{j=1 \\ j\neq i}}^{p} N_j C_{ji} + n_e(U_i + C_{ci})\right] \\ & + \sum_{j=p+1}^{p*} N_j(n_e C_{ji} + A_{ji}) \\ & - N_i\left[\sum_{j=1}^{i-1} A_{ij} + n_e\left(\sum_{\substack{j=1 \\ j\neq i}}^{p*} C_{ij} + C_{ic}\right)\right] + D_i \end{aligned} \tag{3.1}$$

where the A_{ji} (1/sec) are the spontaneous decay rates; C_{ij} and C_{ji} (cm^3/sec) are the collisional rate coefficients between levels i and j; C_{ic} and C_{ci} (cm^3/sec) are the collisional ionization and recombination rate coefficients, respectively; U_i is the radiative recombination rate coefficient; D_i (cm^3/sec) is the net rate at which atoms in level i diffuse into the volume of interest; and n_e is the electron density. The levels 1 through p ($1 \leq i \leq p$) were explicitly included in the model while the levels between p and $p*$ ($p < i \leq p*$) were assumed to be in LTE.

3.3 Solution Techniques

The resulting finite set of p rate equations may be concisely expressed in matrix form:

$$\frac{d\mathbf{N}}{dt} = \mathbf{A} \cdot \mathbf{N} + \mathbf{B} \tag{3.2}$$

where $\mathbf{N}$ is the $(p \times 1)$ column vector of level populations N_i, $\mathbf{A}$ is the $(p \times p)$ matrix of coupling coefficients a_{ij} linking the levels i and j (which includes collisional ionization processes and rates to levels with $i > p$), and $\mathbf{B}$ is the $(p \times 1)$column vector of recombination rates b_i from higher levels $(i > p)$ and the continuum. For example, the a_{ij} element of $\mathbf{A}$ represents the rate (1/sec) of transitions into level j, from level i, while a_{ii} represents the total rate out of level i.

With the addition of laser irradiation to the model, the rate matrix $\mathbf{A}$ in equation (3.2) was modified by the addition of time-dependent rates for laser photoexcitation and stimulated emission:

$$\begin{aligned} a^{\mathrm{L}}_{ii} &= a_{ii}(t) - R^{\mathrm{L}}_{ij}(t) \\ a^{\mathrm{L}}_{ij} &= a_{ij}(t) + R^{\mathrm{L}}_{ji}(t) \\ a^{\mathrm{L}}_{ji} &= a_{ji}(t) + R^{\mathrm{L}}_{ij}(t) \\ a^{\mathrm{L}}_{jj} &= a_{jj}(t) - R^{\mathrm{L}}_{ji}(t) \end{aligned} \tag{3.3}$$

where R_{ij} and R_{ji} represent the laser-induced photexcitation and stimulated emission rates, respectively, and the L superscript on the rate matrix elements indicates the inclusion of these laser-induced rates. The laser photoexcitation rate is simply the product of the Einstein B_{ij} coefficient and the laser's average spectral intensity $\langle J_\nu \rangle$:

$$R^{\mathrm{L}}_{ij}(t)(1/\mathrm{sec}) = B_{ij}(\mathrm{cm}^2/\mathrm{erg} \cdot \mathrm{sec}) \cdot \langle J_\nu \rangle(\mathrm{erg}/\mathrm{sec} \cdot \mathrm{cm}^2 \cdot \mathrm{Hz}) \tag{3.4}$$

(Values for the B_{ij} coefficient may be calculated from tabulated absorption oscillator strengths, as shown in Appendix G. In addition, the calculation of a laser's average spectral intensity is described in that same appendix.) Similarly, the laser-stimulated emission rate is the product of the Einstein B_{ji} coefficient and the laser's average spectral intensity:

$$R^{\mathrm{L}}_{ji}(t)(1/\mathrm{sec}) = B_{ji}(\mathrm{cm}^2/\mathrm{erg} \cdot \mathrm{sec}) \cdot \langle J_\nu \rangle(\mathrm{erg}/\mathrm{sec} \cdot \mathrm{cm}^2 \cdot \mathrm{Hz}) \tag{3.5}$$

The Einstein coefficients are related by the statistical weights of the upper and lower states of the target transition (see Appendix G):

$$B_{ji} = \frac{g_i}{g_j} \cdot B_{ij} = \frac{2i^2}{2j^2} \cdot B_{ij} \tag{3.6}$$

Thus, the laser-stimulated emission rate may be obtained directly from the laser photoexcitation rate:

$$R^{\mathrm{L}}_{ji}(t) = \frac{i^2}{j^2} \cdot R^{\mathrm{L}}_{ij}(t) \tag{3.7}$$

If the rate matrix **A** and the recombination vector **B** of equation (3.2) are time-independent and are not explicit functions of the level populations, this set of rate equations may be solved by obtaining the eigenvalues of matrix **A**. This solution technique was used in the model by Johnson and Hinnov (1973) and, more recently, by Burgess, *et al.* (1980). The solution obtained by this method gives the level populations for steady-state conditions only. In addition, since the ground state may be decoupled from this system of equations, the "quasi" steady-state populations obtained are for a specified electron density and temperature and ground state population. (See Koopman, *et al.* (1978) for further details on this technique.)

In order to obtain a time-dependent solution to this system of rate equations, a time iteration technique which allows the level populations to relax to their steady-state values was used by Gohil and Burgess (1983). One advantage of the time iteration technique used by them was that it did not require the rate matrix **A** or the recombination vector **B** to be independent of the level populations **N**. That is, the set of rate equations could actually be non-linear. In addition, the time iteration technique made it possible to observe the time-dependent behavior of the processes involved, which is critical if the plasma is not actually in steady-state, as was assumed by earlier investigators.

A common method used to implement this time iteration makes use of the divided-difference expression of Gear's technique for the solution of "stiff" differential equations. (Gear, 1971) In this technique, the level populations are obtained by numerical time iteration, with information from previous time steps used to determine the optimum length of the current time step. The accuracy and stability of this method are controlled

by requiring that the relative error in each of the computed level populations be less than a specified error tolerance parameter.

Using a similar numerical technique, Gohil and Burgess (1983) modeled the atomic hydrogen level populations for a wide range of electron temperatures and number densities. They found that the excited state populations equilibrated with the ground state population in a time on the order of nanoseconds, while the ground state population slowly relaxed to a steady-state value in a time on the order of 10 - 100 microseconds. Gohil and Burgess (1983) found that this time iteration technique gave exactly the same quasi steady-state level populations as the matrix inversion (eiqenvalue) technique used by Johnson and Hinnov (1973), and later by Burgess, *et al.* (1980), for a given (constant) ground state population.

However, neither of these solution techniques was able to correctly reproduce the behavior of the hydrogen plasma used in the experiments by Burgess, *et al.*, (1980). As described in the survey of previous work (Chapter 2), the numerical model used by Burgess, *et al.*, failed to model the fluorescence observed in their laser-induced fluorescence (LIF) experiment. More importantly, however, their model showed a "remarkable discrepancy" in predicting the initial (prior to laser irradiation) population of the $n = 2$ level of hydrogen. A major discrepancy in modeling the unperturbed $n = 2$ population would clearly obviate any detailed analysis of the fluorescence signal, which arises due to populations being moved from the $n = 2$ state to the $n = 3$ state. Although such discrepancies between reality and numerical models are (regretably) not uncommon, this discrepancy was particularly significant because the plasma conditions were quite similar to those encountered in astrophysical situations where such models have been widely used. With this in mind, it seemed essential that the assumptions associated with this model and the suggestions of other investigators, as described in the survey of previous work, be carefully examined. As a result of this examination, both an expanded rate equation model and a kinetics model of LIF in a hydrogen plasma were developed.

3.4 Plasma Model Evolution

The evolution of the models used to investigate the behavior of a z-pinch hydrogen plasma is shown in Figure 3.1. The original Burgess model (Burgess

et al., 1980) considered only H, H^+, and e^-, used Johnson's collisional rates, and assumed that the populations of these species were in steady state at all times. In the present investigation, the first model developed, the atomic rate equation model (ARM_J), considered these same atomic species and used Johnson's rates. However, a time-dependent solution technique was employed, as in the model by Gohil and Burgess (1983). The initial species populations, for given n_e and T_e, were obtained by allowing the system of equations to relax to steady state. At each subsequent time step, T_e was set to the experimentally measured value, while n_e was determined by simply requiring plasma neutrality. The next model developed, ARM_{VS}, was the same as ARM_J except dthat the collisional rates of Vriens and Smeets were used in place of Johnson's rates. Using the ARM_{VS} model as a starting point, additional species and processes were added to produce an extended rate equation model, ERM. This model included the species H^-, H_2, H_2^+, and H_3^+ and many of their associated processes. In addition, both ion and neutral diffusion, radiation trapping, and a two-temperature electron population (empirically determined) were included. The ERM model also used initial populations which were obtained from experimental measurements and were not necessarily steady state populations. These quasi steady state populations were sustained for tenths of microseconds by empirically choosing populations for the other species in the model. This model was used to determine which of the processes were significant in the hydrogen plasma beign modeled. These processes were then incorporated in a full kinetics model (KM) of the plasma. Using quasi steady state populations similar tc those in the ERM model, and the experimentally measured plasma temperature, the kinetics model allowed the atomic and molecular species concentrations and electron density and distribution to evolve self-consistently with time.

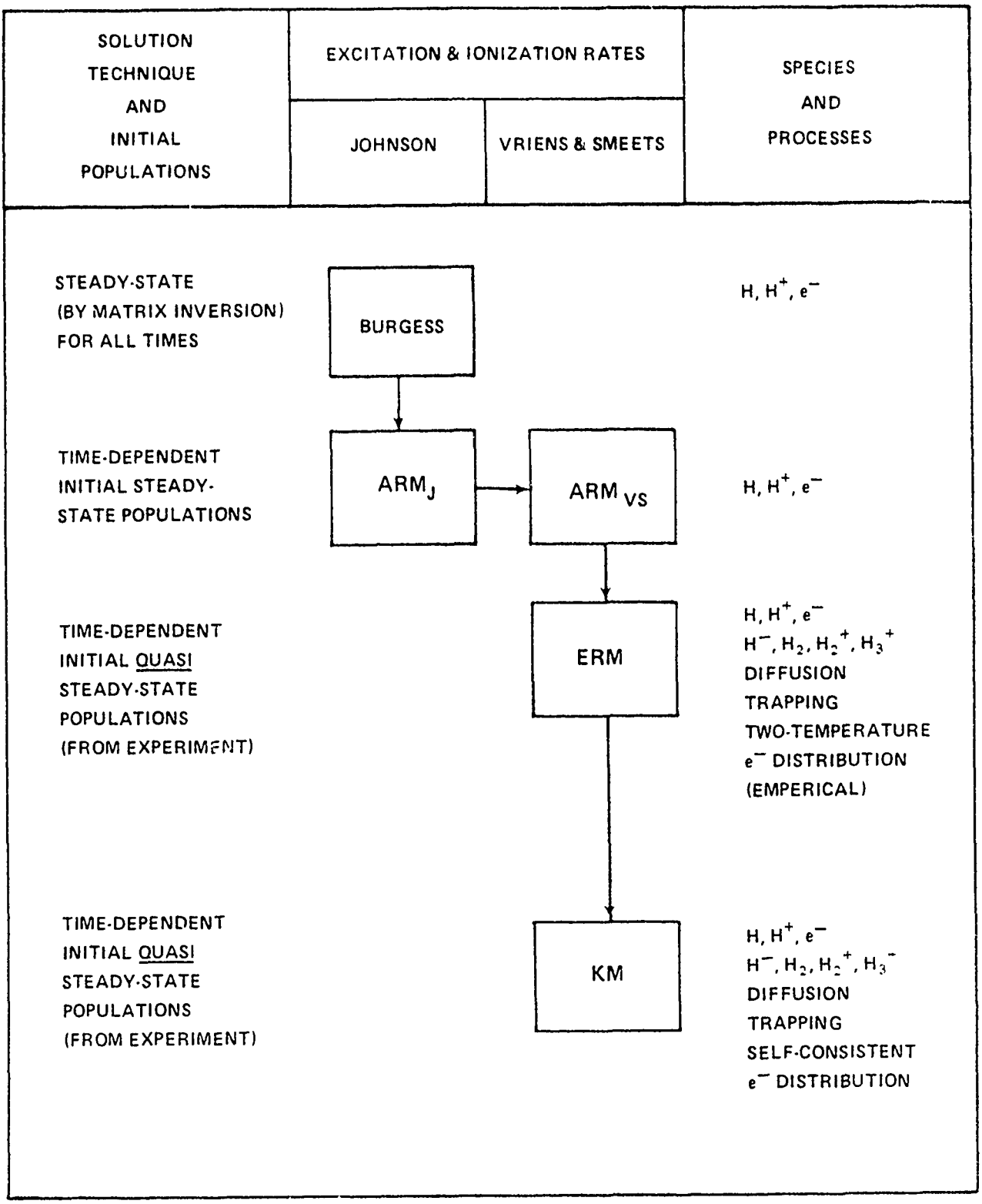

Figure 3.1: Hydrogen Plasma Model Evolution

Bibliography

Burgess D D, Myerscough V P, Skinner C H, and Ward J M 1980 *J. Phys. B: At. Mol. Phys.* **13** 1675–1701

Gear C W 1971 *Communications of ACM* **14** 176

Gohil P and Burgess D D 1983 *Plasma Physics* **25** 1149–67

Johnson L C 1972 *Astrophysical J.* **174** 227

Johnson L C and Hinnov E 1973 *J. Quant. Spectrosc. Radiat. Transfer* **13** 333

Koopman D W, McIlrath T J, and Myerscough V P 1978 *J. Quant. Spectrosc. Radiat. Transfer* **19** 555–67

Seaton M 1959 *Mon. Not. R. Astron. S.* **119** 90

Chapter 4

Rate Equation Model

4.1 Additional Species and Processes

An expanded rate equation model was developed in order to improve upon existing models of hydrogen plasmas, and of laser-induced fluorescence in such plasmas, in particular. Additional species and processes were included and the best available rates were obtained for all processes. In particular, molecular hydrogen, the positive ions H_2^+ and H_3^+ as well as the negative hydrogen ion H^-, were added to the model. The most "significant" processes associated with these species were also added to the model. These processes included: mutual neutralization of H^+ and H^-, dissociative recombination of electrons with H_2^+ and with H_3^+, dissociative attachment of electrons with H_2^+, proton exchange between H and H_3^+, and laser photoionization of atomic hydrogen in the $n = 3$ level. For each of these additional processes, as well as for the electron collisional excitation and ionization processes, the most accurate rates were obtained. For example, the electron collisional excitation and ionization rates of Johnson (1972), which had been used in all previous models, were replaced by those given by Vriens and Smeets (1980). Rates for many of the other processes were obtained from the compilation by Janev *et al.* (1987). For a complete description of the rates used for each of these added processes (and their inverses), see Appendix F.

4.2 Diffusion and Wall Recombination

The macroscopic plasma processes of ion and neutral species diffusion were also included in the expanded rate equation model. The loss of ionic species from the axial core region of a cylindrical plasma, as in the experiments of Burgess *et al.* (1980), was modeled as ambipolar diffusion to the walls. As demonstrated in the simulations of Long and Newton (1971), such diffusion produces a radial concentration profile which may be approximated using a zeroth-order Bessel function of the first kind, $J_0(x)$. (See Figure 4-1.) Upon reaching the walls, these ions are neutralized and may react with other hydrogen species near or adsorbed in the walls, forming a wall sheath of cool atomic and molecular hydrogen. The rapid formation of such a wall sheath was also demonstrated in the simulations by Long and Newton (1971). In addition, citing the experimental results of Newton and Sexton (1969), Jones (1982) argued that hydrogen plasmas produced by nearly complete ionization may have over 40% of the hydrogen initially present attached to the walls in an active state for several hundreds of microseconds. (See Appendix E.) Cool atomic and molecular hydrogen in such a wall sheath would gradually diffuse back into the plasma's axial core, cooling the plasma as a whole and producing a radial concentration profile which may be approximated using a zeroth-order modified Bessel function of the first kind, $I_0(x)$. (See Figure 4.1.)

4.2.1 Ion Diffusion

In the expanded rate equation model, the concentrations of the plasma ions (H^+, H^-, H_2^+, and H_3^+) in the axial core were decreased by their diffusive loss to the walls of the cylindrical discharge tube. Separating variables in the diffusion equation,

$$\frac{\partial n}{\partial t} = D \nabla^2 n,$$

with

$$n(\mathbf{r},t) \equiv T(t)S(\mathbf{r}),$$

the temporal solution was found to be of the form

$$T(t) = T_0 e^{(-t/\tau)},$$

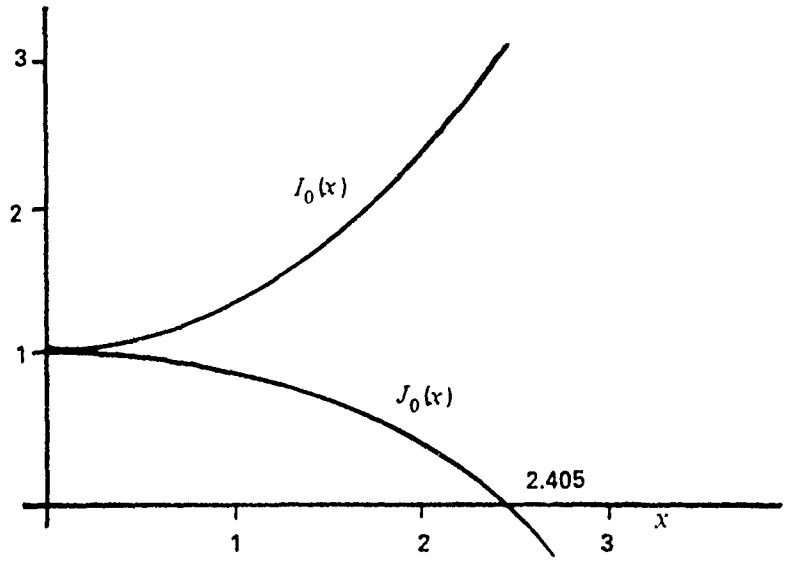

Figure 4.1: Bessel Functions $I_0(x)$ and $J_0(x)$

where τ is the time constant for the density decrease. Assuming that the ion density vanished at the walls and was finite on axis, the spatial solution was found to have the form of a Bessel function of the first kind. Since higher order inhomogeneities in the radial density profile would damp out quickly, the spatial solution was assumed to be of the form of the zeroth-order function, $J_0(x)$. Combining the spatial and temporal solutions, the density of each ionic species could be expressed as:

$$n(r,t) = Ae^{-t/\tau}J_0(r/\sqrt{D\tau}).$$

Assuming that the initial number density on axis for a given ionic species was $n_0(core)$, then $A = n_0(core)$. Thus, the ionic number densities could be given by equations of the form:

$$n(r,t) = n_0(core)e^{-t/\tau}J_0(r/\sqrt{D\tau}).$$

Applying the boundary condition at the wall, the time constant for the diffusion of a given ionic species was found to be

$$1/\tau = (2.405/a)^2 D_a,$$

where a is the radius of curvature of the cylindrical wall, 2.405 is the first zero of $J_0(x)$, and D_a is the ambipolar diffusion coefficient for the species in a mixture of atomic and molecular hydrogen. Consequently, the rate at which this species diffused out of the plasma could be represented simply as:

$$R_{\text{diff}}^{\text{ion}}(1/\text{sec}) = 1/\tau = \Big(2.405/a(\text{cm})\Big)^2 D_a(\text{cm}^2/\text{sec}) \qquad (4.1)$$

The ambipolar diffusion coefficient in this equation may be obtained from experimentally-measured or theoretical values for the specific ion's mobility in a mixture of atomic and molecular hydrogen. The diffusion coefficients used for the ionic species included in the expanded rate equation model are described in Appendix 1.

4.2.2 Neutral Diffusion

When these diffusing ions reach the walls, they will be neutralized and possibly recombine with hydrogen already adsorbed in the walls. This atomic and molecular hydrogen would further augment the high concentration of

hydrogen atoms and molecules which Jones (1982) claimed would already be at the walls as a result of the initial formation of the plasma. The resulting wall sheath would, in turn, act as a source of relatively "cool" neutral atoms and moleules. The rate at which these particles would re-enter the plasma "core" would be determined by their diffusion rates in a mixture of atomic and molecular hydrogen.

In order to obtain values for these diffusion rates in a cylindrical z-pinch plasma similar to that of Burgess *et al.* (1980), the diffusion equation was solved subject to the boundary conditions in the plasma core (along the cylinder's axis) and at the walls. The number densities of atomic and molecular hydrogen were required to be finite in the plasma core, with values given by the solution of the rate equation model. In the cylindrical wall sheath, the number densities of these same species had to be larger, but still finite. With these boundary conditions, then, the spatial solutions could be represented in terms of modified Bessel functions of the first kind, $I_0(r)$, as shown in Figure 4.1. In addition, this form of radial profile agreed well with the simulations of Long and Newton (1971) and with the predictions of Jones (1982), which were based on experimental observations.

Combining the spatial solution with the temporal solution to the differential equation, as in the preceding section on ion diffusion, the number density at time t and radial position r in the plasma could be represented as:

$$n(r,t) = Ae^{+t/\tau} I_0\left(\frac{r}{\sqrt{D\tau}}\right) .$$

So, if the initial number density on axis for a given neutral species is $n_0(core)$, then $A = n_0(core)$. Thus, the number density of a neutral species could be given by:

$$n(r,t) = n_0(core)e^{+t/\tau} I_0\left(\frac{r}{\sqrt{D\tau}}\right) .$$

If the species' initial number density at the wall ($r = a$) is $n_0(wall)$, then

$$n(r = a, t = 0) = n_0(wall) = n_0(core) I_0\left(\frac{a}{\sqrt{D\tau}}\right) .$$

So, in order to satisfy these boundary conditions,

$$I_0\left(\frac{a}{\sqrt{D\tau}}\right) = \frac{n_0(wall)}{n_0(core)} .$$

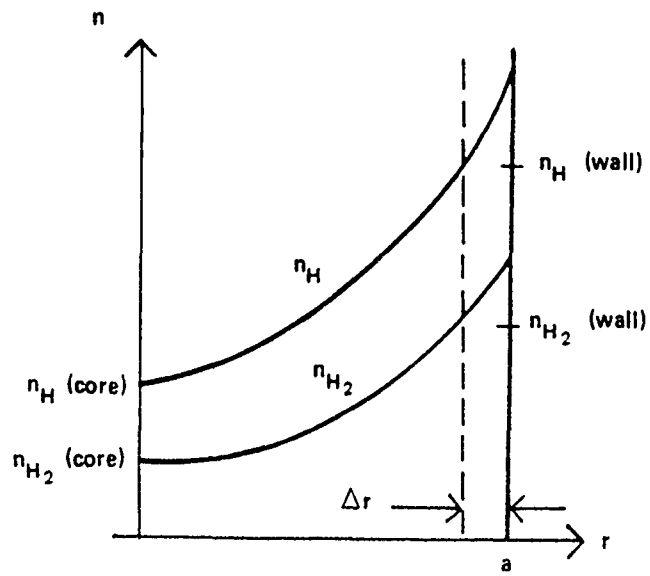

Figure 4.2: Radial Distributions of H and H_2

Taking the inverse of this equation numerically and solving for the time constant τ, the "neutral" diffusion rate is found to be:

$$R_{\text{diff}}^{\text{neutral}}\,(1/\text{sec}) = \frac{1}{\tau} = \left(\frac{D}{a^2}\right)\left\{I_0^{-1}\left[\frac{n_0(wall)}{n_0(core)}\right]\right\}^2 \qquad (4.2)$$

where a is the radius (cm) of the cylinder and D (cm^2/sec) is the mutual diffusion coefficient for atomic and molecular hydrogen in a mixture of these species. An analytic expression for this mutual diffusion coefficient, which is a function of the gas temperature and pressure, is given in Appendix J. (Since the distance from the wall to the plasma core is many mean free paths, the diffusion coefficient's temperature dependence is primarily due to the temperature in the Plasma core and not in the wall sheath.) In order to calculate this diffusion rate for a given neutral species, it was also necessary to know the relative concentrations of that species in the plasma core and in the wall sheath, $n_0(core)$ and $n_0(wall)$, respectively. Values for the neutral concentrations in the plasma core were obtained directly from the rate equation solutions. However, values for the wall concentrations had to be estimated by a more complicated approach. (See Appendix K.)

The wall concentrations of atomic and molecular hydrogen were determined by invoking particle conservation and using measured recombination coefficients for hydrogen atoms incident on the walls. That is, assuming that a quasi steady state prevailed in the wall sheath, the H_2 production rate by wall recombination was required to equal the H_2 loss rate by diffusion back into the plasma. This assumption resulted in a simple expression for the ratio of atomic and molecular hydrogen concentrations in the wall sheath. (See Appendix K.) The individual concentrations of the atomic and molecular hydrogen at the walls were then obtained by assuming (as suggested by Jones (1982)) that a certain fraction of the hydrogen used to initially fill the cylindrical container remained "attached" to the walls for several hundreds of microseconds after the formation of the plasma. The appropriate fraction of such hydrogen was determined empirically, within the bounds suggested by Jones (1982), in order to best model the experimental data given by Burgess *et al.* (1980).

4.3 Bi-Maxwellian Electron Distribution

A major assumption of each of the rate equation models for the laser induced fluorescence experiment by Burgess *et al.*(1980) was that the plasma's electron energy distribution was Maxwellian. However, as shown by Lee *et al.* (1983), the experimental results that Burgess *et al.* presented clearly indicated that the electron distribution became significantly non-Maxwellian as the plasma cooled. From the experimental data, Lee and his collaborators obtained electron distribution functions at three successive times (35, 45, and 55 μsec) after the plasma was formed, as shown in Figure 2.2 of the *Survey of Previous Work* chapter. At 35 μsec the distribution appeared to be completely Maxwellian. However, as the plasma cooled and recombined, the atomic hydrogen ground state population increased and since the Lyman$_\alpha$ radiation was efficiently trapped, the $n = 2$ state presumbably became overpopulated relative to the LTE population. Then, superelastic collisions of electrons with atoms in the $n = 2$ state caused an increase in the number of "hot" electrons. Although these hot electrons would normally collisionally redistribute their energy to other electrons, the accompanying decrease in the electron density as a function of time reduced the rate at which this thermalization occurred. Therefore, by 45 μs the number of hot electrons was only slightly reduced, while the primary distribution of electrons had cooled from .8 eV to .58 eV and the electron density had decreased from 1.1×10^{15} 1/cm^3 to 5.0×10^{14} 1/cm^3. As a consequence, the fraction of hot electrons probably increased. These trends appeared to be accentuated even more in the next 10 μs, with the electron temperature and number density dropping to .43 eV and to 2.2×10^{14} 1/cm^3, respectively.

In an attempt to investigate the effects of such non-Maxwellian electrons using a rate equation model, a bi-Maxwellian electron distribution was added to the expanded model. When this option was selected, a certain (small) fraction of the electron distribution was given an elevated temperature. The temperature of the hot component was assumed to start at .8 eV (at 30 μs after pinch initiation) and approach a limitibng value of 10.2 eV according to a negative exponential. The fraction of electrons which were assumed to be hot was determined empirically. This fraction was also increased according to a negative exponential (with time constant 3.5 μs), to a maximum at 48 μs, and then decreased exponentially (with time constant 1.25 μs). The fraction of hot electrons peaked at approximately 8.7×10^{-9}

of the total electron density at 48 μs. By 65 μs this fraction was reduced by over four orders of magnitude. Although the number of hot electrons is small compared to the total concentration of electrons, it does constitute a significant increase over the normal Maxwell-Boltzmann fraction of electrons at these energies.

To include the effect of these hot electrons, separate rate matrices were calculated for the electrons at the experimentally measured plasma temperature and for the hot electrons. (The hot electron rate matrix was constructed using only a selected set of electron-impact processes.) These rate matrices were then added together to obtain the total rate matrix for both groups of electrons. The total electron density was determined simply by requiring charge neutrality among all the charged species included in the model.

This bi-Maxwellian model provided a means of crudely foreshadowing the results of a more thorough kinetics equation model, discussed in chapter 7. Because of the complexity of such kinetics models, only those processes which had been proven to be significant by the expanded rate equation model were incorporated into the kinetics model.

Bibliography

Burgess D D, Myerscough V P, Skinner C H, and Ward J M 1980 *Journal of Physics B: Atomic and Molecular Physics* **13** 1675-1701

Janev R K, Langer W D, Evans K Jr, and Post D E 1987 *Elementary Processes in Hydrogen-Helium Plasmas* (New York: Springer-Verlag)

Johnson L C 1972 *The Astrophysical Journal* **174** 227-36

Jones W M 1982 *Plasma Physics* **24**(4) 361-68

Lee R W, Morgan W L, Whitten B L, and Kolbe G 1983 *Lawrence Livermore National Laboratory, CA* **UCRL**-88714

Long J W and Newton A A 1971 *Numerical Simulation of Hydrogen Afterglow Proceedings of 10th International Conference on Phenomena in Ionized Gases, Oxford (ed R N Franklin)*

Newton A A and Sexton M C 1969 *Journal of Physics B: Atomic and Molecular Physics* **2** 1069-74

Vriens L and Smeets A H M 1980 *Physical Review* **22** 940

Chapter 5

Validation of Atomic Rate Equation Model

5.1 Introduction

The expanded rate equation model which was developed was first validated by using the same atomic species, processes, and initial conditions as those used in the colisional-radiative model of Burgess, *et al.* (1980). In order to validate this model, both the unperturbed plasma behavior and the behavior under laser illumination were investigated. The results of this atomic rate equation model (ARM) were compared to the model results and experimental observations of Burgess *et al.*. Twenty atomic hydrogen energy levels and the collisional rates of both Johnson (1972) and Vriens and Smeets (1980) were considered. Using Johnson's rates in the current model, the results of Burgess' model (which also made use of these rates) were essentially reproduced in nearly all instances. However, the use of Vriens and Smeets' rates in the current model produced, in some cases, significant changes in the behavior of the plasma; while some changes improved the agreement with the experimental results, other changes made things even worse.

5.2 Unperturbed Plasma Behavior

5.2.1 Quasi Steady State Species Populations

In the ARM model, the quasi steady state level populations were obtained for plasma conditions (n_e and T_e) at 30, 40, and 50 μs after peak current in the plasma-forming pinch (referred to as cases 1, 2, and 3, respectively). The initial populations of these levels for each case were determined empirically, by simply allowing the populations to relax to quasi steady state levels, usually in a time less than .2 μs. These populations were then used as the initial conditions for that particular case.

The quasi steady state $n = 2$ populations which were determined by the relaxation technique were within 2% of the Burgess model values at 30 and 50 μs and approximately 12% too large at 40 μs. However, as Burgess, *et al.* (1980) noted, the actual $n = 2$ populations were significantly higher at early stages of the recombination phase: 16 times greater than predicted at 30 μs, 5 times greater at 40 μs, and within experimental error ($\pm 10\%$) at 50 μs. (See Figure 5.1, which shows the experimental results and theoretical predictions of Burgess, *et al.* (1980), as well as the theoretical predictions from the ARM model.) Using the rates given by Vriens and Smeets increased the quasi steady state $n = 2$ population at each time (electron density), from an increase of 20% at 30 μs to an increase of 35% at 50 μs. These increases improved the agreement with the experimentally measured populations in cases 1 and 2, but worsened the agreement in case 3. (However, the increased discrepancy in case 3 is probably not significant, given the rapid variation in the $n = 2$ population with electron density, as can be seen in Figure 5.1.)

5.2.2 Long-term Plasma Behavior

Using this set of quasi steady state initial populations, the long-term plasma behavior (atomic hydrogen, H^+, and electrons only) is as shown in Figure 5.2 for an initial time of 30 μs. As shown in the figure, the recombination of the H^+ produces a cascade through the excited atomic levels, ending in the ground state. Although the calculated electron density decreases as this recombination proceeds, it is not nearly as fast as the experimentally observed, exponential decrease. This effect was also observed in the kinet-

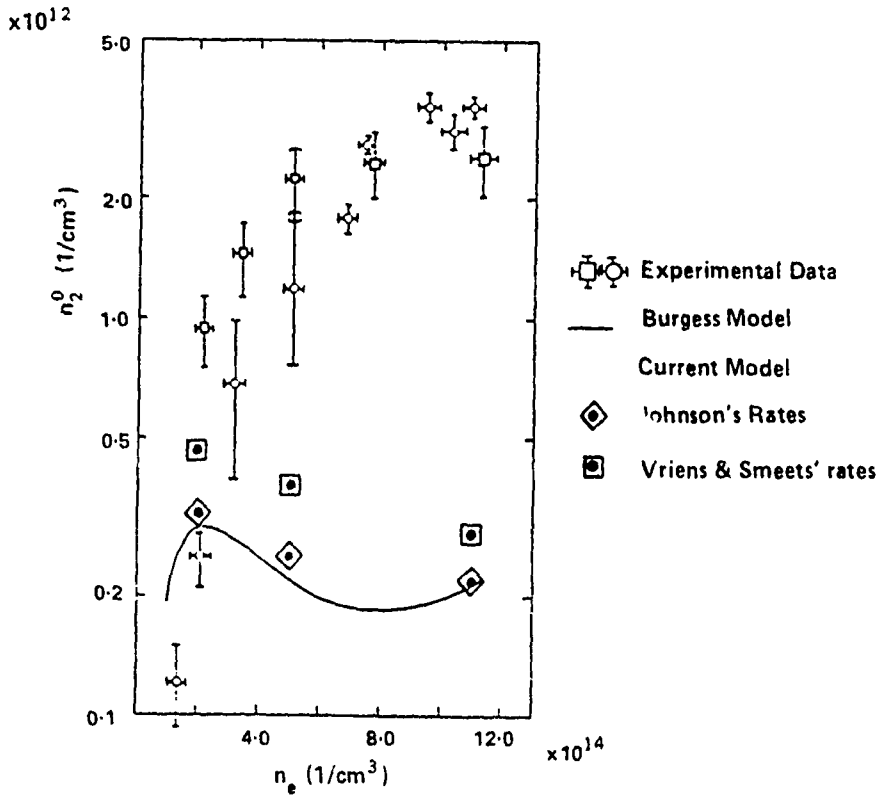

Figure 5.1: $n = 2$ Level Populations, n_2^0, in the Unperturbed Plasma

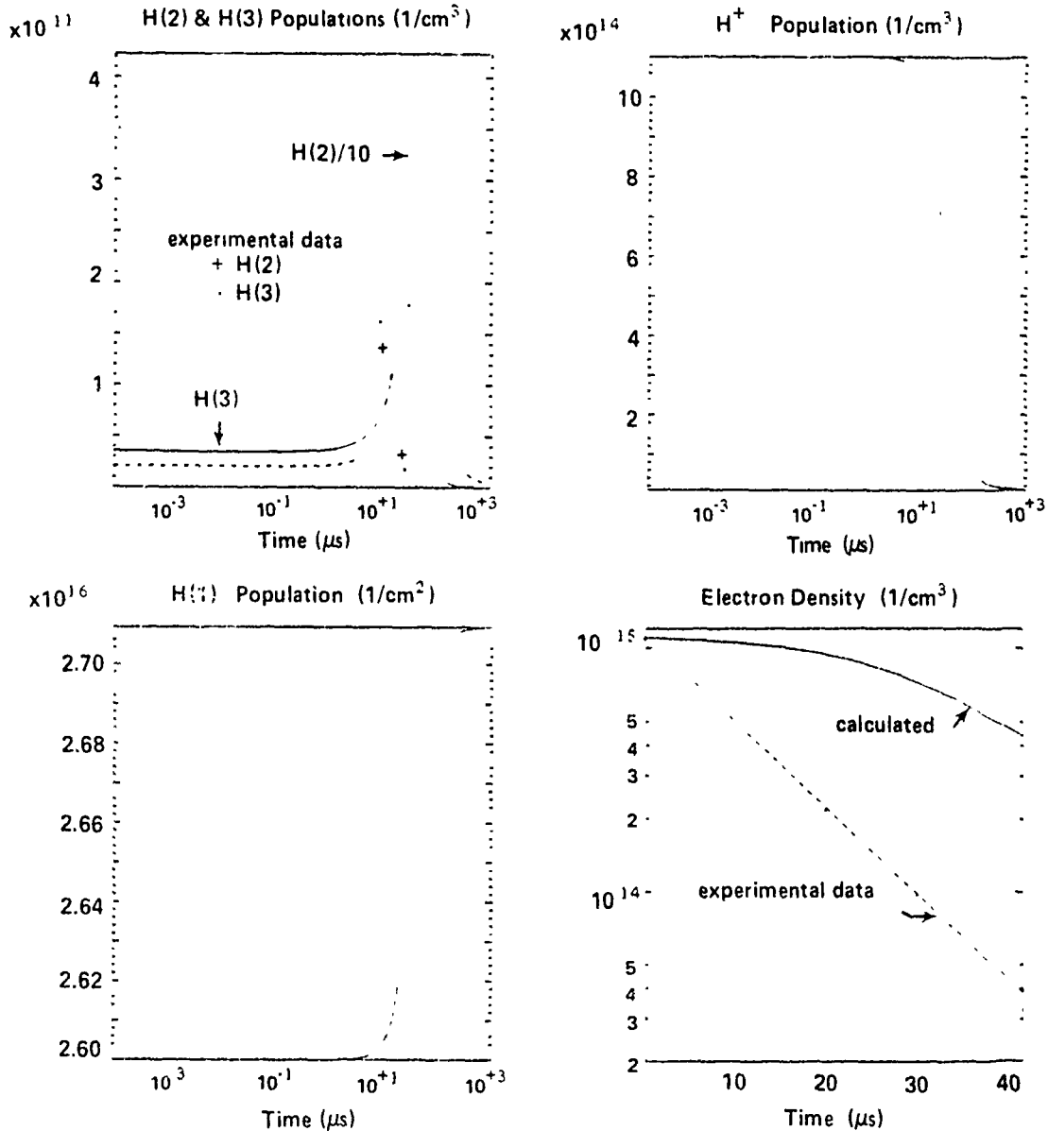

Figure 5.2: Long Term Plasma Behavior (ARM Model, Initial Time 30 μs, Johnson's Rates)

ics simulations of Lee *et al.* (1983), who reported a bulk recombination rate much slower than that observed experimentally. However, this information was not available from the work done by Burgess *et al.* since they used an equilibrium model with electron densities set at the experimentally observed values.

5.3 Plasma Behavior Under Laser Illumination

Under laser illumination, the populations of the $n = 2$ and $n = 3$ states, for an initial time of 50 μs, is as shown in Figure 5.3. (The normalized laser pulse is shown as a dotted line.) The calculated population of the $n = 3$ state shows the same qualitative behavior as the LIF observed experimentally in a helium plasma, as shown in Figure 2.1. (Burgess and Skinner, 1974) That is, the H(3) population (fluorescence) rises quickly to a peak, decays to a plateau while the laser remains on, and returns to its unperturbed value after the laser turns off. The short term behavior of this atomic rate equation model was investigated by comparing three parameters associated with this fluorescence peak – the peak enhancement ratio, the fluorescence plateau ratio, and the decay rate of the fluorescence peak. The values of these parameters for the Burgess model and for the atomic rate equation model were compared to those measured experimentally by Burgess *et al.* (1980).

5.3.1 Peak Enhancement Ratio

Although the $n = 3$ population was not measured experimentally, the peak enhancement ratio, $n_3^L(peak)/n_3^0$, was. Since the $n = 2$ level should be the major source of these $n = 3$ atoms under IIα laser illumination which saturates the transition, it was assumed that this ratio should be essentialy equal to that of n_2^0/n_3^0. Thus, using the quasi steady state $n = 3$ and $n = 2$ populations obtained theoretically, Burgess, *et al.* (1980) obtained theoretical values for the peak ratios, $n_3^L(peak)/n_3^0$. In the ARM model, this assumption was not borne out. Using Johnson's rates (and the same processes, initial conditions, and assumptions as in the Burgess model),the quasi steady state n_2^0/n_3^0 ratios obtained were found to be higher than the

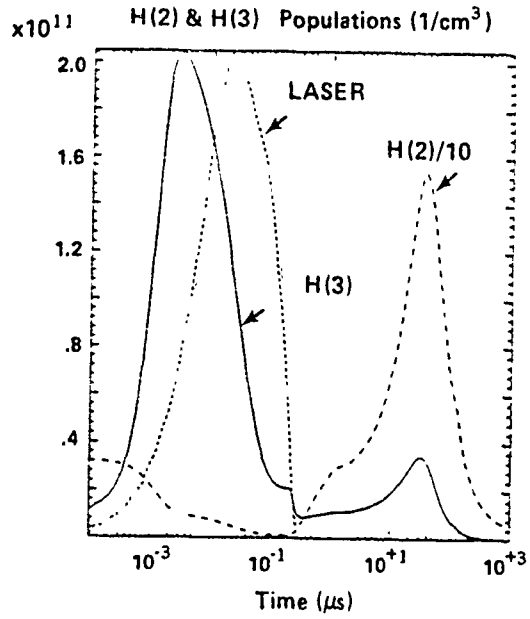

Figure 5.3: $n = 2$ and $n = 3$ Level Populations Under Laser Illumination (ARM Model, Initial Time 50 μs, Johnson's Rates)

$n_3^L(peak)/n_3^0$ ratios: from 71% higher at 30 μs to 48% higher at 50 μs. Similar results were obtained using the rates of Vriens and Smeets, though the discrepancies between the n_2^0/n_3^0 and $n_3^L(peak)/n_3^0$ ratios were slightly reduced. Thus, the simple (atomic hydrogen only) rate equation model produces much smaller peak enhancements than predicted by the ratio of the initial quasi steady state populations.

Although the Burgess model and the ARM model gave similar values for the peak enhancement ratios (within 15% at early times and identically at later times), these values differed significantly from the experimental results. Both models' peak enhancement ratios were greater than the experimentally measured ones: from approximately 20% greater in case 1 to 58% greater in case 3. Using the rates given by Vriens and Smeets only increased these discrepancies with the experimental results, with peak ratios 54% above the experimental value in case 1 and 158% above the experimental value in case 3. (See Figure 5.4, which shows the experimental data and the predictions of the current model and of Burgess, *et al.* (1980).

5.3.2 Fluorescence Plateau Ratio

The ARM model (using Johnson's rates) also agreed well with that of Burgess in the values obtained for the $n = 3$ fluorescence plateau, giving values that were slightly low, though not by more than 8%. However, both models were incredibly bad at reproducing the experimental values, giving values as much as 67% below those of the experiment. Using the rates of Vriens and Smeets slightly improved the agreement by raising the fluorescence plateau ratio, particularly at late times. Thus, the use of Vriens and Smeets' rates, which are, in general, somewhat slower than those of Johnson, did not have nearly the effect reported by Burgess (and confirmed with the present model) when Johnson's collisional rates were arbitrarily reduced by a factor of ten. Thus, the use of Vriens and Smeets' rates in the ARM model resulted in only minimal improvements in the plateau ratio, and then only at later times in the recombination. (See Figure 5.5, which shows the experimental and theoretical results of Burgess, *et al.* (1980) and the results of the ARM model.)

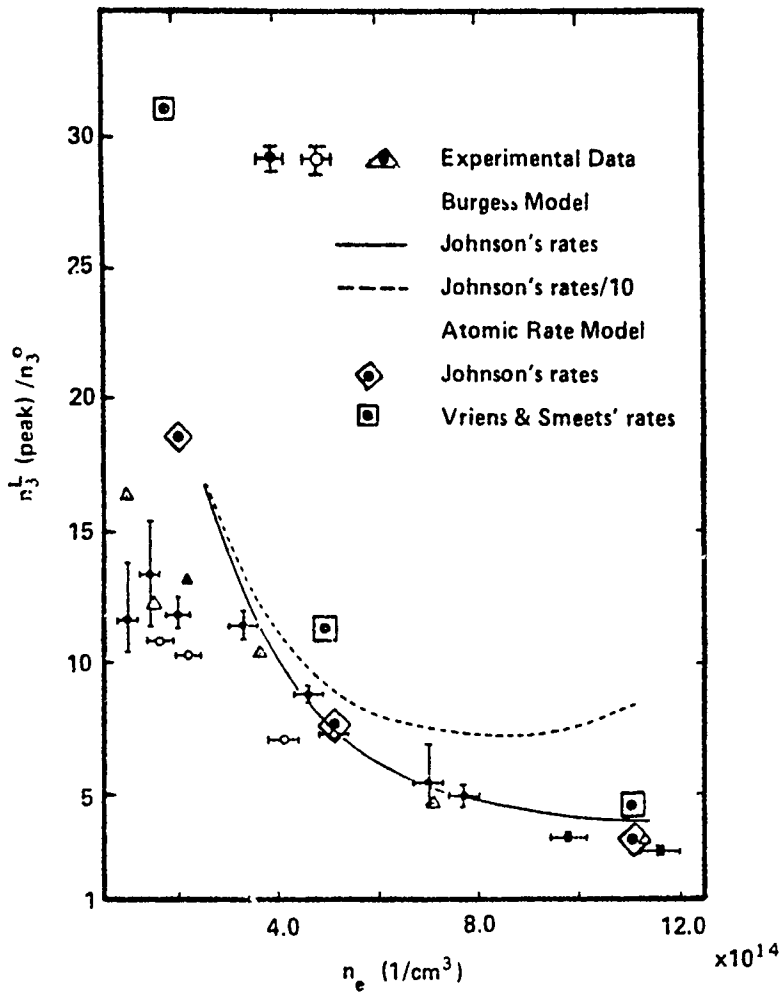

Figure 5.4: Peak Enhancement Ratio Comparisons $n_3^L(peak)/n_3^0$

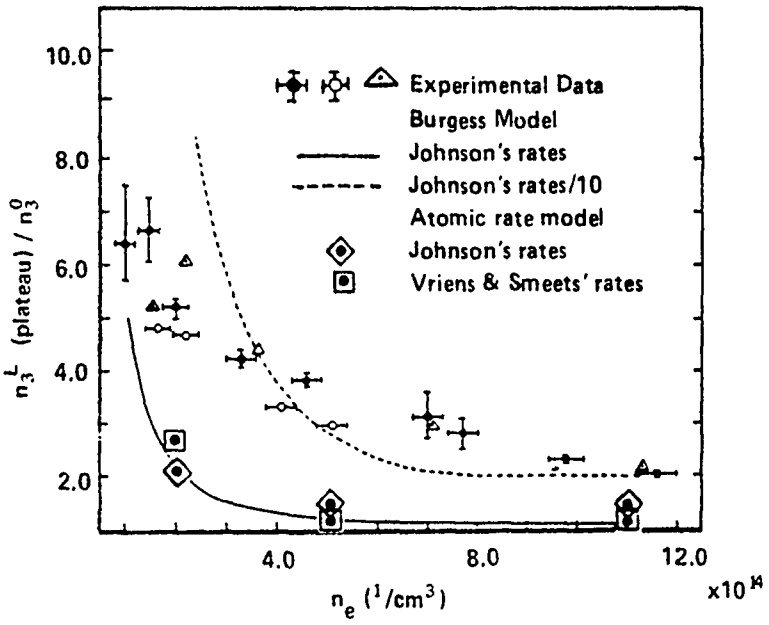

Figure 5.5: Fluorescence Plateau Ratio Comparisons $n_3^L(plateau)/n_3^0$

5.3.3 Decay Rate of Fluorescence Peak

The effect of using Vriens and Smeets' rates on the decay rate of the Hα fluorescence peak was much more encouraging. The theoretical decay rates given by Burgess, *et al.* (1980), for the "appropriate eigenvalue controlling the decay", were much larger than the experimentally obtained rates - from eight times faster than the actual rate early in the recombination, to double the actual rate late in the recombination. (See Figure 5.6.) Using Johnson's

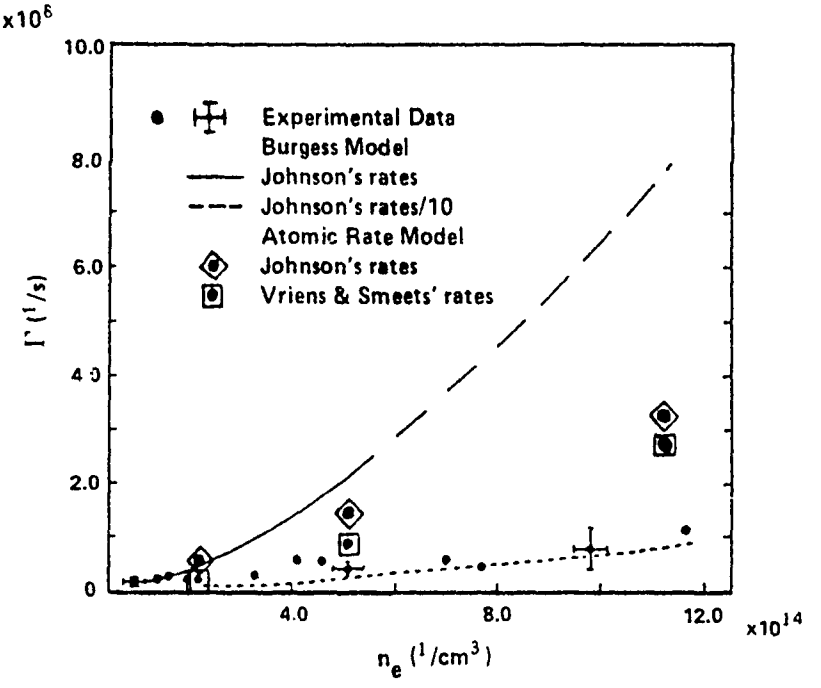

Figure 5.6: Fluorescence Decay Rate Comparisons

rates in the ARM model reduced these discrepancies somewhat, to a factor of 3.1 at 30 μs and 1.5 at 50 μs. Using Vriens and Smeets' rates in this model further reduced the discrepancies, to a factor of 1.8 at 30 μs and 0.9 at 50 μs (*i.e.* the rate at 50 μs was actually slower than the experimental rate).

Although the decay rates obtained by using Johnson's collisional rates in the ARM model differed greatly from the theoretical decay rates given by Burgess, *et al.* (1980), the comparison is not entirely valid. The decay rates

for the current model were obtained by allowing the populations to relax to their plateau values. However, the rates quoted by Burgess were obtained theoretically by determining the "appropriate eigenvalue controlling the decay". In the current model, the "appropriate eigenvalue" varied by a factor of over 10 during the course of the fluorescence decay to the plateau (which occurred in less than 100 ns). Thus, it does not appear that too much significance should be attached to the discrepancy between the decay rate of the fluorescence peak in the current model and the theoretical values given by Burgess.

5.4 Summary of Model Validation

As described in the previous sections, using Johnson's rates in the atomic rate equation model (ARM), nearly all of the predictions (many of which are erroneous) of the collisional-radiative model of Burgess, *et al.* (1980), were reproduced. However, both of these models (which considered only atomic hydrogen, H^+, and electrons) produced results which differred significantly from the experimental observations. Replacing Johnson's collisional rates with those of Vriens and Smeets had a generally positive effect, though there were isolated instances in which the agreement with the experiment was worsened.

Thus, using the same assumptions, rates, and initial conditions as those of Burgess *et al.*, the atomic rate equation model which was developed essentially reproduced their theoretical results. However, this model gave results which were significantly different from the experimental results:

- The initial (quasi steady state) $n = 2$ population was much lower than the experimental value at early times (30 - 40 μs).
- The peak ratio $(n_3^L(peak)/n_3^0)$ was higher than the experimental value at all times - slightly high at early times, but very high at late times.
- The plateau ratio$(n_3^L(plateau)/n_3^0)$ was lower than the experimental value at all times, but especially at late times.
- The rate of decay from the peak was too fast at all times - extremely fast at early times and slightly fast at late times.

time (μs)		$n_e(\text{cm}^{-3})$ $\times 10^{14}$	$n_1^0(\text{cm}^{-3})$ $\times 10^{16}$	$n_2^0(\text{cm}^{-3})$ $\times 10^{11}$	$\frac{n_3^L(peak)}{n_3^0}$	$\frac{n_2^0}{n_3^0}$	$\frac{n_3^L(plat)}{n_3^0}$	$\Gamma(\text{s}^{-1})$ $\times 10^7$
30	**E**	**11.**	**-**	**34.0**	**3.00**	**-**	**2.00**	**9.5**
	B	11.	2.60	2.10	4.00	-	1.10	75.
	ARM_J	11.	2.60	2.11	3.40	5.89	1.06	31.
	ARM_VS	11.	2.60	2.61	4.63	7.20	1.06	28.
40	**E**	**5.1**	**-**	**13.5**	**7.30**	**-**	**3.60**	**4.9**
	B	5.1	2.60	2.15	7.30	-	1.20	20.
	ARM_J	5.1	2.60	2.45	7.50	11.5	1.19	16.
	ARM_VS	5.1	2.60	3.64	11.3	16.9	1.24	9.8
50	**E**	**2.2**	**-**	**3.00**	**12.0**	**-**	**5.00**	**2.3**
	B	2.2	2.60	3.00	19.0	-	2.05	5.0
	ARM_J	2.2	2.60	2.95	19.0	28.1	1.90	4.5
	ARM_VS	2.2	2.60	4.27	31.0	44.9	2.92	2.5

E-experiment B-Burgess model
ARM_J-atomic rate equation model using Johnson's rates
ARM_VS-atomic rate equation model using Vriens and Smeets' rates

Table 5.1: Comparison of Experiment, Burgess Model, and Atomic Rate Equation Model

The use of Vriens and Smeets' rates in the atomic rate equation model had a generally positive impact:

- The $n = 2$ population in the unperturbed plasma was increased (improved).
- The peak ratio was increased (worsened).
- The plateau ratio was increased (improved).
- The peak decay rate was decreased (improved).

Bibliography

Burgess D D, Myerscough V P, Skinner C H, and Ward J M 1980 *Journal of Physics B: Atomic and Molecular Physics* **13** 1675-1701

Johnson L C 1972 *The Astrophysical Journal* **174** 227-36

Vriens L and Smeets A H M 1980 *Physical Review* **22** 940

Chapter 6

Plasma Behavior Using an Extended Rate Equation Model

6.1 Unperturbed Plasma Behavior

With the addition of other species (H^-, H_2, H_2^+, H_3^+) and processes to the atomic rate equation model, it was possible to sustain $n = 2$ and $n = 3$ populations at the higher quasi steady state levels observed (or deduced) experimentally and to model the decay of the electron density. The $n = 2$ and $n = 3$ populations could be sustained for several tenths of microseconds by appropriately choosing the initial values for these additional species. In addition, the experimentally observed exponential decay of the electron density was essentially reproduced for 70 μs after initiation of the plas ... Although the importance of additional species was addressed by Burgess, *et al.* (1980), they discounted their impact on the basis of their theoretically low LTE concentrations. However, no measurements were reported which confirmed the existence of such LTE populations for these species.

This extended rate equation model (ERM) demonstrated that the $n = 2$ and $n = 3$ level populations could be maintained at their elevated quasi steady state levels by simply using concentrations for H^-, H_2, H_2^+, and H_3^+ which are somewhat above their LTE values. For example, at 30 μs the H^- population required was approximately 1000 times greater than the LTE value, but only 1% of the measured electron density. Also at 30 μs, the H_2

population required was approximately 3000 times the LTE value, though less than 5% of the total neutral density at that time. Although the concentrations of the molecular ions, H_2^+ and H_3^+, were elevated to approximately 15 times their LTE values at 30 μs, their combined concentrations were less than .01% of the electron density and an even smaller percentage of the neutral density. By 50 μs the discrepancy was much less pronounced: the quasi steady state populations required of these additional species, in order to reproduce the experimental observations, were only slightly above their predicted LTE values. Although the concentrations of H^-, H_2, H_2^+, and H_3^+ required to sustain the elevated $n = 2$ and $n = 3$ populations are above their LTE values, they are such small fractions of the total concentrations in the plasma that their presence would not have been immediately apparent in the experimental investigations conducted. Thus, it seems possible that such species could actually have been present in the experimental plasma in the required concentrations.

The impact of including these "extra" species and their associated processes was investigated in some detail. The long-term effect of each process was determined by "turning off" individual processes and numerically "observing" the effect on the quasi steady state populations and on the long-term population changes. The effects of the most significant of these processes are described in the following sections.

6.1.1 Mutual Neutralization of H^+ and H^-

If the mutual neutralization of H^+ and H^- was not included in the model, the initial $n = 2$ population could not be maintained beyond .01 μs (10 ns), while the $n = 3$ population could not be sustained for even 1 ns. (See Figure 6.1.) By .1 μs, both $n = 2$ and $n = 3$ level populations had decreased to approximately the same values as for the Burgess model. Without the mutual neutralization of H^+ and H^- to deplete the H^- population, the H^- was nearly doubled by the dissociative attachment of H_2 before the inverse processes of associative detachment and collisional detachment, by both electrons and atomic hydrogen, depleted the H^-.

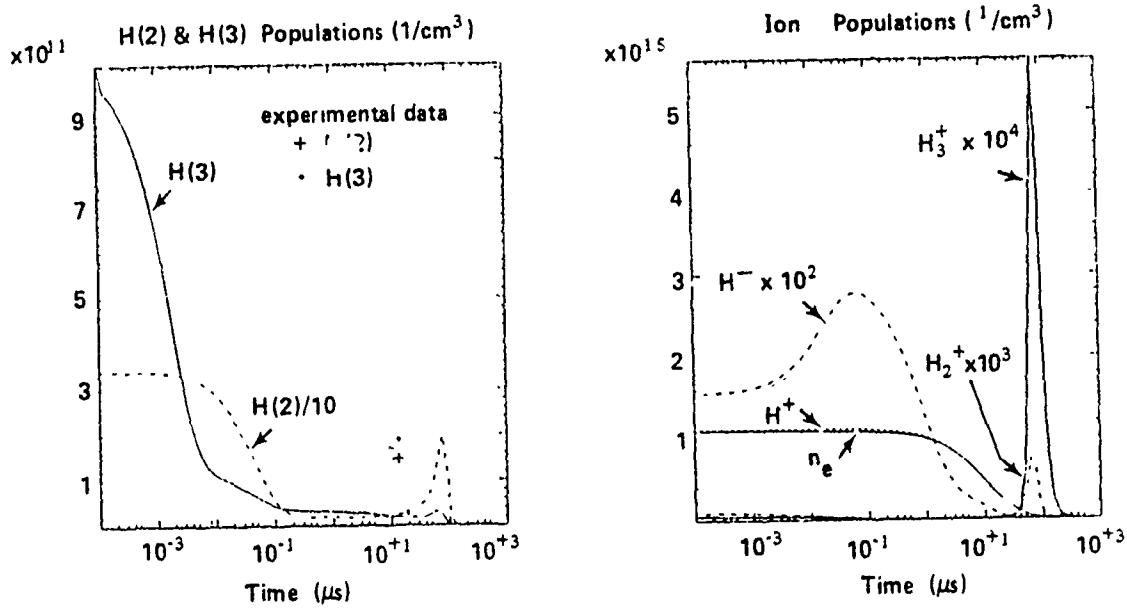

Figure 6.1: Population Profiles with No Mutual Neutralization

6.1.2 Radiation Trapping

The quasi steady state populations of the excited states of atomic hydrogen were also altered by the extent of the radiation trapping which was included. If it was assumed that the Lyman series radiation was completely trapped and no other emissions were trapped, the $n = 2$ population was inflated while the other excited atomic hydrogen level populations were decreased, as expected. (See Figure 6.2.) The current model treated these excited states much more equitably, recalculating the optical depth for each spontaneous transition at each time step. The impact can be seen by comparing

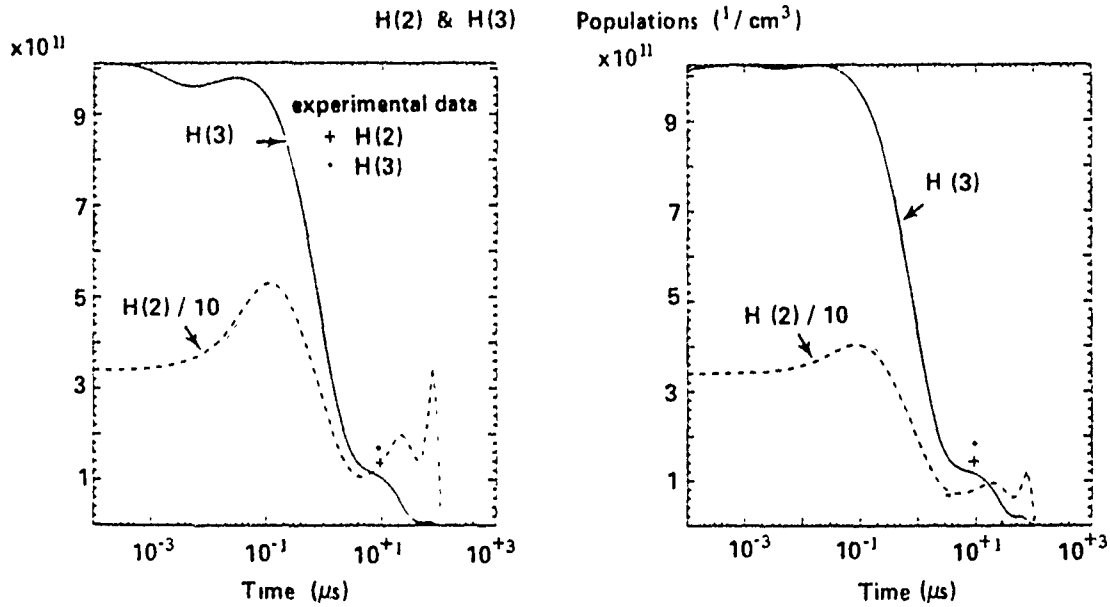

Figure 6.2: The Impact of Radiation Trapping (30 μs): a) Complete Trapping of Lyman Series b) Partial Trapping of all Spontaneous Transitions

the results shown in Figure 6.2, which is for an initial time of 30 μs. The augmentation of the $n = 2$ population which resulted from assuming that the Lyman radiation was completely trapped was especially apparent after 10 μs (40 μs after plasma initiation). The recombination of H^+ initiates a cascade through the excited states of H. However, completely trapping the Lyman radiation produced a bottleneck in the $n = 2$ level, as shown

by the peak at 20 μs. The second peak, at approximately 70 μs, was also due to the Lyman trapping bottleneck. In this instance, however, the influx into the $n = 2$ level was due to the dissociative recombination of H_3^+, which preferentially populates the $n = 2$ level. The increase in dissociative recombination of H_3^+ was a result of the increase in H_3^+ and (especially) the decreasing temperature of the plasma. Although the increase in H_3^+ was due to an increase in H_2 as the plasma cooled and H_2 diffused back in from the walls, it was, again, primarily due to the decrease in temperature, which greatly increased the proton exchange reaction rate

$$H_2^+ + H_2 \Longrightarrow H_3^+ + H \ ,$$

the primary mechanism for H_3^+ production at these temperatures (below .5 eV).

6.1.3 Ground State Population of Atomic Hydrogen

The quasi steady state populations of the excited states of atomic hydrogen also proved to be more sensitive to the value chosen for the atomic hydrogen ground state population than had been suspected by Burgess, *et al.* (1980). They claimed that the ground state was essentially decoupled from the other atomic hydrogen levels for electron temperatures between one and several tenths of an eV and electron densities from 10^{14} to 10^{15} $1/cm^3$. Under these plasma conditions, and with only atomic species present, they assumed that the $n = 3$ and $n = 4$ level populations would "...be determined primarily by collisional processes involving higher levels (and via them the continuum) ...".

However, with the inclusion of H_2 and H^-, and the processes of dissociative attachment and its inverse,

$$e^- + H_2(v*) \Longleftrightarrow H + H^- \ ,$$

the atomic hydrogen ground state population was found to be more significant than previously expected. The balance between the forward and reverse rates for these processes is very sensitive to the species' populations. In addition, the H^- population is very strongly coupled to that of H(3) via mutual neutralization. Thus, variations in the H(1) population were found to have immediate effects on the H(3) population via the intermediary of

H^-. For example, an increased value for H(1) shifted the balance in favor of associative detachment, decreasing the H^- population and thereby decreasing the H(3) population. As shown in Figure 6.3, increasing the ground state population by a factor of 2.6 caused the quasi steady state $n = 3$ population to decrease by a factor of 1.5. (The impact on the H(2) population was not nearly as pronounced since H^- preferentially populates the $n = 3$ state rather than the $n = 2$ state.) Thus, it was possible to support the elevated atomic hydrogen populations experimentally observed by using a reduced ground state population. This effect substantiated the contention by Jones (1980) that a large fraction of the hydrogen in such plasmas may be temporarilly atached to the walls.

These variations in the initial concentrations of the atomic hydrogen ground state also had a significant impact on the long term decay of the electron concentration. In particular, in going from an initial ground state population of 2.6×10^{16} $1/cm^3$ to 1.0×10^{16} $1/cm^3$, the decay of the electron density went from a "diffusive" decay, in which the log of the density decreases linearly with time, to a recombinative decay, in which the decay is faster at higher electron densities. (See Figure 6.4.) With a lower initial density of the atomic hydrogen, the equilibrium electron density would be below the initial value for the electron density. In this case,then, the electron density decays initially by recombination and later decays by ambipolar diffusion. However, with a higher initial density of the atomic hydrogen, the equilibrium electron density would be well above the initial value for the electron density. As a consequence, the electron density decays only by diffusion. The rates of diffusive decay are not the same in the two cases, however. With a lower concentration of atomic hydrogen (the primary constituent of the plasma), the ambipolar diffusion rate (and the neutral diffusion rate) is increased, as may be seen in Figure 6.4 by comparing the slopes of the electron decay curves for late times. To reproduce the observed electron decay between 30 and 50 μs after initiation of the plasma-forming pinch, it was found that the atomic hydrogen concentration should be approximately 1.35×10^{16} $1/cm^3$.

6.1.4 Ambipolar Diffusion

In order for the ground state population of atomic hydrogen to have such a long-term effect on the electron decay, however, it was essential for the

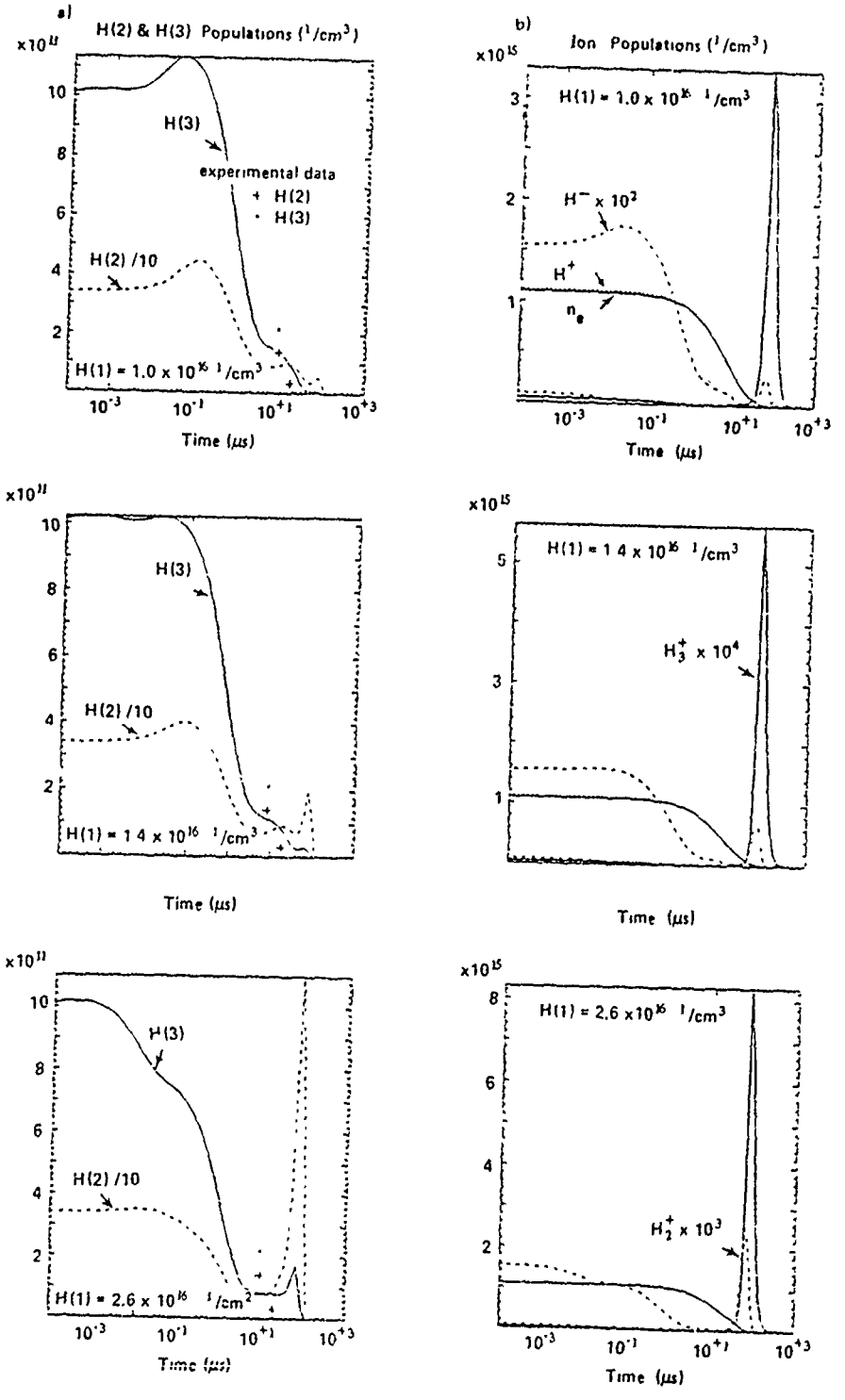

Figure 6.3: The Impact of the Ground State Population of Atomic Hydrogen

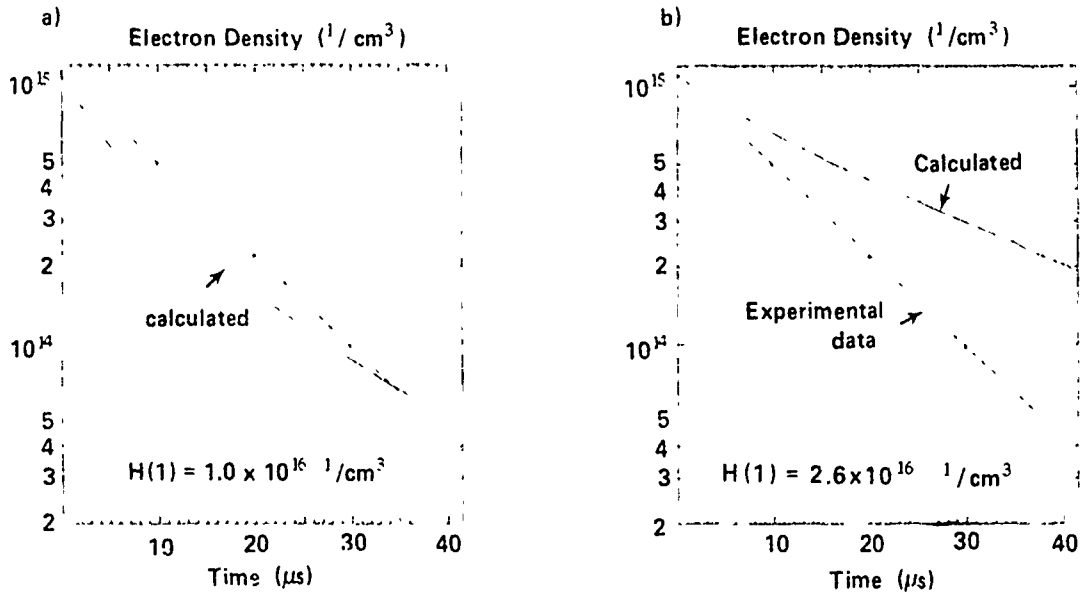

Figure 6.4: The Impact of the Ground State Population of Atomic Hydrogen on the Electron Decay

process of ambipolar diffusion to be included in the model. Without this diffusion of the ionized species, the electron decay was much too slow, as shown in Figure 6.5 for an initial time of 30 μs. Using theoretical values

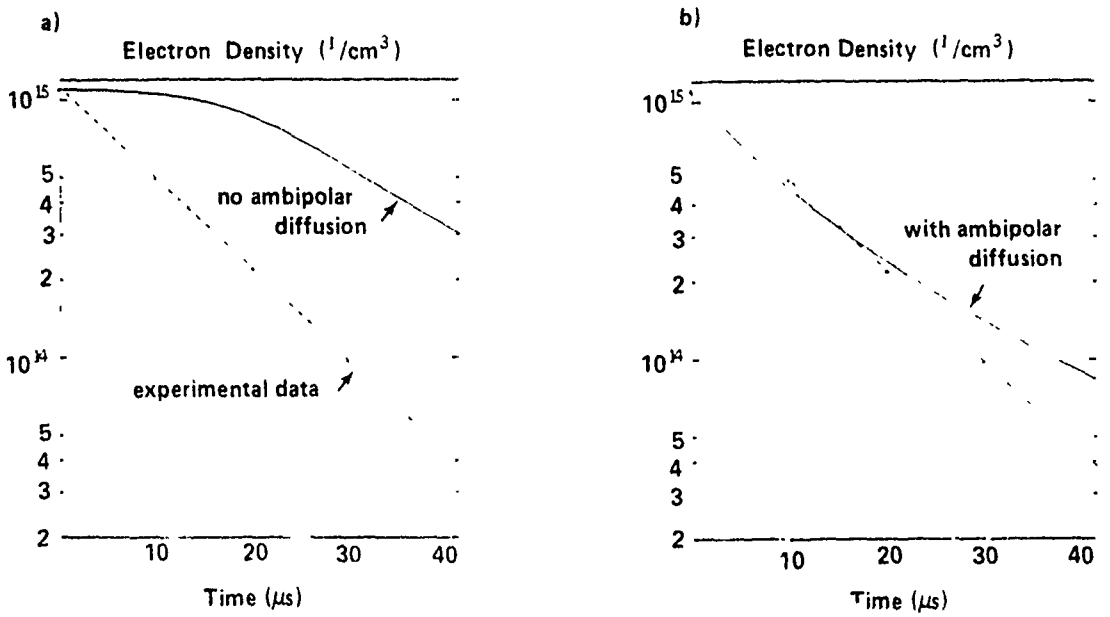

Figure 6.5: Electron Decay: Solid Line, No Ambipolar Diffusion; Dashed Line, Experimental Measurements

for the mobility of H^-, H^+, H_2^+, and H_3^+ in H and extrapolations of the mobilities for these ions in H_2 (see Appendix D), the ambipolar diffusion rates for these ions in a mixture of H and H_2 were estimated. (However, using such **theoretical** mobilities and extrapolating them to a **molecular** gas may be an important source of error in this model.) Even with the inclusion of this diffusion, however, the calculated electron decay rates, for ground state populations between 1.0×10^{16} 1/cm^3 and 2.6×10^{16} 1/cm^3, were still slower than those observed experimentally. By increasing this diffusion rate by a factor of ten, however, it was found that the electron decay rate could be approximately reproduced by choosing an initial atomic hydrogen ground state population of 1.4×10^{16} 1/cm^3 (at 30 μs). (As described previously, Jones (1982) presented evidence to suggest that the atomic hydrogen population in such plasmas is reduced to similar levels.)

Although the electron density was observed to decay exponentially by Burgess, *et al.* (1980), a similar experiment conducted subsequently by Nightingale and Burgess (1983) showed that the electron density in a hydrogen z-pinch plasma fluctuated by at least 15% for times less than 50 μs after plasma initiation. (See Figure C.4 in Appendix C.) They attributed these fluctuations to the existence of cylindrical acoustic waves caused by the initial z-pinch. These radial density fluctuations decreased in magnitude and increased in wavelength with time, indicating that the higher order radial modes damped out more quickly.

The ambipolar diffusion in the plasma was modeled assuming that the ion density varied radially proportional to the zeroth-order Bessel function. If the faster, higher-order modes had been considered, the total ambipolar diffusion rate would have been appreciably faster, particularly for times less than 50 μs after pinch initiation. Thus, increasing the ambipolar diffusion rate used in the ERM model by a factor of ten may actually be a more accurate assessment of the actual diffusion rate in the plasma.

6.1.5 Dissociative Attachment

Deleting the process of dissociative attachment, which is the primary source of H^- in this plasma, had both short and long term effects on the plasma. The drastic drop in the rate at which H− was resupplied had an immediate (within 10 ns) effect on the excited states of atomic hydrogen. Once the initial concentration of H^- was dissipated, the concentrations of the $n = 2$ and $n = 3$ (especially) levels dropped precipitously: with no H^-, mutual neutralization of H^+ and H^- could not keep these excited state populations elevated. The long term effect of deleting the process of dissociative attachment was to break one of the important mechanisms by which molecular hydrogen is transformed into atomic hydrogen. As shown in Figure 6.6, with no dissociative attachment, the atomic hydrogen population did not increase as quickly as usual. The resulting reduction in the atomic ground state population had the same effect on the electron decay as described previously. That is, the electron density decayed more quickly at first (by recombination) and then decayed more slowly as the role of diffusion became more important. Thus, with no dissociative attachment, the atomic hydrogen density was smaller and the ambipolar diffusion was more rapid, improving the agreement with the experimentally measured electron de-

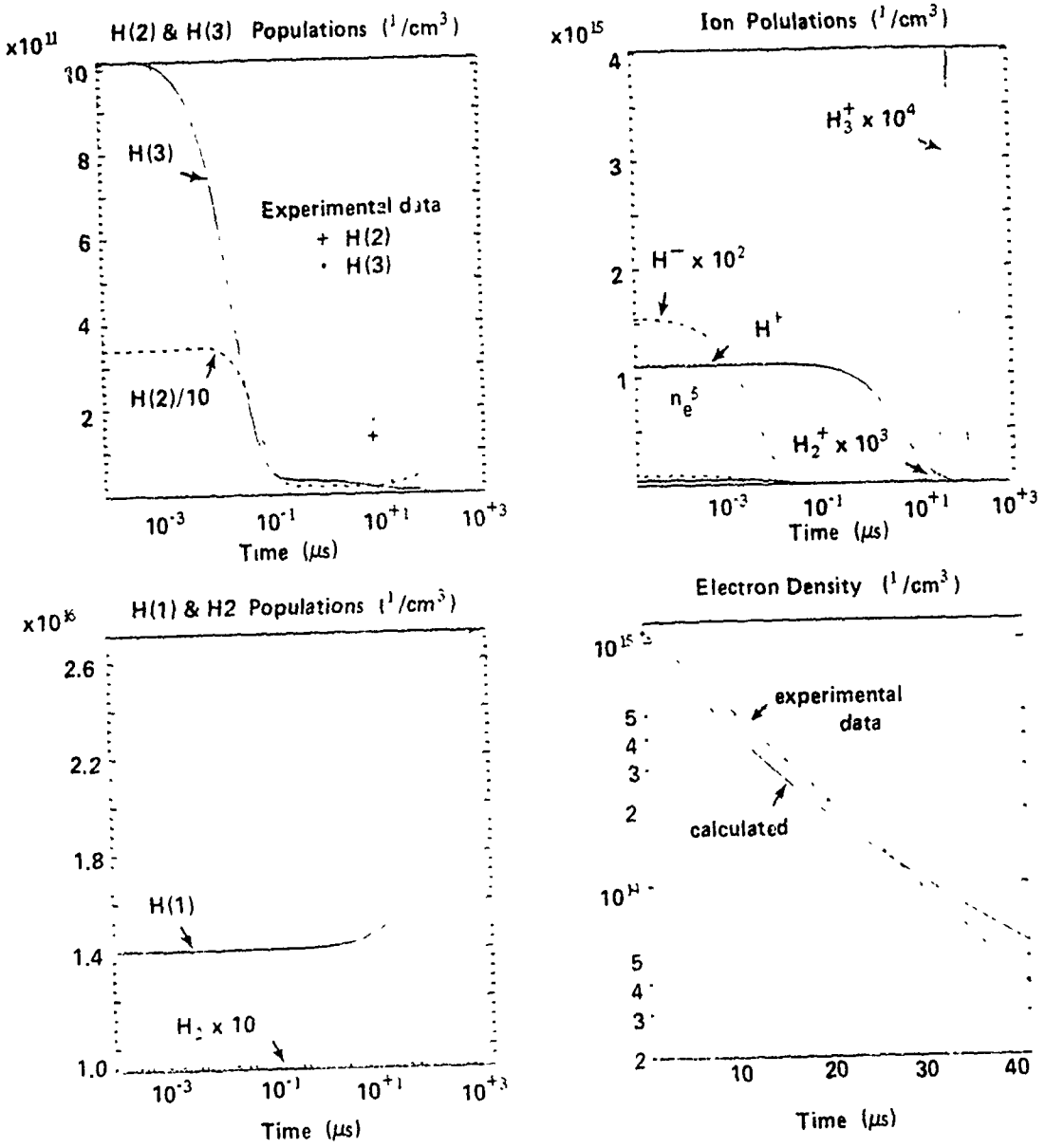

Figure 6.6: Species Populations with No Dissociative Attachment (ERM Model, Initial Time 30 μs): a) H(2) and H(3); b) H^+, H^-, H_2^+, and H_3^+; c) H(1) and H_2 d) n_e

cay. However, this marginal improvement in the agreement with the actual electron decay was more than offset by the disastrous effect on the excited atomic hydrogen populations. Thus, dissociative attachment was found to be a critical process in maintaining the atomic hydrogen at the elevated levels which were observed experimentally.

6.1.6 Non-Maxwellian Electrons

In response to the suggestions, by Burgess *et al.* (1980) and Lee *et al.* (1983), that the electron distribution in this plasma could be significantly non-Maxwellian, a bi-Maxwellian temperature distribution was included in the current model. Based on the work by Lee *et al.*, it was assumed that the dominant "cool" portion followed the experimentally observed electron temperature, while a "hot" portion was added for times greater than 38 μs after the plasma-forming pinch. Although the concentration of hot electrons added was relatively small compared to the total concentration of electrons, they did constitute a significant increase over the normal Maxwell-Boltzmann concentration of electrons at these energies. As shown in Figure 6.7, these hot electrons increased the rates for recombination of H^+ and for de-excitation of excited atomic hydrogen. In addition, the hot electrons reduced the rates of dissociative recombination of both H_3^+ and H_2^+, reducing the late peaks in H(2) and H(3) correspondingly. Indeed, without these processes, there would be no late peaks in H(2) and H(3). The effect of the hot electrons was most apparent at late times, as shown in Figure 6.8, for an initial time of 50 μs. Thus, a miniscule population of hot electrons (at 30 μs: 5.3×10^5 1/cm^3 out of 2.2×10^{14} 1/cm^3, at 6.1 eV) very effectively quenched the excited states of atomic hydrogen, improving the agreement with the experimental results, and increased the rate at which the electrons decayed. Although the rate of electron decay was still not as rapid as in the experiment, it could be increased by simply increasing the time constant for the exponential decay of the hot electron fraction from 1.25 μs to 1.7 μs. Although such an increase in the hot fraction improved the model's agreement with the observed electron decay, it also prematurely reduced the elevated quasi steady state atomic hydrogen populations, as shown in Figure 6.9.

Although the bi-Maxwellian model of the growth of a hot non-Maxwellian component to the electron distribution was admittedly quite crude, it did

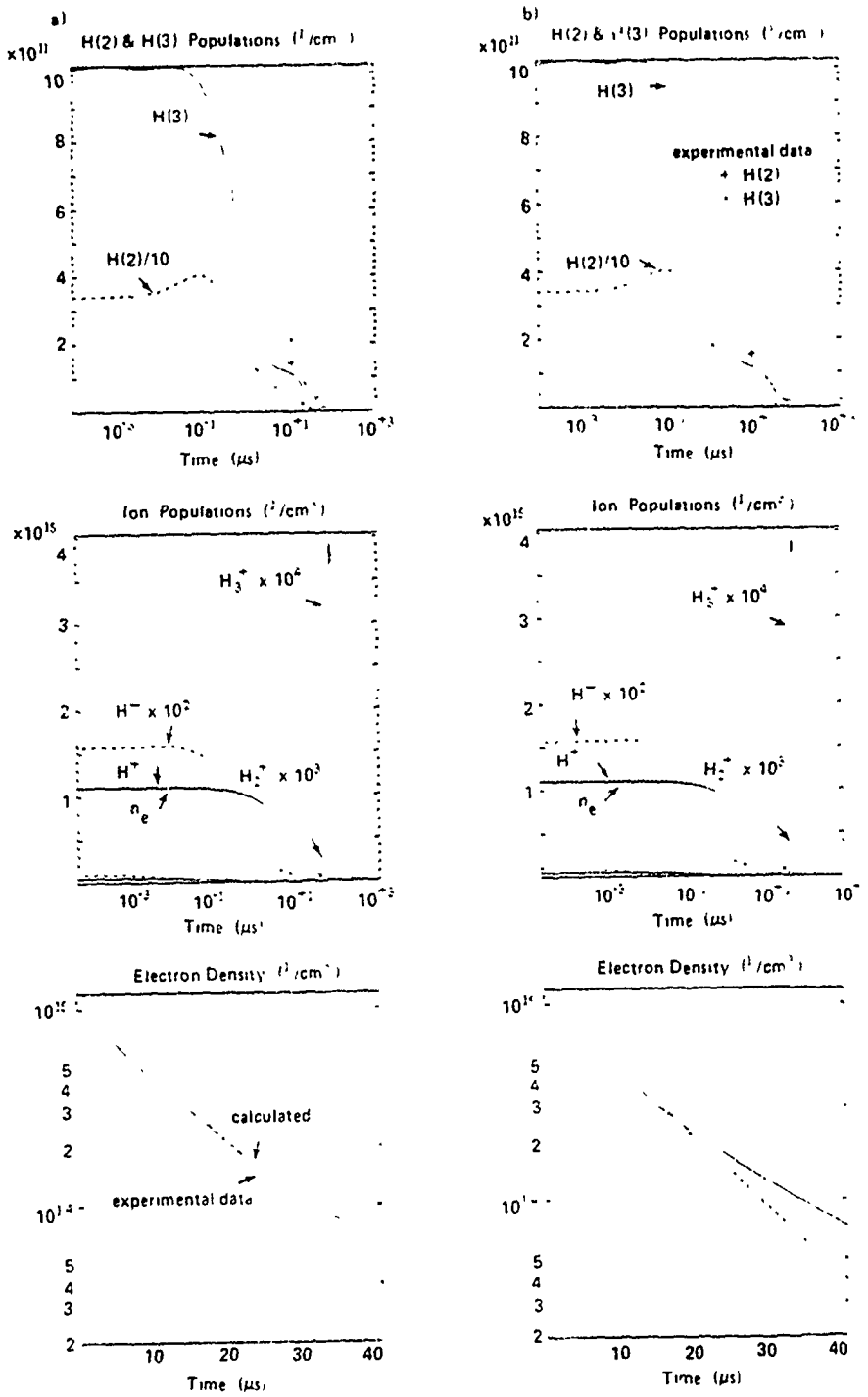

Figure 6.7: Species Populations (ERM Model, Initial Time 30 μs): a) No Hot Electrons b) With Hot Electrons

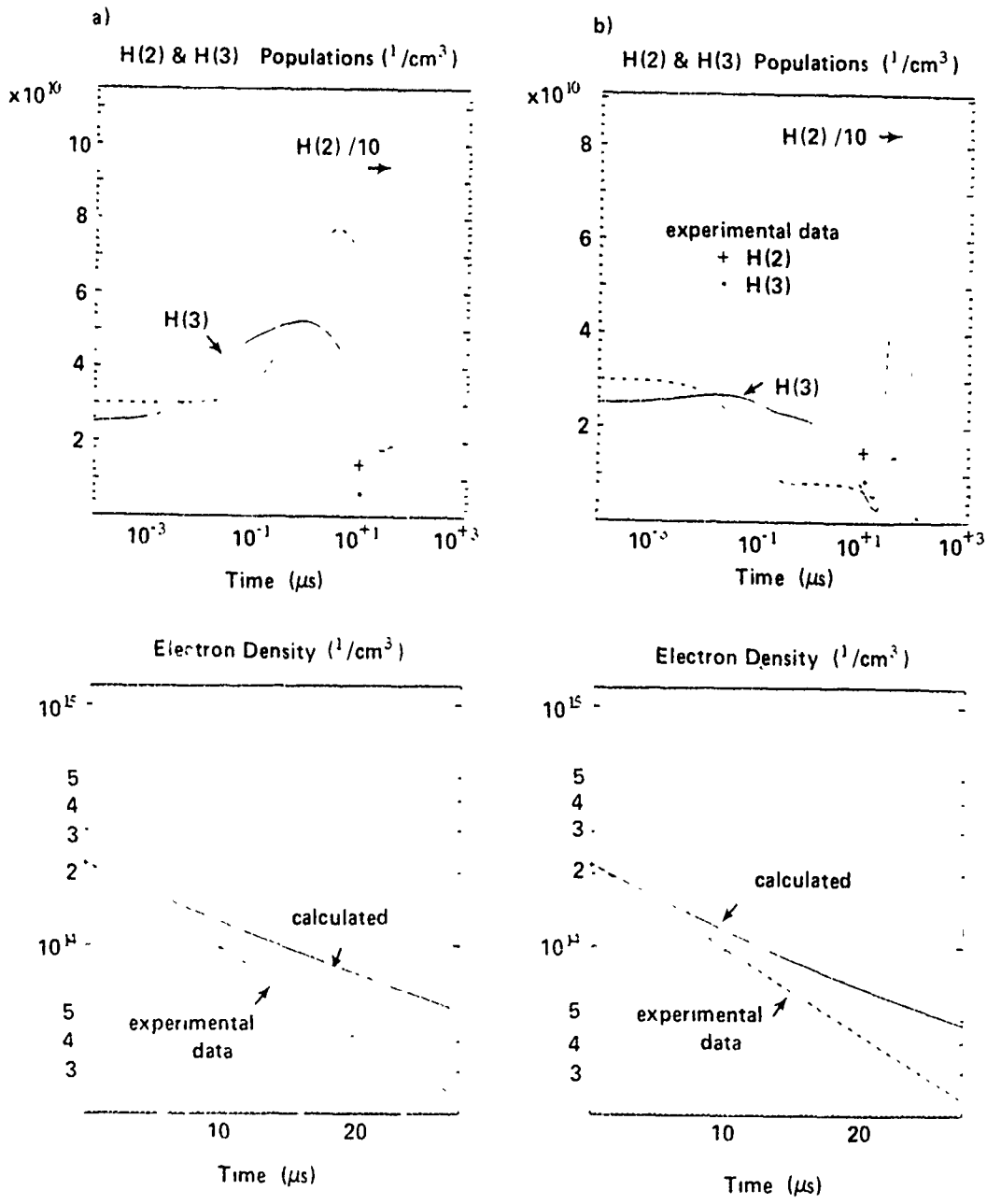

Figure 6.8: Species Populations (ERM Model, Initial Time 50 μs): a) No Hot Electrons b) With Hot Electrons

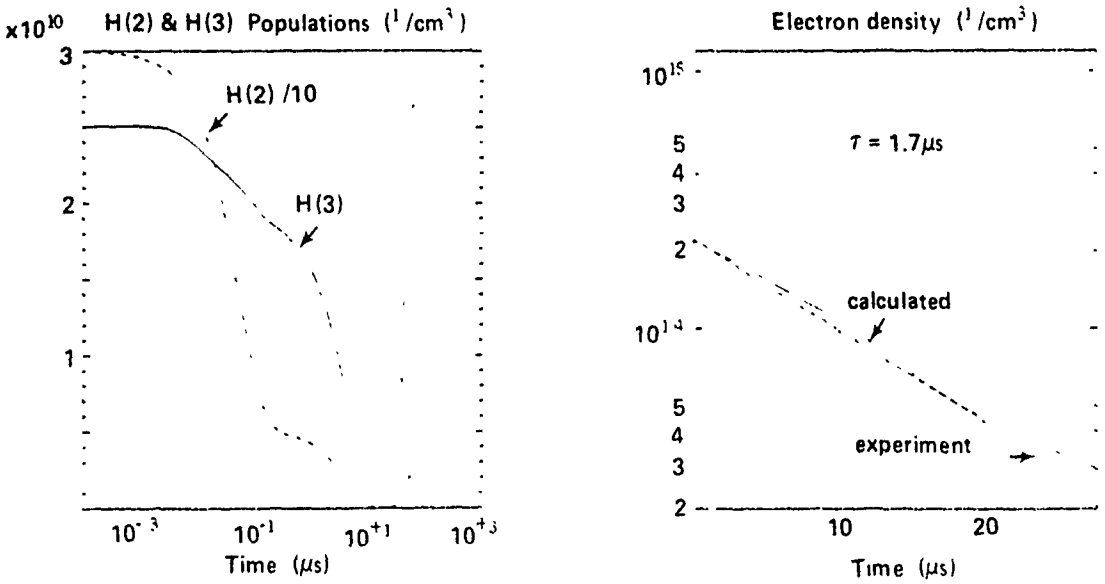

Figure 6.9: Species Populations with Increased Hot Electron Fraction (ERM Model, Initial Time 50 μs)

produce effects in general agreement with the experimental observations. The hot electrons did cause the electron density to decrease at a rate which was faster and thus more comparable to that observed. (However, as mentioned previously, there is evidence to suggest that radial acoustic oscillations may have actually caused large fluctuations in the electron density for times less than 80 μs.) In addition, it was clear that the hot electrons had an important role in quenching the excited atomic hydrogen populations at late times. These results gave additional credence to the assertions by Lee *et al.* (1983) that the electron distribution in this plasma becomes non-Maxwellian as the plasma cools and recombines and traps the Lyman series of radiation.

6.1.7 Summary of Rate Equation Model of Unperturbed Plasma

The extended rate equation model was able to reproduce the general, long term behavior of the hydrogen plasma. Using experimentally observed values for the electron temperature (see Figure C.2 in Appendix C), the electron density decay was nearly identical to that observed experimentally. In addition, the calculated populations of the $n = 2$ and $n = 3$ levels of atomic hydrogen remained constant, for several tenths of microseconds. These initial, experimentally observed, populations, were maintained even though they were often above their theoretical LTE values. The key to maintaining these initially elevated populations was an elevated concentration of molecular hydrogen and a reduced concentration of atomic hydrogen. The H_2, in turn, supported elevated populations of H^-, H_2^+, and H_3^+. The reduction in atomic H allowed H^- production by dissociative attachment to proceed more quickly, supporting the excited atomic hydrogen levels via the process of mutual neutralization. While these heavy species relaxed toward LTE, however, the electron distribution apparently became non-Maxwellian as trapping of the Lyman series augmented the electron distribution near 10 eV. Therefore, in order to correctly model the long-term behavior of the plasma, a detailed kinetics model was required. Only then could the temporal development of the electron distribution, and its impact on the short-term plasma behavior under laser illumination, be investigated with real confidence. As a preliminary step, however, the effect of such laser illumination was first investigated using the extended rate equation model

of the plasma.

6.2 Plasma Behavior Under Laser Illumination

With the long-term plasma behavior relatively well represented by the extended rate equation model, the short-term response of the plasma to laser illumination was investigated. (While the simple atomic hydrogen model of Burgess, *et al.* (1980) used equilibrium populations for their initial conditions, the extended atomic/molecular model used quasi steady state populations which were not as long-lived.) As in the investigation of the Burgess model, the $n = 3$ peak enhancement ratio, the decay rate from this peak, and the fluorescence plateau ratio were considered. These three quantities indicated how well the model performed for progressively longer time periods: the peak ratios indicating how accurate the model was for very short times ($\leq$ 1 ns) and the plateau ratios performing a similar function for relatively long times($\lesssim$ 100 ns). The extended model was able to reproduce the experimentally-observed peak fluorescence ratios, while the calculated decay rates were, in general, about two times too large and the plateau ratios were less than a third of what they were experimentally observed to be.

6.2.1 Peak Enhancement Ratio

The ERM model essentially reproduced the peak fluorescence ratios observed experimentally. However, this could only be done by making the ratio of the initial populations of the $n = 2$ and $n = 3$ states (n_2^0/n_3^0) from 12 tc 30% greater than the ratios assumed by Burgess, *et al.* (They assumed that $n_2^0/n_3^0 \simeq n_3^L\ (peak)/n_3^0$.) The n_2^0/n_3^0 ratio was increased by 12% at 30 μs and by 30% at 50 μs. At 40 μs, the initial ratio was increased by only 5%. As a result, the calculated fluorescence peak ratio was 20% below the experimentally-observed value at that time. Thus, by simply increasing the initial $n = 2$ population, relative to the $n = 3$ population, the calculated fluorescence peak could be made to match the experimental peak. (These empirical changes were restricted so that the $n = 2$ populations used were

within the range of error in the experimental measurements by Burgess, *et al.*

The same effect was observed in the simpler ARM model, using the same assumptions of Burgess, *et al.* That is, using steady state populations for the $n = 2$ and $n = 3$ levels, the peak ratios $(n_3^L\ (peak)/n_3^0)$ obtained were only about 65% of the initial population ratios (n_2^0/n_3^0). In the extended atomic/molecular model (ERM), the calculated peak ratios were about 75% of the initial population ratios. However, the losses from the $n = 3$ state appeared to increase as the plasma cooled, decreasing the effective efficiency of the laser excitation from 82% at 30 μs to 73% at 50 μs. (It should also be noted that the laser flux was more effective at saturating the transition, at the peak in the fluorescence, for later times. That is, the ratio of n_3^L/n_2^L at the peak was 2.12 at 30 μs, 2.21 at 40 μs, and 2.23 at 50 μs, while the theoretical ratio should be $3^2/2^2 = 2.25$ for infinite laser power. For each initial time, however, this ratio approached 2.24 later in the laser pulse.) Thus, the assertion by Burgess, *et al*, that the peak fluorescence ratio $n_3^L\ (peak)/n_3^0$ "essentially represented" the initial population ratio (n_2^0/n_3^0) was not borne out by either the simple atomic hydrogen model (ARM) or by the extended atomic/molecular model (ERM).

6.2.2 Plateau Ratio

As with the simpler ARM model, the plateau ratios $n_3^L\ (plateau)/n_3^0$ calculated by the ERM model were always less than the experimentally-observed ratios. Both models produced about the same plateau ratios at 30 μs, in spite of the fact that the initial $n = 3$ population in the atomic/molecular model was 28 times that in the simple atomic model. At 50 μs, the plateau ratio in the simple model was nearly twice that in the extended model, though the initial $n = 3$ population in the extended model was only three times greater than that in the simple model. Thus, the additional species and processes had no effect on the plateau ratio at 30 μs and made the ratio even worse at 40 and 50 μs. The slight increase in the plateau ratio that Vriens and Smeets' generally lower collisional rates made (see Table 6.1) was more than compensated for by the increase in the net rate out of the $n = 3$ state due to the "extra" species included in the extended model.

In particular, the laser-initiated processes of photodetachment of H^- and photoionization of atoms in the $n = 3$ state contributed to the reduc-

tion in the plateau level. When photodetachment was deleted from the model, the plateau ratio was increased by a factor of nearly two. Similarly, then photoionization was deleted, the plateau ratio was also increased, but by a factor of only 5%. Thus, as predicted by Burgess *et al.* (1980), photoionization had only a minimal impact on the model's results. In contrast, photodetachment appeared to have too great an impact on the model.

6.2.3 Decay Rate

Using the ERM model, the rate of decay from the fluorescence peak was found to agree slightly better with the experimentally observed rate at 30 μs, while the agreement was slightly worse at 40 μs and much worse at 50 μs. (See Table 6.1.) As with the plateau ratio, the improvements made by using Vriens and Smeets' rates were more than compensated for by the increase in the net rate out of the $n = 3$ state due to the "extra" species included in the extended model.

time (μs)		$n_e(\text{cm}^{-3})$ $\times 10^{14}$	$n_1^0(\text{cm}^{-3})$ $\times 10^{16}$	$n_2^0(\text{cm}^{-3})$ $\times 10^{11}$	$\frac{n_3^L(peak)}{n_3^0}$	$\frac{n_2^0}{n_3^0}$	$\frac{n_3^L(plat)}{n_3^0}$	$\Gamma(\text{s}^{-1})$ $\times 10^7$
30	**E**	**11.**	-	**34.0**	**3.00**	-	**2.00**	**9.5**
	B	11.	2.60	2.10	4.00	-	1.10	75.
	ARM_{VS}	11.	2.60	2.61	4.63	7.20	1.06	28.
	ERM	11.	1.40	38.0	3.08	3.77	1.04	26.
40	**E**	**5.1**	-	**13.5**	**7.30**	-	**3.60**	**4.9**
	B	5.1	2.60	2.15	7.30	-	1.20	20.0
	ARM_{VS}	5.1	2.60	3.64	11.3	16.9	1.24	9.80
	ERM	5.1	1.67	13.5	5.83	7.70	1.07	11.6
50	**E**	**2.2**	-	**3.00**	**12.0**	-	**5.00**	**2.3**
	B	2.2	2.60	3.00	19.0	-	2.05	5.0
	ARM_{VS}	2.2	2.60	4.27	31.0	44.9	2.92	2.5
	ERM	2.2	1.70	4.60	11.6	15.9	1.29	5.5

E-experiment B-Burgess model
ARM_{VS}-atomic rate model
ERM-extended rate model

Table 6.1: Comparison of Experiment, Burgess Model, Atomic Rate Model, and Extended Rate Model

Bibliography

Burgess D D, Myerscough V P, Skinner C H, and Ward J M 1980 *Journal of Physics B: Atomic and Molecular Physics* **13** 1675-1701

Jones W M 1982 *Plasma Physics* **24** 361-368

Lee R W, Morgan W L, Whitten B L, and Kolbe G 19832 *Lawrence Livermore National Laboratory, CA* **UCRL**-88714

Nightingale M P S and Burgess D D 1983 *Journal of Physics B: Atomic and Molecular Physics* **16** 4101-4115

Chapter 7

Plasma Behavior Using the Kinetics Equation Model

7.1 Kinetics Equation Model

The effect of a non-Maxwellian electron energy distribution on the atomic hydrogen level and other species populations was investigated using a kinetics equation model (KM). In such a model, the electron energies are not assumed to be Maxwellian and the rate for any electron impact process is determined by using the energy-dependent cross-section for that process. The model which was used was patterned after a time-dependent Boltzmann equation solver initially developed by W. L. Morgan. (Morgan and Penetrante, 1990) In this approach, the time-dependent Boltzmann equation

$$\left(\frac{\partial}{\partial t} + \mathbf{v}\cdot\nabla_r + \frac{e\mathbf{E}}{m}\cdot\nabla_v\right) f(\mathbf{r},\mathbf{v},t) = \left(\frac{\partial f}{\partial t}\right)_{collisions}$$

is solved under the asumptions that the distribution function is spatially uniform and that it can be expressed in terms of a two-term spherical harmonic expansion.

$$f(\mathbf{v},t) = f_0(v) + \frac{\mathbf{v}}{v}\cdot\mathbf{f}_1(v)$$

In order to solve the Boltzmann equation numerically, the electron energy axis is divided into finite segments (energy bins), transforming a partial differential equation into a set of coupled ordinary differential equations at

each time step. At each of these time increments, rates for each microscopic process included in the model are calculated. Using these rates, along with rates for the macroscopic processes of neutral and ambipolar diffusion, the electron bin populations and heavy species concentrations are evolved forward in time using a combination of explicit and implicit methods.

The finite difference approach to solving the Boltzmann equation applied certain constraints on the maximum bin size and maximum allowed electron energy. In order for the finite difference scheme to be accurate, the electron energy bin size had to be small compared to the smallest energy change in any electron impact process and small compared to the energy dependence of each of the electron impact cross sections. In addition, normalization and conservation of electrons required that the allowed energy bins extend into the "tail" of the distribution and that the bin size be much less than the mean energy of the distribution. However, because the model includes electron-electron collisions, increasing the number of bins has a significant impact on the time required to complete a calculation. Thus, accuracy must be sacrificed to efficiency. For the low ($\leq$1 eV) "temperature" hydrogen plasma considered, these requirements were met by using a maximum electron energy of 15 eV and dividing that range into 50 electron bins, of .30 eV each. As described later in this chapter, increasing the number of bins to 75 in this 15 eV interval produced only a 10% increase in the H(3) population at .1 μs, but a 30% increase in the H_3^+ population at 60 μs.

7.2 Processes Included in the Kinetics Model

Rates for electron-impact processes were, in nearly all cases, calculated using energy-dependent cross-sections, while temperature-dependent rate coefficients were used to calculate the rates for collisions of heavy species and temperature-dependent mobilities were used to calculate the neutral and ambipolar diffusion rates. The electron-impact processes incorporated in the kinetics model were: momentum transfer collisions of electrons with other electrons, momentum transfer collisions of electrons with H and H^+, excitation/de-excitation and ionization of H, radiative recombination with H^+, three-body recombination with H^+, dissociative attachment of H_2, dissociative recombination with H_2^+ and H_3^+ and their inverses, electron-impact

detachment of H^- and its inverse, In addition, spontaneous emission and radiation trapping by H and laser-initiated photoionization of H and photodetachment of H^- were included in the model. The heavy species processes included were: mutual neutralization of H^- with H^+, H_2^+, and H_3^+, and their inverses; associative detachment of H^- by H impact; and collisional detachment by H impact on H^- and its inverse. The ambipolar diffusion of H^+, H^-, H_2^+, and H_3^+ to the walls and the diffusion of H and H_2 back into the plasma, from the walls, were also included, as in the rate equation model.

The electron-electron momentum transfer rates were obtained using the method given by Rockwood (1973), which involves obtaining $\partial f_0/\partial t$ by solving the Fokker-Planck equation using the Rosenbluth potentials. Momentum transfer collisions of electrons with H were modeled using the cross sections given by Morgan and Penetrante (1989), while momentum transfer collisions with H^+ made use of the analytic expression for the cross section given by Spitzer (1956). Vriens and Smeets' cross sections for electron impact excitations and ionizations of atomic hydrogen were used to model these processes. The inverse process of collisional (three-body) recombination was modeled using the corresponding ionization rate and invoking detailed balance to obtain the differential recombination cross section ($\sim$ cm^5) for producing electrons in each energy bin. (The relation between the forward and reverse cross sections is given by Shoub (1977).) The processes of dissociative recombination with H_2^+ and dissociative attachment of H_2 were modeled using the cross sections given by Janev, *et al.* (1989). Rates for the heavy species collisional processes and for the diffusion of both neutrals and ions were the same as those used in the extended rate equation model.

A more thorough description of the solution techniques used in solving the Boltzmann Equation may be found in the report by Morgan and Penetrante (1990).

7.3 Unperturbed Plasma Behavior Using the Kinetics Model

Quasi steady state atomic hydrogen populations could also be maintained in the kinetics model, though with slightly different concentrations of H^-, H_2,

H_2^+, and H_3^+ than in the rate model. In fact, it was found that quasi steady state populations could be maintained for about 0.1 μs, which was slightly longer than for the rate equation model. Depending upon the initial time, the heavy species populations required to produce such quasi steady state populations differed from those in the rate equation model by up to 50%. The cause of these differences in the required populations (and of a number of other anomalies) appeared to be the growth of a hot non-Maxwellian component to the electron distribution.

The temporal evolution of the electron distribution function in the kinetics model was nearly identical to that which was deduced by Lee *et al.* (1983) (Figure 2.2) from the experimental data of Burgess *et al.* (1980). The results of the kinetics model at representative times are shown in Figure 7.1. These numerical results were obtained with 50 electron bins between 0 and 15 eV.

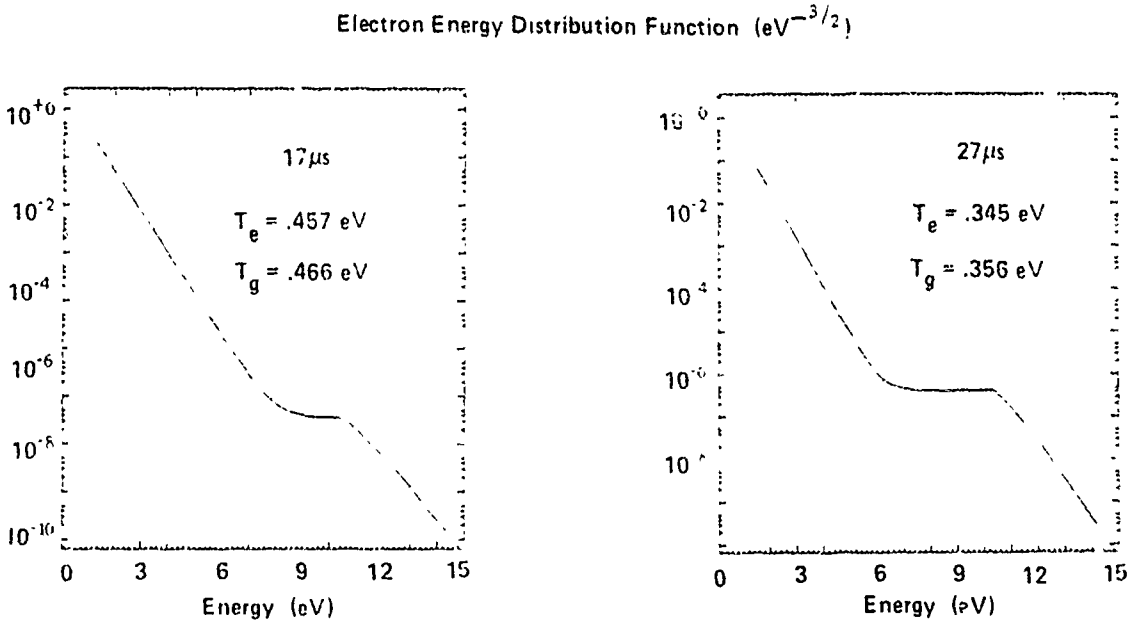

Figure 7.1: Temporal Evolution of Electron Distribution Function (Kinetics Model, Initial Time 30 μs)

The cause of the high energy bump in the distribution was found to

be the trapping of Lyman-series radiation, as had been suggested by Lee *et al.* (1983). A comparison of the kinetics results, with and without radiation trapping, is shown in Figure 7.2. Without trapping, the excited atomic hydrogen populations could not be sustained by the initial values used for H^-, H_2, H_2^+, and H_3^+. In addition, the trapping helped sustain the H^+ population by keeping the excited atomic state populations elevated. Comparing the distribution functions obtained with and without trapping, as shown in Figure 7.2, it can be seen that trapping increased the number of hot electrons which formed by a factor of several orders of magnitude.

Such non-Maxwellian distributions can also be the result of wave-particle interactions in the plasma. In that case, a "bump" at 10 eV could dbe the result of a plasma wave with a speed of approximately 1.9×10^8 cm/sec. As described in Appendix C, cylindrical plasma oscillations have been observed in similar experimental arrangements. (See Figure C.4.) With a tube radius of 2.35 cm and a wave period of approximately 16 μs, the speed of these waves was found to be only 3.0×10^5 cm/sec. Thus, it does not appear likely that the "bump" in the electron distribution is due to a wave-particle interaction. This conclusion appears to be well substantiated by the clear demonstration by the kinetics model that trapping of the Lyman-series radiation is the primary source of this phenomenon.

Although the total electron density was determined differently in the rate and kinetics models, they agreed with each other to within 3%, and with the experimentally observed density to within 6%, at 50 μs after plasma initiation. However, the density in the kinetics model decreased more slowly afterward, becoming 12% higher than the density in the rate model, and 35% higher than the measured density, by 60 μs after plasma initiation. In the rate model, the density of electrons was determined implicitly, by calculating the densities of the heavy species and simply requiring charge neutrality in the plasma. In the kinetics model, however, though the electron density was determined explicitly, with no requirement of charge neutrality, neutrality was actually preserved for over 100 μs in the numerical model. However, by 1 ms, inconsistencies within the model produced an electron density of 1.0×10^{10} 1/cm^3, and a proton density of only 2.4×10^6 1/cm^3. This discrepancy is simply a consequence of not requiring plasma neutrality at each time step, as was done in the various rate equation models. Although such inconsistencies also arose in the rate equation models, the problem was accentuated in the kinetics model be-

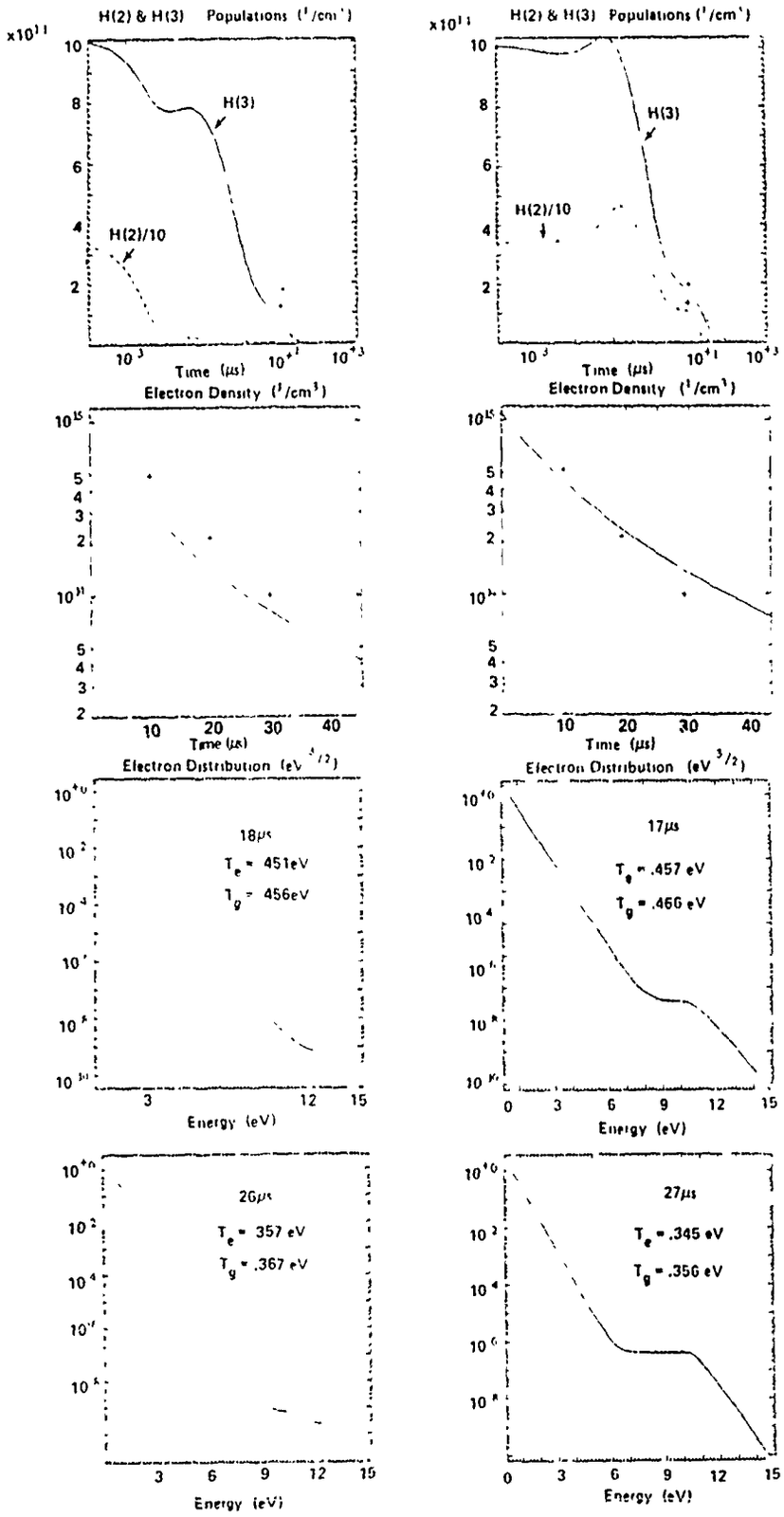

Figure 7.2: Kinetics Model (Initial Time 30 μs): a) No Radiation Trapping b) With Radiation Trapping

cause of the inaccuracies associated with using finite-sized electron energy bins. This discrepancy did not affect the model in the short term, however, since it arose only for times over ten times longer than those of interest in the present investigation.

Although the calculated electron distributions clearly exhibited the growth of a non-Maxwellian component, an approximate (effective) temperature was calculated for the electron distribution at each time step. It was found that the calculated electron temperature was always lower than the experimentally measured (gas) temperature at that time. As shown in Figure 7.2, the "effective" temperature of the electrons (T_e) decreased more quickly than the measured "gas" temperature (T_g) did, with a temperature that was 14% lower than the gas temperature by 130 μs after plasma initiation. In fact, the calculated electron temperature was decreased by 5% on the very first iteration at 30 μs. Thus, the total rates for the electron-impact processes in the kinetics model differed from those used in the rate models, which assumed that the electron and gas temperatures were identical to the measured gas temperature and that the electron energy distribution was Maxwellian.

With such differences in the electon-impact rates, it was not surprising that the long-term behavior of the excited atomic hydrogen states, H^+, H_2^+, and H_3^+ were different in the kinetics model than in the rate model. At late times, the peak in H_3^+ was reduced by a factor of over twenty and the H_2^+ peak was eliminated entirely, as can be seen in Figure 7.3. With these reductions in H_2^+ and H_3^+, the late surges in the $n = 2$ and $n = 3$ level populations were eliminated, though they did not decrease as quickly as with the bi-Maxwellian approximation of the hot electrons in the rate model.

The sensitivity of the kinetics model's results to the number of electron bins used was investigated by increasing the number of bins from 50 to 75. (With a maximum electron energy of 15 eV allowed by the model, this increase in bins corresponded to reducing the bin size from .3 to .2 eV. The electron density in each of these bins was assumed to be distributed uniformly with respect to energy. Thus, for a distribution which is approximately Maxwellian, the number of lower energy electrons in each bin is consistently under-represented, while the number of higher energy electrons in each bin is over-represented. Thus, a large bin size tends to artificially reduce the rate for any electron impact process with a cross sec-

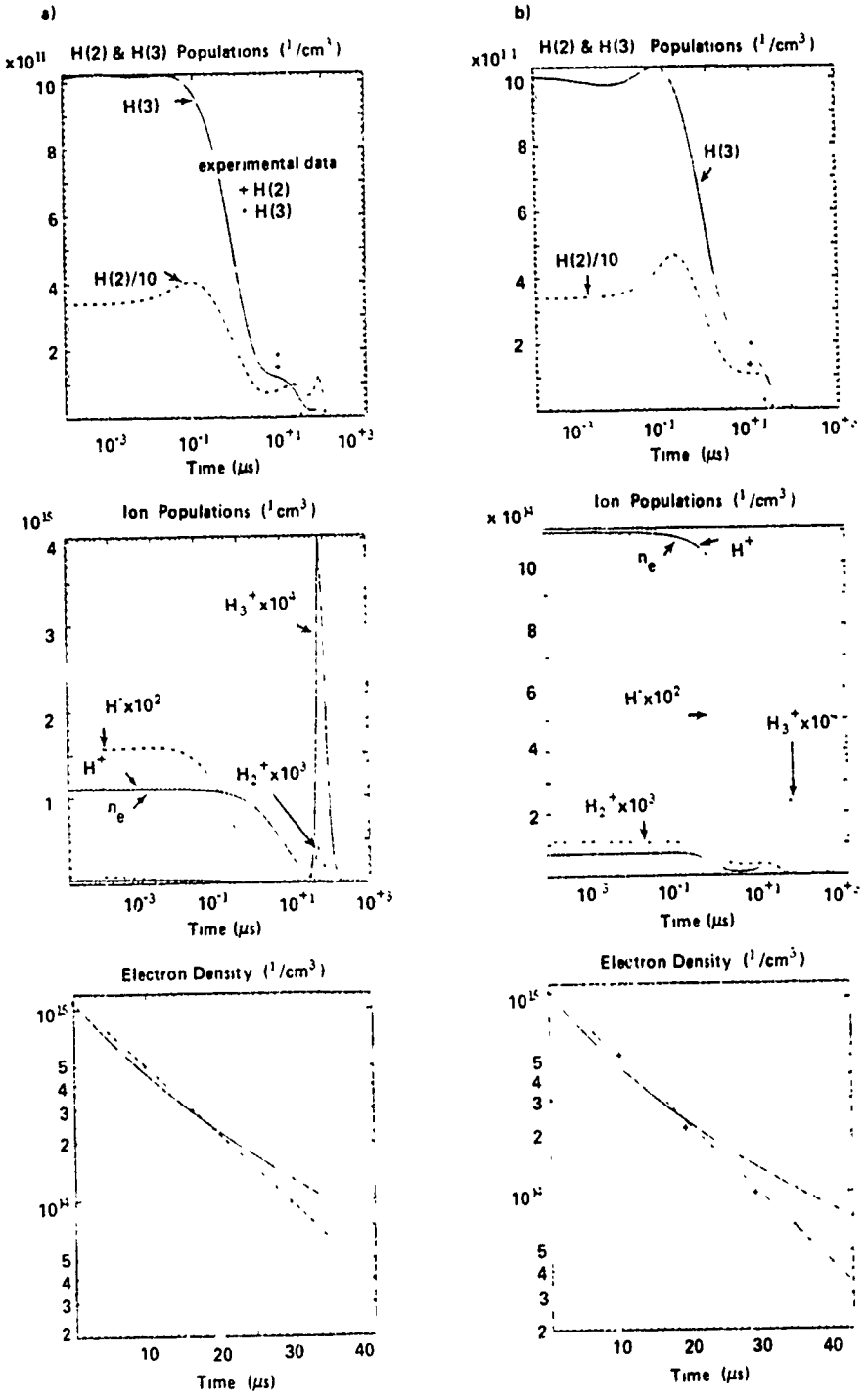

Figure 7.3: Comparison Between Rate Equation and Kinetics Models (Initial Time 30 μs): a) Rate Equation Model b) Kinetics Equation Model

tion which increases at lower energies. In particular, since the three-body collisional recombination cross section increases at lower electron energies, the rates into the excited atomic hydrogen states are reduced for larger bin sizes. This effect can be clearly seen by comparing the short-term $n = 2$ and $n = 3$ level populations obtained using 50 electron bins and 75 electron bins, as shown in Figure 7.4.

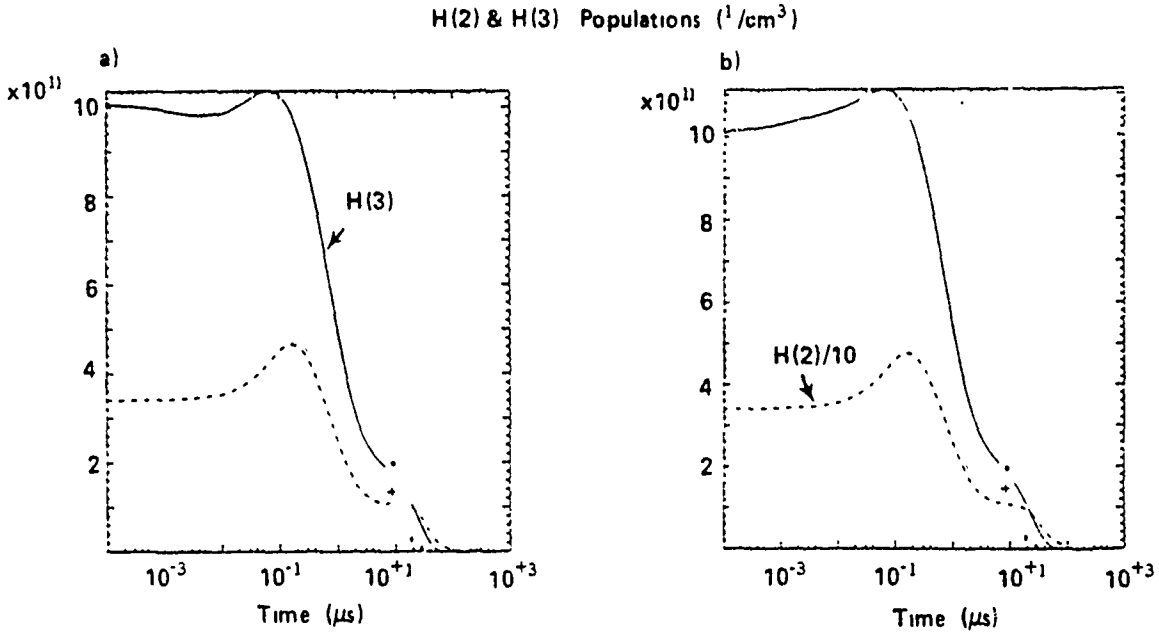

Figure 7.4: Comparison of Excited Atomic Hydrogen Populations for a) 50 Electron Bins b) 75 Electron Bins

For the same reason, the rates out of H^+ are reduced for larger bin sizes, keeping H^+ elevated. (The effect on H^+ is not as apparent as that on the excited atomic hydrogen states, however, because of the much larger concentration of the positive ion.) The smaller concentrations of excited atomic hydrogen also had an effect on the concentrations of the positive molecular ions. With smaller populations of the $n = 2$ and $n = 3$ states, the H_3^+ and H_2^+ populations, which are strongly coupled to these states, are also reduced with large electron bins. This effect can be seen in Figure 7.5, where it is clear that the late peak in H_3^+ is reduced with larger electron

bins.

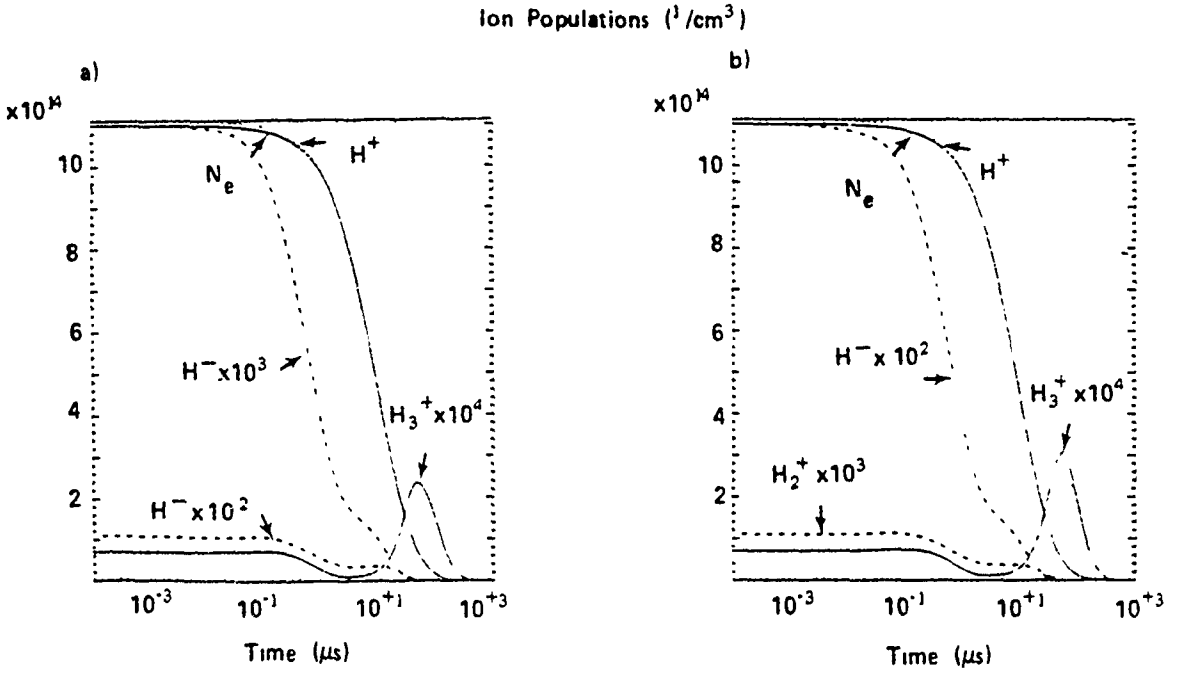

Figure 7.5: Comparison of Ionic Populations for a) 50 Electron Bins b) 75 Electron Bins

The discretization of the electron energy distribution also had an effect on the calculated effective temperature of the electrons. As described previously, it was assumed that the electrons were uniformly distributed with respect to energy within each bin, with the result that the number of lower energy electrons in each bin was consistently under-represented, while the number of higher energy electrons was over-represented. In addition, if the energy gain or loss in a process was less than the energy bin width, it was assumed that only those electrons within that energy increment of the bin boundary were moved to the next bin. For example, for such small energy changes, the number of electrons promoted to the next higher energy bin for recombinations and de-excitations, and the number demoted for ionizations and excitations, was only a fraction of the total number of electrons in each bin. Although the two approximations appeared to compensate for

each other, the assumption that the electrons were uniformly distributed in each bin resulted in an increase in the rates to lower energy bins when the bin size was increased. Thus, the effective temperature of the electron distribution was reduced for larger bin sizes. As shown in Figure 7.6, at 57 μs after plasma initiation the calculated electron temperature was .363 eV for 75 bins and .345 eV for 50 bins, while the gas temperature was .356 eV.

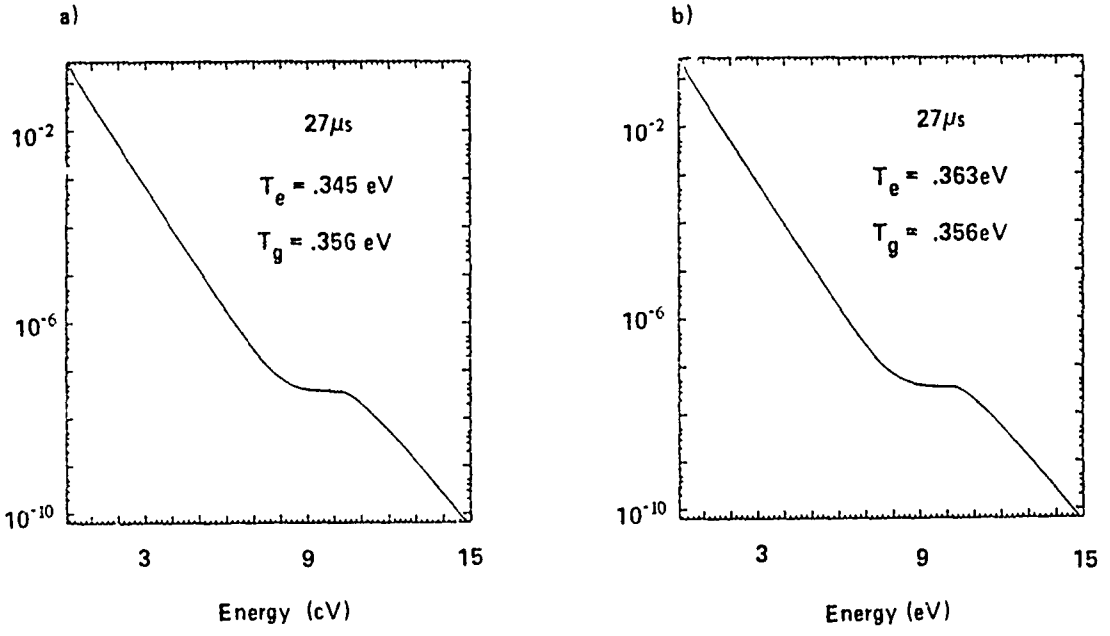

Figure 7.6: Comparisons of Electron Distributions for a) 50 Electron Bins and b) 75 Electron Bins

The errors associated with the assumption that the electrons were uniformly distributed in each energy bin were even more apparent when the number of bins was reduced to 25. In that case, the calculated electron temperature at 57 μs was .317 eV. In fact, the electron temperature was reduced immediately, to such an extent that it more than compensated for the fact that, in each bin, the lower energy electrons were under-represented and the higher-energy electrons were over-represented. Thus, the recombination rates were increased, increasing the excited atomic hydrogen populations

and decreasing the H^+ population. Similarly, the H_2^+ and H_3^+ populations were increased because of the lower electron temperature.

7.4 Plasma Behavior Under Laser Illumination

During laser illumination, the kinetics model (KM) improved on the results of the extended rate equation model (ERM) in nearly every category. In a few instances, however, the simple atomic rate equation model (ARM_{VS} actually gave better results. The fluorescence peak ratios closely matched those of the Burgess *et al.* (1980) experiment, improving the agreement at 40 μs. Although the LIF plateau ratios were improved, especially at later times, they were still significantly less than the experimentally measured plateau levels. The peak decay rates were also improved, only slightly at 30 μs, but very significantly at 50 μs, bringing Γ to within 18% of the experimental value at that time. (However, the decay rate obtained using Vriens and Smeets' rates in the simple atomic rate equation model (ARM_{VS}) was even closer to the experimental value.) At 30 μs, the decay rate of the peak was over two times greater than the experimental value.

The large discrepancies between the calculated and experimentally measured decay rates seem to be a function of the ratio of initial populations of the $n = 2$ and $n = 3$ levels, n_2^0/n_3^0. In general, the smaller this ratio, the greater the decay rate of the peak. Apparently, if the $n = 3$ level population is artificially large, the laser fluorescence peak is very short-lived.

time (μs)		n_e(cm^{-3}) $\times 10^{14}$	n_1^0(cm^{-3}) $\times 10^{16}$	n_2^0(cm^{-3}) $\times 10^{11}$	$\frac{n_3^L(peak)}{n_3^0}$	$\frac{n_2^0}{n_3^0}$	$\frac{n_3^L(plat)}{n_3^0}$	Γ(s^{-1}) $\times 10^7$
30	**E**	**11.**	**-**	**34.0**	**3.00**	**-**	**2.00**	**9.5**
	ARM_{VS}	11.	2.60	2.61	4.63	7.20	1.06	28.0
	ERM	11.	1.40	38.0	3.08	3.77	1.04	26.0
	KM	11.	1.40	38.0	3.13	3.77	1.08	23.5
40	**E**	**5.1**	**-**	**13.5**	**7.30**	**-**	**3.60**	**4.9**
	ARM_{VS}	5.1	2.60	3.64	11.3	16.9	1.24	9.80
	ERM	5.1	1.67	13.5	5.83	7.70	1.07	11.6
	KM	5.1	1.67	16.0	6.49	8.65	1.18	8.93
50	**E**	**2.2**	**-**	**3.00**	**12.0**	**-**	**5.00**	**2.3**
	ARM_{VS}	2.2	2.60	4.27	31.0	44.9	2.92	2.50
	ERM	2.2	1.70	4.60	11.6	18.4	1.29	5.50
	KM	2.2	1.73	4.60	11.6	15.9	1.42	2.70

E-experiment ARM_{VS}-atomic rate equation model
ERM-extended rate equation model KM-kinetics equation model

Table 7.1: Comparison of Experiment, Atomic Rate Equation Model, Extended Rate Equation Model, and Kinetics Equation Model

Bibliography

Janev R K, Langer W D, Evans K Jr, and Post D E 1987 *Elementary Processes in Hydrogen-Helium Plasmas* (New York: Springer-Verlag)

Lee R W, Morgan W L, Whitten B L, and Kolbe G 1983 *Lawrence Livermore National Laboratory, CA* **UCRL**-88714

Morgan W L and Penetrante B M 1990 *Computer Physics Communications* bf 58 127

Rockwood S D 1973 *Physical Review A* **8** 2348

Spitzer L 1956 *Physics of Fully Ionized Gases* (New York: Interscience)

Chapter 8

Conclusions and Recommendations

The present work has illustrated the complexity of what had been thought to be a simple problem. A number of the conjectures of previous investigators were confirmed and some new insights into the behavior of such plasmas were obtained. However, there are still significant discrepancies remaining between the present theoretical models and experimental measurements. In order to reconcile these differences, more detailed diagnostic experiments should be conducted to verify the conclusions of these theoretical models. Then, having confirmed the accuracy of this theoretical model, or modifying it appropriately, the remaining discrepancies can be attacked.

8.1 Conclusions

The major observations and inferences obtained from the present theoretical model are as follows.

- The use of Vriens and Smeets' collisional rates improved the agreement between the numerical model and the experiment. (Vriens and Smeets' excitation rates are generally half those of Johnson, while the ionization rates are generally twice Johnson's.)

- H^- is a significant source of atomic hydrogen in the $n = 2$ and $n = 3$ (especially) states through the process of mutual neutralization with

H^+. However, the H^- population required to sustain the experimentally measured/deduced H(2) and H(3) populations changes by over two orders of magnitude in 20 μs (from 1.1×10^{13} $1/cm^3$ at 30 μs to 7.3×10^{10} $1/cm^3$ at 50 μs).

- Vibrationally excited H_2 is the primary source for H^- through the process of dissociative attachment. (The cross-section for this process peaks at .2 eV and drops to nearly zero at 10 eV.) Thus, if "extra" vibrational excitation is not included in the model, the H_2 population required to sustain the H^- population is too high, causing increased production of H_3^+ and thus H(2). Even with such extra vibrational excitation, the required H_2 population cannot be sustained at the high levels required in the early recombination phase because dissociative attachment depletes it too quickly.

- Photodetachment of H^- causes the LIF plateau level to be greatly reduced. Under laser illumination, the H(2) population is depleted rapidly and not sufficiently replenished by other processes while the laser remains on. This effect is seen in both the extended rate equation and kinetics equation models. However, a reduction in the plateau level was not seen in the ARM_J or ARM_{VS} models since the lower initial populations in these cases were not dependent upon H^- as a source. Experimental observations indicate that there is a short-lived dip in the fluorescence plateau. The impact of photodetachment may be exaggerated because the laser energy flux used to saturate the $n = 2$ to $n = 3$ transition in the models was approximately 20 times that reported experimentally. Thus, the enhanced effect of photodetachment may simply be the result of incorrectly modeling the process of photo-excitation.

- H_3^+ is an important source of H(2) through the process of dissociative recombination. H_3^+ is produced primarily by proton exchange between H_2 and H_2^+. Since this cross-section increases as the temperature decreases and the rate is proportional to the H_2 population, H_3^+ becomes the dominant ion as the plasma cools and recombines.

- H_2^+ is an important source of H(3) through the process of dissociative recombination. Low energy electrons are primarily responsible for

the production of H(3) by this process since the cross-section is much greater at low electron energies. As the plasma recombines and the population of H_2 increases, the primary loss process for H_2^+ is by H_3^+ production through proton exchange with H_2.

- Ambipolar diffusion of H^+ and e^- appears to be responsible for the faster than expected exponential decay of the electron density. Diffusion dominates recombination because the z-pinch forces ions and electrons to the walls initially, significantly reducing the plasma charge and neutral densities for several hundred microseconds. As a result, the initial diffusion is more rapid than would normally be expected and overshadows the loss of electrons by recombination.

- The diffusion rates of neutral H and H_2 back into the plasma were modified to reflect the contention by Jones (1982) that these species remained at the walls for several hundred microseconds before returning to the plasma. Thus, the theoretical diffusion rate of atomic hydrogen was reduced, while that of molecular hydrogen was increased. This neutral diffusion had no impact on the short term modeling of the LIF in the plasma .

- The kinetics model demonstrated that a hot non-Maxwellian component of the electron distribution was produced by the trapping of $Lyman_\alpha$ radiation.

- The kinetics model demonstrated that as the plasma cools and recombines, the electron temperature and the (experimentally measured) gas temperature diverge. The lower electron temperatures produce small variations in the rates for certain electron impact processes and their inverses.

- The presence of a hot electron component was found to decrease H^+ and to quench the excited atomic hydrogen levels more quickly. Comparing the results of the extended rate equation and kinetics models, it was found that the two-temperature scheme used in the extended rate equation model appeared to overestimate the effect of these hot electrons.

8.2 Recommendations

In order to extend and improve our understanding of z-pinch hydrogen plasmas, the following suggestions should be considered in future theoretical models and in the design of follow-on experiments.

- Because the H^- population is an important source of H(3) and the $H_2(v*)$ population controls H^- via dissociative attachment, it is critical to model the vibrational excitation and relaxation of H_2 by electron collisions, wall recombination, and mutual neutralization with H_2^+ and H_3^+. In addition, since the vibrational distribution of H_2 is primarily determined by electron collisions, and since the cross-sections for all $\Delta v = 1$ transitions are approximately equal, the temperature used to calculate the vibrational distribution of H_2 may actually be the electron temperature and not the gas temperature. Finally, since the dissociative attachment rates may vary by a factor of from 5 to 100, depending upon the rotational state of the molecular hydrogen (Hiskes, 1982), rotation should also be included if it is desired to model the dissociative attachment process accurately.

- The laser energy flux required for saturation of the H_α transition was found to be approximately 20 times higher than that which was reported by Burgess *et al.* (1980). This discrepancy should be resolved in any future investigations.

- Since it now seems certain that there is more molecular hydrogen present in such plasmas than was at first thought, the absorption of laser radiation and the resulting photodissociation or vibrational excitation should be considered in any future models. For example, since the $n = 2$ population was determined by measurements of the axial H_β transmission, the absorption of radiation by molecular hydrogen would result in an overestimate of the actual H(2) population. Thus, any future numerical models should consider this effect and the experimental data reported by Burgess *et al.* (1980) may have to be modified to reflect this reality.

- It has also been shown (Cathernot, *et al.*, 1978) that excited atomic hydrogen levels may be quenched by molecular hydrogen in ground

and metastable states. For example, quenching of H(3) by $H_2(a\ ^3\Sigma_g^+)$ produces H(2) and H_2 in an even higher level. This molecular hydrogen then fluoresces (at 6568 Å). As a result, the H(3) population, which was experimentally deduced (Burgess, *et al.*, 1980) by measuring the peak in the H_α fluorescence (at 6563 Å), may actually be less than previously thought. This possibility should be considered in any future models of this plasma and in deducing level populations from the observed fluorescence signals.

- Oscillations in the electron and neutral densities have been observed in z-pinch hydrogen plasmas similar to those used in the Burgess *et al.* (1980) experiment. These oscillations could be modeled using a time-dependent factor which modifies the populations of all species simultaneously. As shown by both rate and kinetics models, the behavior of the H(2) and H(3) populations is very sensitive to both electron and neutral densities. Thus, these oscillations could significantly alter the initial conditions for the LIF.

- The ambiolar diffusion of electrons and ions has been shown to be an important factor in correctly modeling the electron density decay. However, the mobilities used to calculate the diffusion coefficients for each species were determined in an approximate factor. In order to reproduce the experimentally observed electron decay, it was necessary to empirically increase the ambipolar diffusion coefficients by a factor of ten. However, there may exist higher-order, shorter-lived radial modes which could increase the diffusion coefficients initially. This possibility should be investigated and, if appropriate, incorporated in future plasma models.

- The interaction of hydrogen with the walls of the plasma containment vessel presented many complications in modeling the simple LIF process. Follow-on experiments to validate the LIF technique may be more successful it they are carried out with a less reactive gas, such as helium.

- In order to better understand the detailed kinetics in a hydrogen plasma, the present model's long-term errors in charge neutrality should be eliminated and energy balance (including radiative losses)

should be included. That is, the kinetics model should include conservation of charge and energy to increase the accuracy of the electron distributions obtained.

Bibliography

Burgess D D, Myerscough V P, Skinner C H, and Ward J M 1980 *Journal of Physics B: Atomic and Molecular Physics* **13** 1675-1701

Catherinot 1978 *Physical Review A* **18** 1097-102

Hiskes J R, Karo A M, Bacal M, Bruneteau A M, and Graham W G 1982 *Journal of Applied Physics* **53** 3469

Jones W M 1982 *Plasma Physics* **24**(4) 361-68

Appendix A

Laser-Induced Fluorescence as a Local Plasma Diagnostic

Laser-Induced Fluorescence (LIF) is an experimental technique which may be used in the measurement of basic plasma parameters, such as electron temperature and density, and in the measurement of macroscopic properties, such as plasma flow velocity.

In the first half of this century, plasma parameters were often measured by inserting a probe of some sort into the plasma to sample its condition over a small region. More recently, with the advent of high-power lasers, it has become possible to use Thompson scattering by free electrons in the plasma to measure electron densities and temperatures without placing probes directly into the plasma. However, because the Thompson cross-section is so small, high-power lasers must be used and the technique can only be used for high density plasmas. In addition, with such high laser powers, the plasma could be significantly altered right at the point of observation.

However, in 1968, a "new" approach for obtaining localized plasma diagnostics was reported (Measures, 1968). This technique involves the "selective excitation" of one or more specific atomic transitions in one of the constituents of a plasma. Since the cross-section for such "resonance" excitations is about ten orders of magnitude greater than the Thompson cross-section, the effects of such resonance excitation can be observed with much lower power lasers. Consequently, this technique presents a much smaller danger of altering the plasma being investigated.

One of the diagnostic techniques proposed by Measures involves the observation of the fluorescence produced by a pump laser pulse which is of sufficient power to "saturate" a target transition. That is, the laser pump power is such as to produce a level population ratio corresponding to the Boltzmann level populations,

$$\frac{n_U}{n_L} = \frac{g_U}{g_L} e^{-\Delta\epsilon/kT_e}, \tag{A.1}$$

with an effectively infinite temperature. (g_U and g_L are the statistical degeneracies of the upper and lower states, respectively.) Measures described theoretically the temporal behavior of the "intensification factor" for the upper level population and of the "diminuition factor" for the lower level in response to a pump pulse which may be short or long compared to the equilibration time of the levels. For a long pulse, he showed that the spontaneous emission from the upper level quickly rises to a peak and then decays exponentially to a plateau value while the laser remains on. By comparison, a short excitation pulse does not yield a plateau and the decay from the peak is altered. However, both long and short excitation pulses produce the same peak intensification, given by

$$(\frac{n_{L0}}{n_{U0}} + 1)/(\frac{g_L}{g_U}), \tag{A.2}$$

where n_{U0} and n_{L0} are the upper and lower level populations prior to the laser pulse and g_L and g_U are the level degeneracies. Thus, a measurement of the peak fluorescence intensification resulting from either a long or short laser pump pulse would yield a value for the ratio of the initial level populations, $\frac{n_{L0}}{n_{U0}}$. (Note that the expression obtained by Measures for the peak intensification assumes that the plasma is optically thin at this emission frequency. See Hinnov and Ohlendorf (1969).) If these levels were initially in LTE, their initial population ratio would also be given by the Boltzmann relation

$$\frac{n_{U0}}{n_{L0}} = \frac{g_U}{g_L} e^{-\Delta\epsilon/kT_e}, \tag{A.3}$$

where T_e is the electron temperature. Thus, using the measured peak intensification and the initial LTE ratio, the electron temperature can be determined in the plasma region where the laser beam and the fluorescence detection system's field of view intersect. Alternatively, two lasers could

be used to excite separate transitions with the same upper state. Comparing the fluorescence peaks for these two transitions, the ratio of the two lower level populations could then be obtained. If these levels are in LTE, the Boltzmann relation could again be used to determine the electron temperature.

To use this intensified fluorescence for such localized plasma diagnostics, the fluorescence must be distinguishable from the background radiation. This background is composed of natural radiation from the rest of the plasma and of laser radiation scattered by the walls, small particles, etc. In order to easily distinguish fluorescence radiation from scattered laser radiation, the pumped transition can be chosen so that the observed fluorescence is to an intermediate level, a level somewhat above the lower level of the pumped transition. (Although the same problem arises with Thomson scattering diagnostics, such a simple solution is not possible.) In fact, if the atomic species in the plasma do not have such "conveniently" arranged energy levels, the plasma can be "seeded" with another species which has a more useful energy level arrangement. For example, Measures (1968) describes the use of barium for this purpose, as a controlled impurity in a low-temperature plasma.

The intensification in the fluorescence must also be distinguishable from the natural radiation from the excited state. For this to occur, the thermal population of the lower level in the fluorescing transition must be much greater than that of the upper level, $n_{L0} \gg n_{U0}$. Thus, the energy separation of these levels must be much greater than the mean thermal energy, $\Delta\epsilon \gg kT$. Since it is this energy separation that the pump laser is tuned to, this requirement imposes a limit on the temperature, in terms of the wavelength of the pump laser, for which the intensification will be adequate. Claiming that an intensification of at least 3% is required, Measures (1968) obtained the following requirement:

$$\lambda T \leq 0.225 \text{ cm} - ^\circ \text{K}. \tag{A.4}$$

Thus, to accurately measure plasma temperatures above 1 eV using this technique, pump laser wavelengths must be less than 200 nm. This requirement places an additional constraint on the energy level structure of the target atom if the two-transition technique, mentioned previously, is used. In this case, to obtain accurate results for the temperature, the lower levels of the two transitions must also be separated by (at least) several kT.

Since the upper excited state can decay by either radiative or collisional de-excitation, varying the electron density determines which method is dominant. In fact, if the electron number density is too high, collisional de-excitation may be so rapid that any fluorescence increase would go completely unnoticed. Thus, there is an upper limit on the electron number density in the plasma in order for this technique to be feasible. (Decreasing the electron number density increases the relative impact of radiative de-excitation upon the decay from the fluorescence peak. As a consequence, varying the electron density in the plasma allows both the collisional and radiative *in situ* rates to be determined, as described in Appendix B.)

Measures also described the use of LIF in estimating the local value of the velocity in a supersonic flow. In this technique, a laser is tuned to match the doppler-shifted resonance frequency of a plasma species at a given location. The beam is then rotated through 90° about the point of interest and the frequency is again varied to match the doppler-shifted resonance from this direction. Using these two resonance frequencies, the flow velocity at the point of interest in the plasma is determined.

Bibliography

Hinnov and Ohlendorf 1969 *Journal of Chemical Physics* **50**(7) 3005-3010

Measures R M 1968 *Journal of Applied Physics* **39** 5232-45

Appendix B

Burgess and Skinner Model of Laser Induced Fluorescence

The traditional use of fluorescence in the measurement of collisional or radiative rates relies on the use of short excitation pulses. In 1974, Burgess and Skinner proposed a method for measuring such rates using long laser pulses with intensities sufficient to saturate the pumped transition. This method had been proposed earlier by Measures (1968), but only in the context of local plasma diagnostics (see Appendix A), not in the measurement of atomic rates. Burgess and Skinner illustrated the utility of their proposed technique using a simple two-level model.

Consider two levels in an atomic system with a number of other possible levels. A laser is tuned to excite a transition from the lower level (L) to the upper level (U). The populations of these two levels are assumed to be small enough that the resulting fluorescence does not substantially alter the populations of any of the other levels in the system. Assume that the laser is turned on at $t = 0$ and immediately rises to an intensity sufficient to "saturate" the transition, *i.e.* to populate the upper and lower levels in the ratio of their statistical weights. (Due to the high collision rates in the plasmas generally investigated by Burgess, *et al.*, laser fluxes of 1 $kWcm^{-2}$ or more were required to approach such a saturated condition.) As long as this saturation is maintained, direct excitation and de-excitation processes between these two levels need not be considered in the model.

Let the rate at which the lower level is populated from all other levels in the system, except the upper level, be C_L. Similarly, let the rate at which

the upper level is populated from all other levels, except the lower level, be C_U, as shown in Figure B.1. In addition, let the corresponding decay

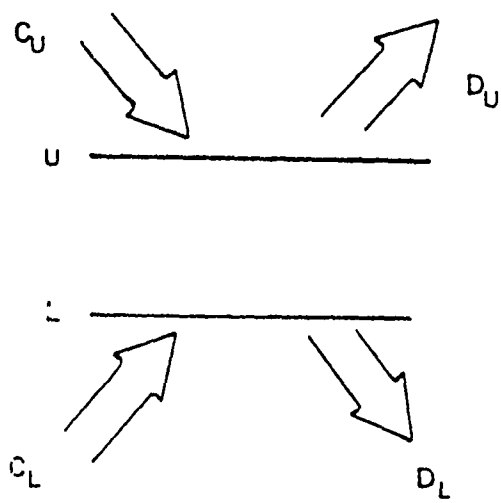

Figure B.1: Two-level Model of LIF

rates, per atom, to all other levels be D_U and D_L. In the equilibrium level populations before the laser is turned on are n_{L0} and n_{U0}, the rates in and out of the two levels, as a combined system, must be equal:

$$C_L + C_U = n_{L0}D_L + n_{U0}D_U, t < 0 \tag{B.1}$$

After the laser is turned on, assuming that it immediately saturates the transition, the two level populations are related by their statistical weights:

$$n_L(t) = \frac{g_L}{g_U} n_U(t), t > 0 \tag{B.2}$$

If the total concentration of both levels is designated as n^+, at any time t it is given by

$$n^+(t) = n_L(t) + n_U(t). \tag{B.3}$$

Then, in particular, before the laser is turned on,

$$n^+(0) = n_{L0} + n_{U0}. \tag{B.4}$$

Once the laser is on the the time rate of change of this combined population is

$$\frac{dn_+}{dt} = (C_L + C_U) - n_L(t)D_L - n_U(t)D_U \qquad \text{(B.5)}$$

Using the relationship between n_L and n_U given in equation (B-2) to express the joint population, n_+, in terms of the upper level population, equation (B-5) may be expressed as:

$$\frac{dn_U}{dt}(1 + \frac{g_L}{g_U}) = (C_L + C_U) - n_U(\frac{g_L}{g_U}D_L + D_U) \qquad \text{(B.6)}$$

Thus, the solution for the time-dependent upper level population is:

$$n_U(t) = \left(\frac{n_{L0} + n_{U0}}{1 + \frac{g_L}{g_U}} - \frac{C_L + C_U}{\frac{g_L}{g_U}D_L + D_U}\right)e^{-\frac{\frac{g_L}{g_U}D_L + D_U}{1 + \frac{g_L}{g_U}}t} + \frac{C_L + C_U}{\frac{g_L}{g_U}D_L + D_U} \qquad \text{(B.7)}$$

As Burgess and Skinner (1974) noted, the time-dependent population of this upper level, and hence the observed flurorscence, may take two possible forms, as shown in Figure B.2. In both cases, the initial rise in

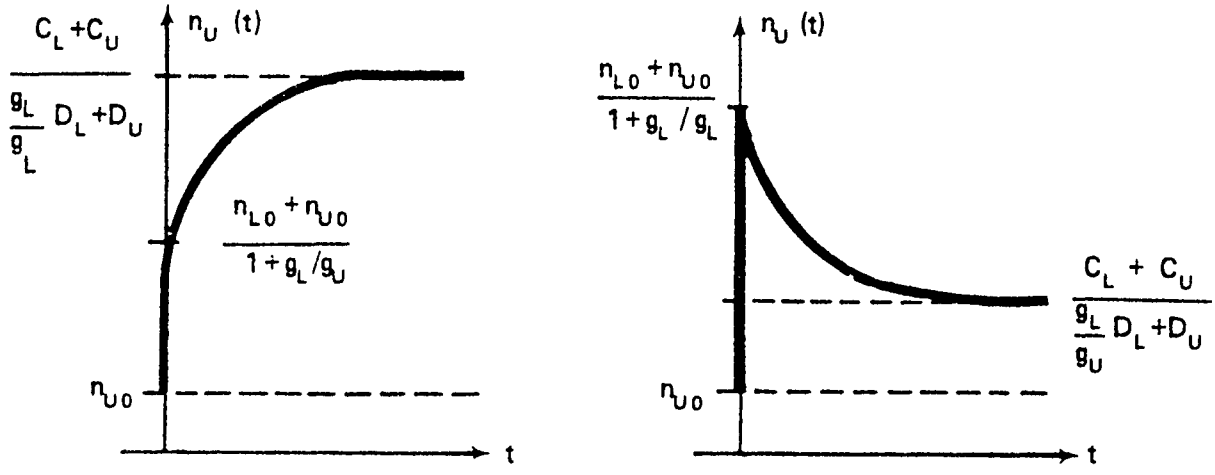

Figure B.2: Theoretical Fluorescence Profiles for Two-Level Model

the fluorescence results from the laser's rapid saturation of the transition.

If the rate out of the pair of levels is less than the rate in by a factor approximately equal to the combined population of the two levels, $n_{L0}+n_{U0}$, the coefficient of the exponential in equation (B.7) will be negative and the initial rapid rise in the fluorescence will be followed by an additional (but slower) increase to a plateau value. (See Figure B.2 a.) However, if the rate out of the pair of levels is comparable to the rate in, the initial rapid rise in the fluorescence is followed by an exponential decrease to the plateau level.

In many cases of experimental interest, a system of levels is observed while it is relaxing to a lower degree of excitation. In these cases, the latter fluorescence profile (Figure B.2 b) is obtained. The initial increase in the upper level population, which occurs primarily at the expense of the lower level population, is short-lived because of the large rate out of the upper level. A measurement of the intensity of this initial fluorescence spike, relative to the background fluorescence, yields the ratio of the initial populations, n_{U0}/n_{L0}. In addition, a measurement of the exponential decay rate from this spike gives the combined decay rates out of both levels, weighted by their statistical weights. The final equilibrium plateau which is reached indicates the relative importance of processes into the upper (fluorescing) level compared to those into the lower level. With the combined decay rate obtained from the exponential decay, a measurement of this plateau intensity can be used to determine the combined rate into both levels, $(C_L + C_U)/n_{U0}$. Then, using the initial equilibrium relation for the rates (equation (B.1)) (assuming that they have not changed appreciably during the laser pulse), separate values can be obtained for the rates out of each of the two levels, D_L and D_U.

There are, therefore, two primary advantages of the long-pulse LIF technique over the traditional, short-pulse technique. First, the use of a saturating laser intensity in the long-pulse method removes the effects of any decays from the upper to the lower level. Secondly, and more importantly, while a **short** laser excitation pulse can be used to determine the decay rate out of the upper level, a **long** excitation pulse can be used to determine the decay rates out of **both** upper and lower levels in the excited transition.

Bibliography

Burgess D D and Skinner C H 1974 *Journal of Physics B: Atomic and Molecular Physics* **7**(9) L297-301

Measures R M 1968 *Journal of Applied Physics* **39** 5232-45

Appendix C

Laser-Induced Fluorescence in Hydrogen Experiment

An experimental investigation of laser-induced fluorescence (LIF) in a well-diagnosed hydrogen plasma was conducted by Burgess, *et al.* (1980) in an attempt to explain discrepancies between the theory and results of an earlier experiment. (Burgess, *et al.*, 1978)

C.1 Hydrogen Plasma

The experimental setup used is shown in Figure C.1. The plasma was formed by a z-pinch discharge in a pyrex tube 70 cm long and 4.7 cm in diameter, with quartz windows at each end. The initial fill pressure of molecular hydrogen in the tube was .45 Torr. Power was supplied to the discharge by a 1 μF capacitor charged to 20 kV. The current through the discharge peaked at 2 μs after initiation and was critically damped with a time constant of 6 μs. All of the experimental measurements were made between 28 and 60 μs after the peak current, during the plasma's "recombination" phase, so that no currents or magnetic fields of consequence were present. During the experiments, electron densities and temperatures varied between $10^{14} \leq n_e\,(1/\mathrm{cm}^3) \leq 10^{15}$ and $0.3 \leq T_e\,(\mathrm{eV}) \leq 0.8$, respectively.

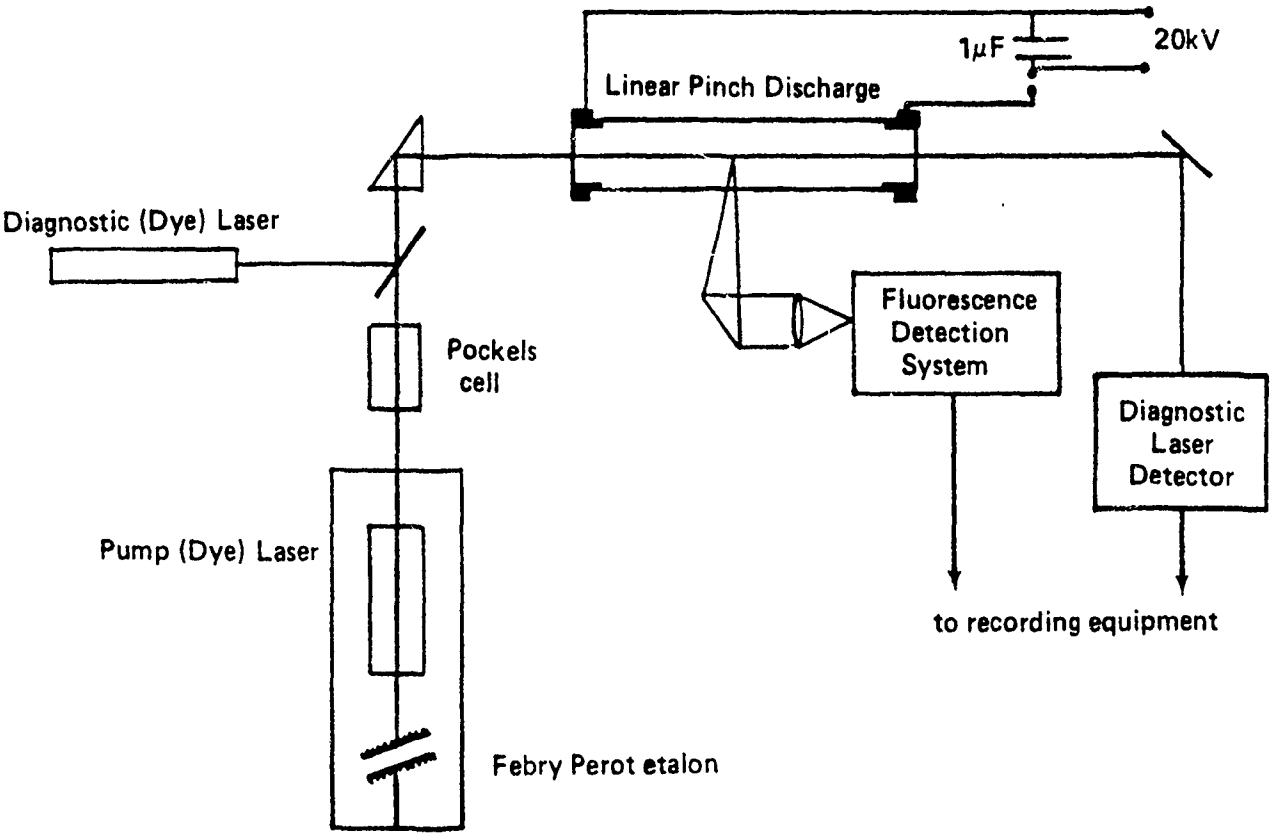

Figure C.1: Setup for LIF Experiment by Burgess *et al.*, (1980)

C.2 Pump Laser

The laser used to pump the plasma at either H_α or H_β was a coaxial xenon flashlamp-pumped dye laser. Different dyes were used to produce the H_α or H_β output. Tuning was accomplished using one or two intra-cavity Fabry-Perot etalons. In most instances, the output linewidth used was about 5 Å, although some experiments were done with a linewidth of only .5 Å. (There was no observed effect due to this variation in the pump laser's bandwidth.) A Pockells cell switch was used to shape the laser pulse, producing a pump pulse from 150 to 200 ns long, with rise and fall times of about 1 ns. During such a pulse, the maximum energy supplied by the laser was 60 mJ. Using baffles on the input side of the system, the pump laser beam was limited to a diameter of 1.4 cm. (Burgess, *et al.*, 1980) In addition, Burgess' group directly verified that the beam diameter was unaltered in the plasma at the location from which the fluorescence was observed. Thus, the apparent scattering volume in the plasma was not significantly enlarged by effects such as diffusion or radiation trapping.

C.3 Diagnostics

Assuming that the electron energies had a Maxwellian distribution, electron temperatures were determined by Thomson scattering of a high power laser. A 200 MW, 20 ns pulse, at 6943 Å, was provided by a ruby laser sustem. The incident beam was aligned coaxially with the discharge tube and was focused to a 2 mm diameter spot in the center of the tube. Observing the scattered light at 90° to the incident beam, spectral profiles were obtained and fit to a Gaussian to determine values for T_e at selected times. These measurement times were quite accurately known since the measured response of the detection system was better than 5 ns. The values obtained by Burgess, *et al.*, (1980), as a function of time after peak current in the pinch, are reproduced in Figure C.2. Experimental results are indicated by open circles, while an exponential fit to the data, given by the formula

$$T_e(t) = .14 + 2.2660155\, e^{-(t/24.32028)} \qquad \text{(C.1)}$$

is shown as a solid curve. (T_e is in units of eV and t is in units of μs.)

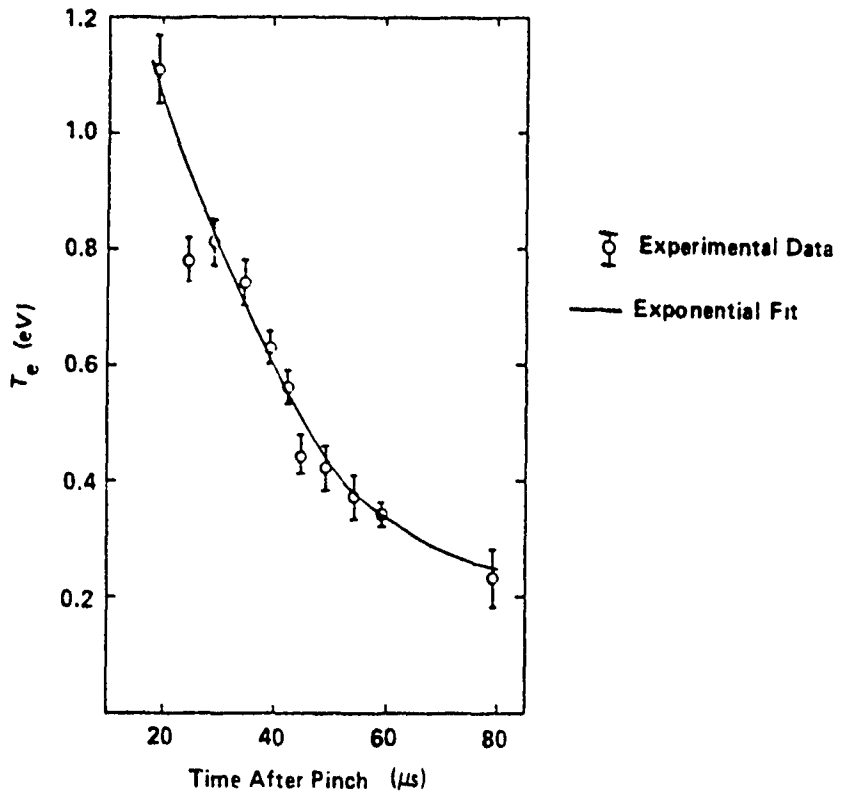

Figure C.2: Electron Temperature (eV) as a Function of Time (μs) After Peak Current

Electron number densities were obtained interferometrically using a HeNe laser to axially illuminate the plasma. The laser, which was operated simultaneously on the 3.39 μm and 6328 Å transitions, was placed in a 4.5 m cavity which also contained the discharge plasma. Since light at 6328 Å was prevented from entering the plasma by a germanium filter, the effect of the plasma's electron density on the 3.39 μm fringes was detected on the 6328Å output of the laser via the Ashby-Jephcott feedback technique. (Ashby and Jephcott, 1963). The values obtained by Burgess *et al.* (1980) for the electron density, as a function of time after peak current, are reproduced in Figure C.3. Experimental results are indicated by open

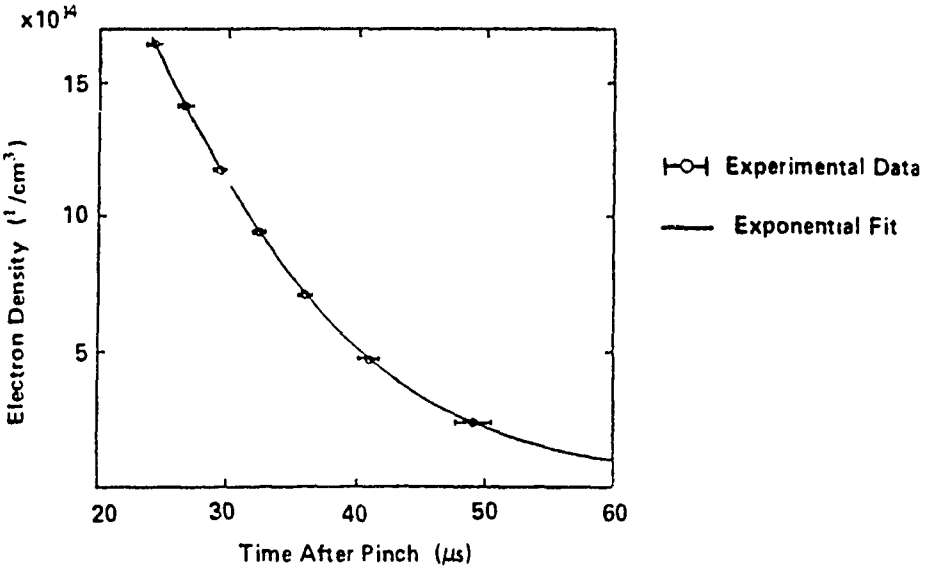

Figure C.3: Electron Density as a Function of Time (μs) After Peak Current

circles, while an exponential fit to the data, given by the formula

$$n_e(t) = 1.286504 \times 10^{16}\, e^{-(t/12.2891156)}\,, \qquad \text{(C.2)}$$

is shown as a solid curve.

However, more recent experimental measurements (Nightingale and Burgess, 1983a and 1983b) in similar plasmas have shown large oscillations in the

electron density. (See Figure C.4.) A CW ring laser system was used to obtain temporal measurements which were much better resolved than the measurements of Burgess *et al.* (1980). The oscillations were much more pronounced for a helium plasma, though the oscillations in both hydrogen and helium plasmas were nearly gone by 80 μs after peak current. These oscillations were attributed to a cylindrical acoustic pulse propagat-

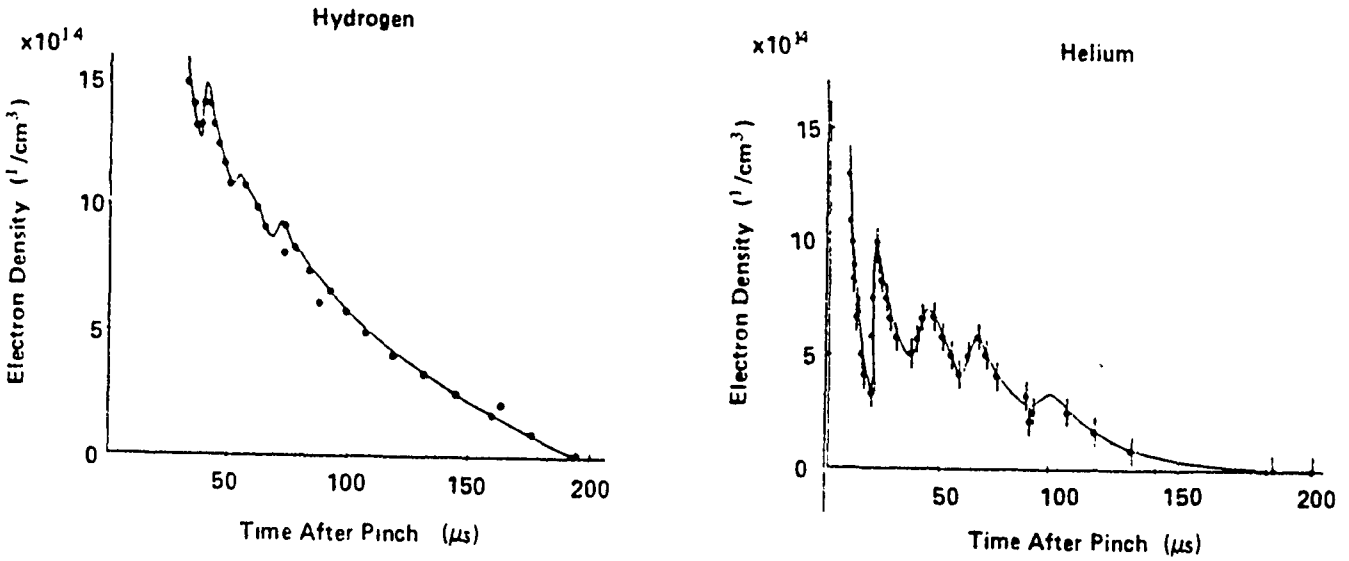

Figure C.4: Electron Densities in .45 Torr Hydrogen and Helium Plasmas

ing through the plasma, producing variations in both electron and neutral species densities. With a cylinder radius of 2.35 cm and an oscillation period of approximately 15 μs at 50 μs after peak current in the pinch (see Figure C.4), the wave speed is approximately 3.1×10^5 cm/s. (By comparison, the theoretical sound speed at this temperature in molecular hydrogen is 7.3×10^5 cm/s and in atomic hydrogen is 1.1×10^6 cm/s.) In fact, assuming that these pulses traveled at the neutral speed,

$$v_s = \sqrt{\frac{\gamma kT}{M}}$$

(γ is the specific heat ratio, M is the atomic mass, and T is the plasma

temperature), Nightingale and Burgess (1983a) deduced time-dependent plasma temperatures from the measured oscillation frequencies. These temperatures agreed will (within 20%) with those obtained from Thomson scattering measurements. Although the temperatures measured in the previous experiments by Burgess *et al.* (1980) were fit to a smooth exponential curve, the temperatures seemed to mimic the oscillations in the electron density (see Figure C.2). The excursions of the temperature from the exponential fit were most significant at about 25 μs, when the measured temperature was over 21% below the temperature used in the numerical models . In addition, Nightingale and Burgess (1983a) reported large absorption peaks at times corresponding to axial electron density maxima. These variations in the absorption were clear evidence that the oscillations also altered the neutral species concentrations.

The number density of hydrogen atoms in the $n = 2$ state was determined by longitudinal (line-of-sight integrated) measurements of the plasma's H_β optical depth, *i.e.* the number of H_β photon mean free paths for absorption. These measurements, using a 1 mW CW dye laser, with a beam diameter of 5 mm, were made before, during, and after illumination by the high-intensity H_α pump laser. As a check, the population of the $n = 2$ state in the unperturbed plasma was also determined by measurements of the plasma's transverse H_α optical depth. The $n = 2$ populations which Burgess *et al.* (1980) obtained using these two methods are presented, as a function of the electron density, in Figure C.5. These investigators also noted that the measured H_α radial optical depths were always less than 0.9. From this, they concluded that trapping of H_α radiation had a negligible effect on the observed H_α fluorescence, *i.e.* on the $n = 3$ level population.

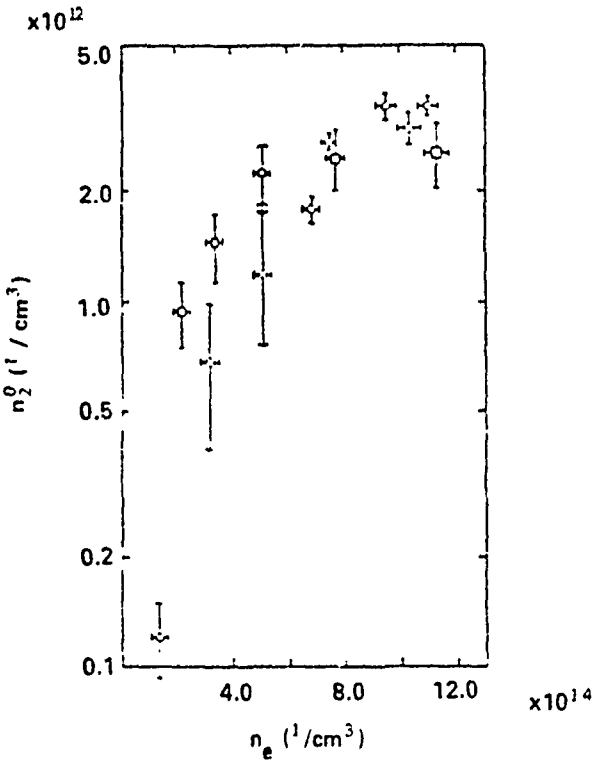

Figure C.5: Population of the $n = 2$ State in the Unperturbed Plasma

Bibliography

Ashby D E T F and Jephcott D F 1963 *Applied Physics Letters* **3** 13-18

Burgess D D, Myerscough V P, Skinner C H, and Ward J M 1980 *Journal of Physics B: Atomic and Molecular Physics* **13** 1675-1701

Burgess D D, Kolbe G, and Ward J M 1978 *Journal of Physics B: Atomic and Molecular Physics* **11** 2765-78

Nightingale M P S and Burgess D D 1983a *Journal of Physics B: Atomic and Molecular Physics* **16** 4091-4100

Nightingale M P S and Burgess D D 1983b *Journal of Physics B: Atomic and Molecular Physics* **16** 4101-4115

Appendix D

Energy Density in a Hydrogen Plasma

D.1 Energy Dissipated in a Z-Pinched Hydrogen Plasma

The "recombination phase" plasma investigated by Burgess, *et al.* (1980) was produced by the discharge of a 1 μF capacitor through hydrogen flowing in a pyrex tube. The electrical circuit used to produce the z-pinch is shown in Figure D.1. Six current "return bars" spaced symmetrically outside of the discharge tube provided the 100 KΩ resistance in parallel with the discharge. The 3 Ω resistor was used to critically damp current oscillations (ringing) in the discharge circuit. The plasma vessel itself, shown in Figure D.2, consisted of a pyrex cylinder, of radius 2.35 cm, with hollow ring electrodes of brass at each end. Quartz windows at each end of the plasma vessel allowed diagnostic and pump lasers to illuminate the plasma axially. (Kolbe, 1985)

According to Burgess, *et al.* (1980), the current through the hydrogen peaked at two microseconds after initiation of the pinch. After this peak, the current decayed approximately exponentially, being critically damped with a time constant of 6 μs. (However, as described in Appendix C, the electron density oscillated for times less than 80 μs after initiation. These oscillations were thought to be due to a cylindrical acoustic wave produced by the initial pinch.) With such a time constant, a 3 Ω damping resistor,

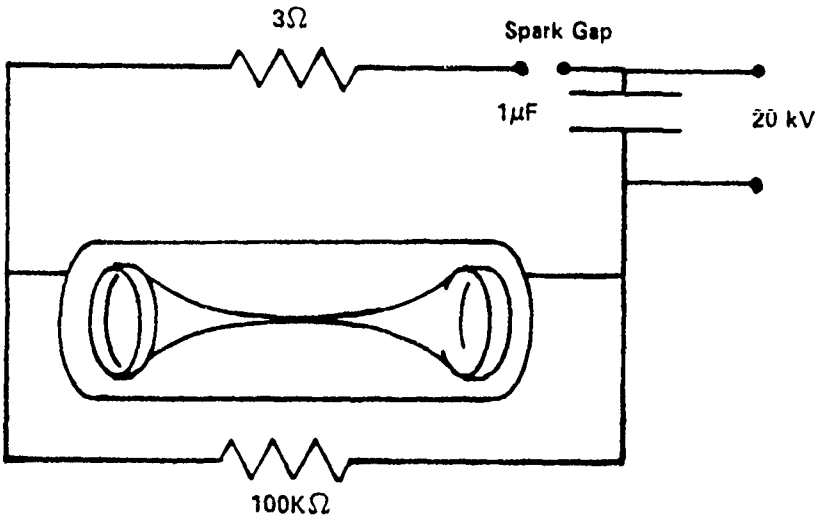

Figure D.1: Electrical Circuit for Z-Pinch

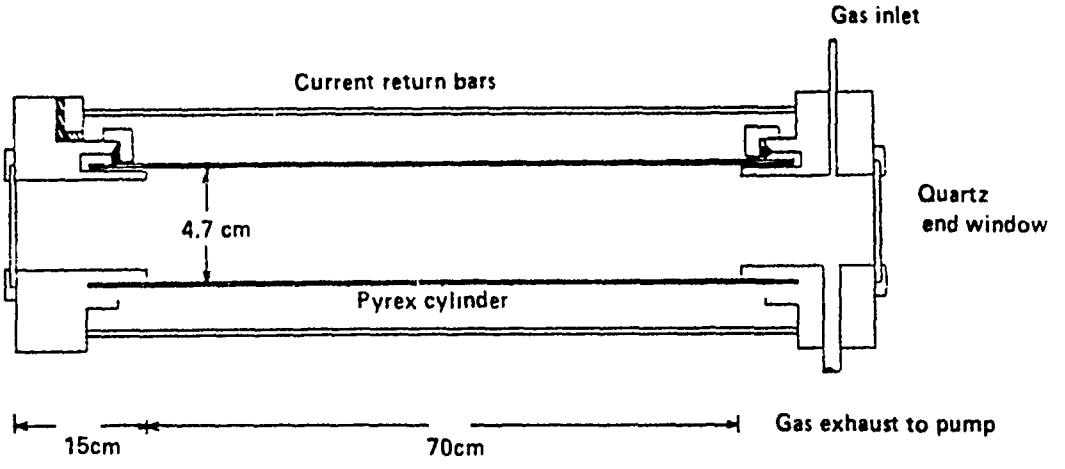

Figure D.2: Z-Pinch Plasma Vessel

a 1μF capacitor, and the plasma itself in series, the hydrogen plasma must have presented an average resistance of about 3 Ω. Thus, the initial energy stored in the capacitor was dissipated approximately equally between the damping resistor and the plasma. The energy dissipated in the plasma is approximately:

$$\begin{aligned} W_D &\approx \tfrac{1}{2}(\tfrac{1}{2}CV^2) \\ &\approx .25 \cdot 1 \times 10^{-6} \cdot (2 \times 10^4)^2 \\ &\approx 100 \text{ Joules} \end{aligned}$$

Assuming that this energy was deposited between the ring electrodes, as shown in Figure D.2, the density of the energy dissipated in the plasma is:

$$w_D \approx \frac{100J}{\pi \cdot (2.35\text{cm})^2 \cdot (70\text{cm})} = 82.3 \text{ mJ/cm}^3$$

D.2 Energy Density to Dissociate and Ionize Hydrogen

The energy density required to fully dissociate and ionize a molecular hydrogen gas of a given pressure may be determined using the approximation by Newton and Sexton (1969).

$$w_{d\&i} \approx n_H \cdot (\frac{1}{2}\epsilon_{dH_2} + \epsilon_{iH}) \qquad \text{(D.1)}$$

where ϵ_{iH} is the ionization evergy of atomic hydrogen and ϵ_{dH_2} is the dissociation energy of molecular hydrogen. (The radiative loss of energy during ionization is negligible for hydrogen.) So, for a fill pressure of .45 Torr at 300°K and dissociation and ionization energies of 4.48 eV and 13.6 eV, respectively, the energy density required to dissociate and ionize this density of hydrogen is approximately

$$w_{d\&i} \approx 73.5 \text{ mJ/cm}^3$$

Thus, if more energy than this is given to the plasma, the remainder will simply go into kinetic energy of the electrons and ions or be radiated away.

Bibliography

Burgess D D, Myerscough V P, Skinner C H, and Ward J M 1980 *Journal of Physics B: Atomic and Molecular Physics* **13** 1675-1701

Kolbe G 1985 *PhD Thesis* (London: Imperial College of Science and Technology)

Newton A A and Sexton M C 1969 *Journal of Physics B: Atomic and Molecular Physics* **2**(2) 1069-74

Appendix E

Surface Recombination of Hydrogen

The surface and bulk interactions of solids with hydrogen are important in a number of areas: the recombination of hydrogen atoms to form molecular hydrogen on interstellar dust grains, the embrittlement of metals by dissolved hydrogen, the effects of hydrogen on reactor wall integrity, and the absorption of hydrogen by metals for fuel storage.

Some of the early work on the interaction of hydrogen with solid surfaces was done by Wood and Wise (1961,1962). Their experiments focused on the recombination of hydrogen atoms as the result of interactions with surfaces of various compositions. They considered two possible mechanisms by which this recombination could occur. One, the Rideal mechanism, involves a collision between the incident atom and a surface-adsorbed atom (adatom). The second, the Hinshelwood mechanism, involves the adsorption of the incident atom and its subsequent collision with another surface-bound atom. Using experimental data, Wood and Wise calculated "average" recombination coefficients, with both mechanisms occurring, assuming a steady state condition in which the number of atoms incident on the surface is equal to the number which return to the gas as atoms or molecules. The recombination coefficients which they presented are defined as the fraction of hydrogen atoms striking a surface which recombine to produce molecular hydrogen. The value obtained by Wood and Wise for the recombination coefficient of hydrogen atoms incident on a pyrex surface at a temperatue between 288°K and 303°K was $5.8 \pm 1.8 \times 10^{-3}$

recombinations/sec/atom. In order to obtain an estimate of the recombination coefficient for hydrogen atoms incident on the brass ring electrodes used in the Burgess *et al* (1980) experiment, the data given by Wood and Wise for copper (at 333°K) was used. (Such brass is nominally 80% copper and 20% zinc.) Thus, the recombination coefficient for hydrogen atoms on brass was approximated as 0.14 recombinations/sec/atom.

However, these recombination coefficients may underestimate the actual recombination coefficients for the walls of the z-pinch discharge being modeled. Because of the cylindrical plasma shock wave which hits the walls shortly after the pinch, the walls could be nearly saturated, with adsorbed hydrogen atoms in almost all of the available interstitial sites. In that case, the steady state model used by Wood and Wise would be invalid. As a result, the effective recombination coefficient, the probability that a hydrogen atom which strikes a surface will recombine with an adsorbed hydrogen atom to produce a hydrogen molecule, could be significantly larger. In fact, the experimental results obtained by Wood and Wise prompted them to conclude: "It appears that the presence of large amounts of hydrogen in the solid enhances the recombination process." In an attempt to explain this enhanced recombination, they speculated that the adsorbed hydrogen atoms may somehow distort the lattice structure of the solid, forming additional electronic states which may make the surface more favorable for recombination reactions. (Wood and Wise, 1961)

These same researchers also noted that the surface recombination of hydrogen was accompanied by the release of energy in the form of internal and/or kinetic energy of the desorbing hydrogen molecule. Citing work by other individuals, they described the existence of two distinct binding states for hydrogen in pyrex: a strongly chemisorbed state with an estimated bond (activation) energy of 44 kcal/g-atom (1.91 eV/H atom) and a weakly-bound state, which becomes significantly populated at low temperatures, with an estimated bond energy of 5 kcal/g-atom (.22 eV/H atom).

More recently, experimental work has also been done on the desorption of molecular hydrogen from copper surfaces. This work, as summarized by Kubiak *et al* (1985), found bond (activation) energies for desorption of hydrogen atoms of approximately 9 kcal/mole of H_2 (.20 eV/H atom). In addition, they observed that the dissociative adsorption of molecular hydrogen required from 10 to 12 kcal/mole of H_2 ($\approx$ .24 eV/H atom). These observations appeared to be consistent with a model originally proposed by

Lennard-Jones (1932). Their model assumes that the potential energy curve crosses between atomic and molecular potentials above the surface of the solid. This model, as applied to copper, is shown in Figure E.1. According

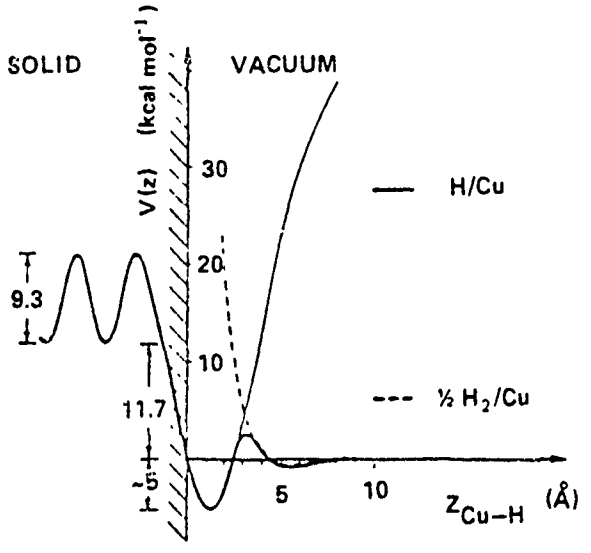

Figure E.1: Potential Energy Curves at the Surface of Copper

to this model, it appears that copper may exhibit both a strongly-bound state, .20 eV/H atom (9.3 kcal/mole of H_2), within the solid and a weakly-bound state, .11 eV/H atom (5.0 kcal/mole of H_2), at the surface. Thus, an incident hydrogen atom of sufficient energy may surmount the potential barrier at the copper surface, recombine with an adsorbed hydrogen atom, and leave the solid as molecular hydrogen with up to 1 eV of kinetic and/or internal energy.

This potential energy model for copper appears to agree qualitatively with that for pyrex, as indicated by the experimental observation, by Wood and Wise (1961), of both strongly and weakly bound states in pyrex. In addition, Kubiak indicated (private communication, 1987) that dielectric surfaces such as pyrex (as compared to conductors such as copper) would probably have an even greater exothermic energy for the desorbed molecular hydrogen. This conjecture is supported by the experimental measurement, by Wood and Wise (1961), of the relatively large, 1.91 eV/H atom,

recombination activation energy for pyrex. However, Wood and Wise did not measure the total exothermic recombination energy, so the total energy available to the molecular hydrogen, as kinetic and/or internal energy, is not known. In spite of this lack of quantitative data, it seems reasonable to assume that this exothermic recombination energy is of the order of several eV per H atom, which would seemingly guarantee the production of a sizeable fraction of the molecular hydrogen in excited electronic and/or vibrational states.

Thus, the impact of hydrogen atoms on the walls of the pyrex tube used in the experiment by Burgess *et al.* (1980) could result in the production of vibrationally-excited molecular hydrogen. This vibrationally-excited molecular hydrogen and the remaining atomic hydrogen would then slowly diffuse back into the plasma core, as suggested by Jones (1982) and Newton and Sexton (1969).

Bibliography

Jones W M 1982 *Plasma Physics* **24**(4) 361-68

Kubiak G D, Sitz G O, and Zare R N 1985 *Journal of Vacuum Science and Technology A* **3**(3) 1649-54

Lennard-Jones J E 1932 *Transactions of the Faraday Society* **28** 333

Wood B J and Wise H 1961 *Journal of Physical Chemistry* **65** 1976-83

Wood B J and Wise H 1962 *Journal of Physical Chemistry* **66** 1049-53

Appendix F

Forward and Reverse Reaction Rates

F.1 Forward Rates

The probability that a particular reaction between particles will occur is often expressed as a cross-section. For binary collisions, this cross-section may be viewed as the effective area presented by each of the target particles. The reaction rate coefficient (cm^3/sec) for such a process is the integrated product of this cross-section, $\sigma(v_r)$ (cm^2), the particles' relative impact velocity, v_r (cm/sec), and the normalized velocity distribution function of the "incident" particles, $f(v_r)$:

$$\langle \sigma v \rangle = \int_{v_{r0}}^{\infty} f(v_r)\sigma(v_r)dv_r$$

where $f(v_r)dv_r$ is the fraction of the collisions in which the relative velocity lies between v_r and $v_r + dv_r$ and the cross section is, in general, a function of this relative velocity.

Such rates are generally available, in the form of analytic formulas or polynomial fits, for reactions in which the incident particles are assumed to have a Maxwellian velocity distribution. (In the rate equation model it is assumed that the electron distribution function remains Maxwellian at all times.) Analytic expressions from various sources were used for collisional excitation and ionization, spontaneous emission, stimulated emission, photoexcitation, photoionization, and radiative recombination of atomic hy-

drogen. The rates for other (collisional) processes included in the model were obtained from polynomial fits by Janev *et al* (1987) to combinations of experimental and theoretical rates. For electron impact reactions, these fits were of the form

$$\log \langle \sigma v \rangle = \sum_{n=0}^{N} b_n (\log T_e)^n$$

where $N = 8$ and T_e is the electron temperature in eV. Reaction rates for heavy particle interactions were modeled using a double polynomial fit in both E and T. (E and T are the temperatures, in eV, of the two species involved. In the current model, it was assumed that these temperatures were equal.) The fits were of the form

$$\log \langle \sigma v \rangle = \sum_{n=0}^{N} \sum_{m=0}^{M} a_{mn} (\log T)^m (\log E)^n$$

where $N = M = 8$.

However, these polynomial fits did not always apply at the low temperatures ($\leq$1 eV) in the experiment being modeled. For electron temperatures much less than the threshold energy for a given process, only the "tail" of the electron distribution function overlaps with the process' cross-section. In those instances, an analytic expression was adapted from Zel'dovich and Raizer's (1966) (p.388) formula for electron impact ionizations. Their expression for such rate coefficients was derived under the assumption that the cross-section for the process is approximately linear, with slope m, for electron energies in the vicinity of the threshold energy, ϵ_{TH}. Integrating the cross-section over a Maxwellian electron energy distribution, $f_M(\epsilon)$, the expression they obtained for the rate coefficient is

$$\langle \sigma v \rangle = \bar{v}_e \, m_e \, (\epsilon + 2\, k_B T_e) \, e^{-\epsilon_{TH}/k_B T_e} \; (\mathrm{cm}^3/\mathrm{sec}) \qquad \text{(F.1)}$$

where

$$\bar{v}_e = \sqrt{\frac{8 k_B T_e}{\pi m_e}} = 6.7 \times 10^7 \sqrt{T_e(\mathrm{eV})} \; (\mathrm{cm/sec}) \qquad \text{(F.2)}$$

is the average thermal speed of the incident electrons at a temperature of T_e and

$$f_M(\epsilon) = \frac{2\sqrt{\epsilon}}{\sqrt{\pi}(k_B T_e)^{3/2}} e^{-\epsilon/k_B T_e}. \qquad \text{(F.3)}$$

In order to calculate the value of the slope m, the rate for the process at the lowest valid temperature for the polynomial fit is equated to the rate given by equation (F.1) at that temperature. The resulting relationship is then solved for m. Thus, the Zel'dovich and Raizer expression provides estimates for reaction rates at temperatures below the minimum valid energy for polynomial fits to these rates.

F.2 Reverse Rates

For each process considered in the rate equation model, the rate for the reverse process was also included. In some cases an analytic expression or polynomial fit for the reverse rate was available. However, in most instances, the reverse rate was obtained by invoking the principle of detailed balance between the forward and reverse reactions. That is, in equilibrium, each individual process is exactly balanced by the precise reverse process. Thus, any process which creates a state is exactly matched by an inverse process which destroys the state. For example, consider the species A-E which undergo forward and reverse reactions as indicated.

$$A + B \Longleftrightarrow C + D + E \tag{F.4}$$

Detailed balance dictates that the forward and reverse reactions must exactly "balance."

$$n_A\, n_B\, R_{forward} \;=\; n_C\, n_D\, n_E\, R_{reverse} \tag{F.5}$$

Thus, the reverse rate, $R_{reverse}$ may be expressed in terms of the forward rate, $R_{forward}$.

$$R_{reverse} = \frac{n_A\, n_B}{n_C\, n_D\, n_E}\, R_{forward} \tag{F.6}$$

In order to obtain this reverse rate, then, the ratio of species concentrations must be known. If LTE prevails, the chemical potentials on each side of the reaction equation (F.4) must be equal.

$$\mu_A + \mu_B = \mu_C + \mu_D + \mu_E \tag{F.7}$$

For each species, of total number N, at temperature T, and with total partition function Q, the chemical potential is:

$$\mu = -kT\frac{\partial}{\partial N}\ln(Q) \tag{F.8}$$

The total partition function for a species of N indistinguishable particles is simply the product of the individual partition functions for each category of energy they may have (translational, electronic, *etc.*).

$$Q = \frac{1}{N!}\left(q^{translational} q^{electronic} q^{rotational} q^{vibrational} \cdots\right)^N. \qquad \text{(F.9)}$$

Thus, the chemical potential is approximately given by

$$\mu \approx +kT\left[\ln N - \ln(q^t q^e q^r q^v \cdots)\right] \qquad \text{(F.10)}$$

So, with the reactions shown in equation (F.4) at equilibrium and assuming species B and E are the same for simplicity,

$$\ln N_A - \ln N_C - \ln N_D = \ln(q_A^t q_A^e \cdots) - \ln(q_C^t q_C^e \cdots) - \ln(q_D^t q_D^e \cdots)$$

or

$$\frac{N_A}{N_C N_D} \approx \frac{(q_A^t q_A^e \cdots)}{(q_C^t q_C^e \cdots)(q_D^t q_D^e \cdots)} \qquad \text{(F.11)}$$

In terms of species concentrations, n, rather than absolute numbers of particles, N, where $N = nV$ and V is the volume under consideration,

$$\frac{n_A}{n_C n_D} \approx V \frac{(q_A^t q_A^e \cdots)}{(q_C^t q_C^e \cdots)(q_D^t q_D^e \cdots)} \qquad \text{(F.12)}$$

Then, since the translational partition functions are of the form

$$q^{translational} = q^t = V\left(\frac{2\pi mkT}{h^2}\right)^{\frac{3}{2}}, \qquad \text{(F.13)}$$

the volume cancels out in the previous equation.

$$\frac{n_A}{n_C n_D} \approx \left(\frac{m_A}{m_C m_D}\right)^{\frac{3}{2}}\left(\frac{h^2}{2\pi kT}\right)^{\frac{3}{2}}\left(\frac{q_A}{q_C q_D}\right)^{elect}\left(\frac{q_A}{q_C q_D}\right)^{vib}\cdots \qquad \text{(F.14)}$$

Similarly, the ratio of species concentration for the forward and reverse processes

$$A + B \Longleftrightarrow C + D$$

is

$$\frac{n_A n_B}{n_C n_D} \approx \left(\frac{m_A m_B}{m_C m_D}\right)^{\frac{3}{2}}\left(\frac{q_A q_B}{q_C q_D}\right)^{elect}\left(\frac{q_A q_B}{q_C q_D}\right)^{vib}\cdots \qquad \text{(F.15)}$$

As can be seen in these two expressions, equations (F.14) and (F.15), the theoretical LTE ratio of the species concentrations for a given process and its inverse may be obtained from the species' various partition functions. (The partition functions for the species of interest in a hydrogen plasma are given in Appendix II.) Multiplying this value for the theoretical ratio of species concentrations and the forward reaction rate, the reverse reaction rate is easily obtained.

F.3 Rates for Individual Processes

F.3.1 Collisional Excitation and Ionization

$$e^- + H(i) \Longrightarrow H(j) + e^- \, , \, i < j \qquad \text{(F.16)}$$

$$e^- + H(i) \Longrightarrow H^+ + e^- \, . \qquad \text{(F.17)}$$

The rates for the collisional excitation and ionization of atomic hydrogen were calculated using analytic expressions given by Johnson (1972) and by Vriens and Smeets (1980). The first attempts to model the laser-induced fluorescence experiment of Burgess *et al.* (1980) used Johnson's rates. However, the rates of Vriens and Smeets are now generally considered to be more accurate than those of Johnson. Thus, Johnson's rates were used initially in the expanded model in order to compare the current model to the previous model.

Johnson's (1972) rate is given in his equation (36), while the ionization rate is given in equation (39). Vriens and Smeets' (1980) excitation and ionization rates are given in their equations (17) and (8), respectively. However, the analytic fit to the ionization rates given by Vriens and Smeets is invalid for ionizations from the $n = 1$ level and is rather inaccurate for ionizations from the $n = 2$ level. Consequently, the rates used for these processes in the curent model are taken from polynomial fits to experimental data and theoretical estimates given by Janev *et al.* (1987).

F.3.2 Collisional De-excitation

$$e^- + H(j) \Longrightarrow H(i) + e^- \, , \, i < j \qquad \text{(F.18)}$$

The rate for collisional de-excitation, R_{CD}, is obtained from the excitation rate, R_{CE}, by knowing that detailed balance prevails in thermodynamic equilibrium. Thus,

$$n_e \cdot n_{H(j)^*} \cdot R_{CD} = n_e \cdot n_{H(i)^*} \cdot R_{CE}$$

$$R_{CD}(j,i) = \frac{n^*_{H(i)}}{n^*_{H(j)}} \cdot R_{CE}(i,j) \qquad \text{(F.19)}$$

(In these equations, the * indicates an equilibrium population.) Then, since the chemical potentials on either side of the reaction equation must be equal, the ratio $(n_{H(i)}/n_{H(j)})^*$ of the electronic level populations (the Boltzmann relation) is obtained:

$$\left(\frac{n_{H(i)}}{n_{H(j)}}\right)^* = \frac{g_i}{g_j} e^{Ry(\frac{1}{i^2}-\frac{1}{j^2})/T_H} , \qquad \text{(F.20)}$$

where g_i and g_j are the degeneracies of the two states ($2i^2$ and $2j^2$, respectively), Ry is the Rydberg energy (13.605 eV), and T_H is the temperature (in eV) of the hydrogen. Using the Boltzmann relation in the expression for the collisional de-excitation rate ($R_{CD}(j,i)$) above, the result is:

$$R_{CD}(j,i) = \frac{i^2}{j^2} e^{13\,605(\frac{1}{i^2}-\frac{1}{j^2})/T_H} \cdot R_{CE}(i,j) \ , \ i < j \qquad \text{(F.21)}$$

F.3.3 Collisional (Three-Body) Recombination

$$e^- + e^- + H^+ \Longrightarrow e^- + H(i) \qquad \text{(F.22)}$$

The rate for collisional recombination, R_{CR}, is obtained from the collisional ionization rate, R_{CI} by applying detailed balance. Thus,

$$R_{CR}(i) = \left(\frac{n_{H(i)}}{n_e n_{H^+}}\right) R_{CI}(i) \qquad \text{(F.23)}$$

The ratio of the $H(i)$ concentration to that of H^+ and the electrons is obtained by equating the chemical potentials on either side of the reaction equation.

$$\left(\frac{n_{H(i)}}{n_e n_{H^+}}\right) = V \cdot \left[\frac{q_{H(i)}}{q_e q_{H^+}}\right]^{trans} \cdot \left[\frac{q_{H(i)}}{q_e q_{H^+}}\right]^{elect} \qquad \text{(F.24)}$$

Using the translational and electronic partition functions given in Appendix H, this equilibrium ratio becomes

$$\left(\frac{n_{H(i)}}{n_e n_{H^+}}\right) = \left(\frac{4.14165 \times 10^{-16}}{T_e(^\circ\mathrm{K})^{3/2}}\right) i^2 \, e^{(13.605/i^2)/T_H(eV)} \qquad \text{(F.25)}$$

where T_e is the electron temperature in degrees Kelvin and T_H is the hydrogen temperature in electron volts. With this ratio and the collisional ionization rate, R_{CI}, the collisional recombination rate, R_{rmCR}, is:

$$R_{CR}(i) = \left(\frac{4.14165 \times 10^{-16}}{T_e(^\circ\mathrm{K})^{3/2}}\right) i^2 \, e^{(13.605/i^2)/T_H(eV)} \, R_{CI}(i) \, . \qquad \text{(F.26)}$$

F.3.4 Radiative Recombination

$$e^- + H^+ \Longrightarrow H(i) + h\nu \qquad \text{(F.27)}$$

The radiative recombination rates used in the current model are based on those given by Seaton (1959). For computational ease, these rates were calculated using the formulation of Johnson (1972), equations (4) - (9).

F.3.5 Spontaneous Emission

$$H(j) \Longrightarrow H(i) + h\nu \, , i < j \qquad \text{(F.28)}$$

The spontaneous emission rates for transitions in hydrogen are given by the corresponding Einstein A coefficients. These coefficients were calculated using the theoretical expression given by Rybicki and Lightman (1979, equation (10.34)), with tabulated absorption oscillator strengths, $fos(i,j)$, given by Wiese, *et al.*, (1966):

$$A_{ji} = \left(\frac{8\pi^2 e^2 \nu_{ji}^2}{m_e c^3}\right) \left(\frac{g_i}{g_j}\right) fos(i,j) \, , \, i < j \qquad \text{(F.29)}$$

where ν_{ji} is the transition frequency, m_e is the mass of an electron, and g_i and g_j are the degeneracies of the lower and upper electronic states ($2i^2$ and

$2j^2$, respectively). Inserting numerical values in this equation, the Einstein A coefficient is:

$$A_{ji} = 8.02 \times 10^9 \left(\frac{j^2 - i^2}{i j^3} \right)^2 fos(i,j) \qquad \text{(F.30)}$$

For lower level transitions ($i \leq 20$ and $j \leq 25$) the tabulated oscillator strengths given by Wiese, *et al.* (1966) are used. For higher level transitions, an asymptotic expression is used:

$$fos(i,j) = 1.9603 \left(\frac{i j^3}{(j^2 - i^2)^3} \right) . \qquad \text{(F.31)}$$

F.3.6 Photoabsorption and Radiation Trapping

$$H(i) + h\nu \Longrightarrow H(j) \, , i < j \qquad \text{(F.32)}$$

When a photon is emitted as the result of spontaneous emission, it may be re-absorbed by the plasma. This emission and re-absorption may occur repeatedly until the photon is "destroyed." Photon destruction will occur if the photon produces an ionization or if a photo-excited atom collisionally de-excites. This trapping of photons by the plasma effectively decreases the corresponding Einstein A coefficient. (If a transition's photons are completely trapped, the A coefficient is effectively zero.) In order to quantify the effect of radiation trapping on the spontaneous emission rates in a plasma, escape probabilities may be calculated for individual transitions.

The escape probability, $P_e(\tau)$, is defined as the probability, averaged over the frequency profile of a spontaneous emission line, that a photon emitted at the optical depth for a line-center photon will escape from the medium before being absorbed along its path of flight. (See Mihalas (1978), p.335.) The probability for a photon to be absorbed is largest for a photon with a line-center frequency. As photons are absorbed and re-emitted by the atoms or molecules of the medium, the photons are altered in frequency, distributing them over the emission line (frequency) profile. Thus, after a number of such scatterings, a line-center photon may be emitted in a line "wing" where the opacity of the medium is small and the probability of escape is large.

Clearly, then, the mechansims responsible for the broadening of such an emission line play an important role in determining the photon escape probabilities. For a medium in which both Doppler and pressure (collision) broadening are important, in addition to the natural broadening of individual atoms and molecules, the line has a Voigt profile. This profile may be represented as

$$\phi(\nu) = \frac{H(y,x)}{\Delta\nu_D\sqrt{\pi}} \tag{F.33}$$

where

$$H(y,x) = \frac{y}{\pi}\int_{-\infty}^{+\infty} \frac{e^{-t^2}}{y^2+(x-t)^2}\,dt \tag{F.34}$$

$$y = \frac{\Gamma}{4\pi\,\Delta\nu_D}$$

$$x = \frac{\nu-\nu_0}{\Delta\nu_D}$$

$$\Delta\nu_D = \sqrt{\frac{2kT}{m}}\left(\frac{\nu_0}{c}\right) \tag{F.35}$$

$$\Gamma = \gamma_L + \gamma_U + 2\nu_{coll} \tag{F.36}$$

$H(y,x)$ is the Voigt function itself, $\Delta\nu_D$ is the Doppler width of the line, ν_0 is the line center frequency, y is the Lorentz damping rate (in multiples of $\Delta\nu_D$), x is the frequency offset from line center (in multiples of $\Delta\nu_D$), Γ is the total broadening of the transition, γ_L is the natural and collisional (inelastic) broadening of transitions from the lower level, γ_U is the natural and collisional (inelastic) broadening of transitions from the upper level, and ν_{coll} is the elastic collision frequency. For an emission line with Voigt broadening, Mihalas (1978, p.342) obtains an expression for the escape probability which is valid for optical depths, τ, much greater than one:

$$P_e(\tau) \approx \frac{y}{\pi\,x_1}\,,\ \tau \gg 1$$

where

y = Lorentz damping rate

x_1 = $\sqrt{\frac{y\,\tau(\nu_0)}{\pi}}$

$\tau(\nu_0)$ = optical depth at line center .

For $\tau(\nu_0) \leq 1$, the escape probability may be approximated as

$$P_e(\tau) \approx e^{-\tau(\nu_0)/\tau_0}, \tau \leq 1$$

where τ_0 is determined by requiring that the two expressions for the escape probability are equal for $\tau(\nu_0) = 1$. Thus, the escape probability for line radiation with a Voigt profile may be approximated as

$$P_e(\tau) \approx \begin{cases} e^{-\tau(\nu_0)/\tau_0} & \tau \leq 1 \\ \frac{y}{\pi x_1} & \tau > 1 \end{cases} \quad \text{(F.37)}$$

where

$$\tau_0 = -2\ln(\frac{y}{\pi})$$

and y and x_1 are given above. In this expression for the escape probability, the line center optical depth, $\tau(\nu_0)$, for radiation emitted in the spontaneous transition from level j to level i is given by the product (Mihalas, 1978, p.84)

$$\tau(\nu_0) = n_i \cdot L \cdot \phi_V(\nu_0) \cdot \sigma_{ps} \quad \text{(F.38)}$$

where

n_i	=	lower level concentration
L	=	shortest distance to surface of medium
$\phi_V(\nu_0)$	=	Voigt – broadened line – shape profile at line center
σ_{ps}	=	total photon scattering cross – section
	=	$\frac{\pi e^2}{mc} fos(i,j) = .0265\, fos(i,j)$

The effect of this trapping is incorporated in the present model by using "effective" Einstein A coefficients. The "effective" spontaneous emission rate from state j to state i, $R_{SE}(j,i)$, is obtained by multiplying the Einstein A coefficient by the escape probability for that particular transition:

$$R_{SE}(j,i) = A_{ji} \cdot P_e(\tau).$$

F.3.7 Laser Photoabsorption and Stimulated Emission

$$H(i) + h\nu \Longrightarrow H(j), i < j \quad \text{(F.39)}$$

$$H(j) + h\nu \Longrightarrow H(i) + 2h\nu \ , \ i < j \qquad \text{(F.40)}$$

The rates for laser photoabsorption and stimulated emission are obtained using the theoretical Einstein B coefficients and the time-dependent average spectral intensity of the pump laser. The photoexcitation rate is

$$up = \begin{cases} B_{ij}^{L}\langle J_\nu\rangle(1 - e^{-t/trise}) \ , & t \leq 2.5 \cdot trise \\ B_{ij}^{L}\langle J_\nu\rangle(1 - e^{-2.5}) \cdot (1 - \frac{t-2.5 \cdot trise}{toff}) \ , & t > 2.5 \cdot trise \end{cases} \qquad \text{(F.41)}$$

where B_{ij} is the Einstein B coefficient for photoabsorption, $\langle J_\nu \rangle$ is the average spectral intensity of the pump laser at its peak intensity, *trise* is the rise time of the laser, and *toff* is the time for the laser pulse to linearly decrease to zero. The stimulated emission rate is obtained similarly, but with the photoabsorption Einstein B coefficient replaced by the stimulated emission B coefficient. The simplified result is

$$down = up \cdot \left(\frac{i}{j}\right)^2 . \qquad \text{(F.42)}$$

See Appendix G for a more complete discription of the calculation of these rates.

F.3.8 Laser Photoionization of Atomic Hydrogen

$$H(i) + h\nu \Longrightarrow H^+ + e^- \ , \ i < j \qquad \text{(F.43)}$$

The rate (1/sec) for laser photoionization of a hydrogen atom in level i is obtained by multiplying the cross-section for the process, $\alpha_\nu(i)$, by the photon flux provided by the incident laser beam.

$$R_{phion}^{L}(i)(1/\text{sec}) = \alpha_\nu(i) \frac{10^{10} \cdot flxlsr}{\Delta E} \qquad \text{(F.44)}$$

The laser flux, *flxlsr*, is in units of kW/cm^2, the photon energy, ΔE, is in units of ergs, and the cross-section, α_ν, is in units of cm^2. This expression for the photoionization rate is described in more detail in Appendix G. Only single-photon ionization is considered in this model, so that the photoionization rate is set to zero for $\Delta E < E_{ion}(i)$, where $E_{ion}(i)$ is the ionization energy for hydrogen atoms in electronic energy level i. Thus, the H_α pump laser is able to ionize hydrogen atoms above $i = 2$.

F.3.9 Photodetachment of H^-

$$H^- + h\nu \Longrightarrow H(1s) + e^- \qquad \text{(F.45)}$$

The rate (1/sec) for laser photodetachment of electrons from H^- ions may be obtained from the product of the laser photon flux and the cross-section for the reaction.

$$R^L_{pdhm}(1/\text{sec}) \approx \sigma^L_{pdhm}(\text{cm}^2)\ \frac{flxlsr(\text{kW/cm}^2) \times 10^{10}}{\Delta E(\text{ergs})} \qquad \text{(F.46)}$$

For a laser tuned to H_α transition in hydrogen, the cross-section is $3.57 \times 10^{-17}\text{cm}^2$, yielding a rate of

$$R^L_{pdhm}(1/\text{sec}) \approx (1.18 \times 10^5) \times flxlsr(\text{kW/cm}^2) \qquad \text{(F.47)}$$

See Appendix G for a more detailed description of this process.

The photodetachment of H^- ions may also be caused by trapped plasma radiation. Because of the large ground state population of atomic hydrogen, the Lyman series radiation is nearly completely trapped. Although the peak in the photodetachment cross-section, at approximately 1.2 eV, does not correspond to any of the Lyman transitions, the process does have a resonance at 10.976 eV, for photodetachment to the $n = 2$ level of hydrogen. (The cross-section at this resonance is approximately 75% of the cross-section for H_α photons.) Lyman_α radiation, at 10.2 eV, would not have a significant impact on this process, but it is possible that Lyman_β radiation, at 12.09 eV, could. In addition, radiation from molecular hydrogen transitions could play a role in the photodetachment of H^- ions. However, these possibilities were not included in the current model of the plasma.

F.3.10 Dissociative Recombination of H_2^+

$$e^- + H_2^+ \Longrightarrow H(1s) + H(i)\ , i = 2, 3, \ldots \qquad \text{(F.48)}$$

The rates for the dissociative recombination of H_2^+, R_{DR}, were obtained from a polynomial fit by Janev, *et al.* (1987, p.69) to experimental data and theoretical claculations. The rate to each level of hydrogen, H(i), is

given as a percentage of the total rate, which was determined by numerically integrating the experimentally measured total cross-section over a Maxwellian electron distribution.

$$R_{DR}(i)(\mathrm{cm}^3\,\mathrm{sec}) = factor(i) \cdot R_{DR}(total) \qquad \text{(F.49)}$$

$$factor(i) = \begin{cases} 0.100, & i = 2 \\ 0.450, & i = 3 \\ 0.220, & i = 4 \\ 0.120, & i = 5 \\ 0.069, & i = 6 \\ 10./i^3 & i \geq 7 \end{cases}$$

F.3.11 Associative Ionization

$$H(1s) + H(i) \Longrightarrow e^- + H_2^+ \;,\; i = 2,3,\ldots \qquad \text{(F.50)}$$

The rate at which H_2^+ is produced by the associative ionization of two hydrogen atoms, RAI, is obtained from the corresponding dissociative recombination rate, R_{DR}, by invoking detailed balance and assuming that equilibrium prevails..

$$n_{H(1)} \cdot n_{H(i)} \cdot R_{AI}(i) = n_e \cdot n_{H_2^+} \cdot R_{DR}(i)$$

Thus,

$$R_{AI}(i)(\mathrm{cm}^3/\mathrm{sec}) = \left(\frac{n_e n_{H_2^+}}{n_{H(i)} n_{H(1)}}\right) R_{DR}(i)(\mathrm{cm}^3/\mathrm{sec}) \qquad \text{(F.51)}$$

The ratio of the species concentrations shown is obtained by equating the chemical potentials on each side of the reaction equation.

$$\left(\frac{n_e n_{H_2^+}}{n_{H(i)} n_{H(1)}}\right) = \left[\frac{q_e q_{H_2^+}}{q_{H(1)} q_{H(i)}}\right]^{trans} \cdot \left[\frac{q_e q_{H_2^+}}{q_{H(1)} q_{H(i)}}\right]^{elect} \cdot q_{H_2^+}^{rot} \cdot q_{H_2^+}^{vib}$$

Using the partition functions given in Appendix H, with a common temperature, T, for all of the heavy species and another temperature for the electrons, T_e, the equilibrium concentration ratio becomes:

$$\left(\frac{n_e n_{H_2^+}}{n_{H(i)} n_{H(1)}}\right) = \left[\frac{2}{1836} \cdot \frac{T_e}{T}\right]^{\frac{3}{2}} \left[\frac{e^{(2.792 - 13.6/i^2)/T}}{i^2}\right] \left[\frac{T(^\circ\mathrm{K})}{2\theta_r^{H_2^+}}\right] \left[e^{\theta_v^{H_2^+}/2T(^\circ\mathrm{K})} - e^{-\theta_v^{H_2^+}/2T(^\circ\mathrm{K})}\right], \qquad \text{(F.52)}$$

where θ_r and θ_v are the rotational and vibrational temperatures, respectively, given in Appendix H. Using this expression for the equilibrium concentration ratio in the detailed balance equation, the associative ionization rate is obtained from the corresponding dissociative recombination rate.

F.3.12 Collisional Dissociation

$$e^- + H_2^+ \Longrightarrow e^- + H(i) + H^+ \ , \ i = 1,2 \qquad \text{(F.53)}$$

The rates for the collisional dissociation of H_2^+ to H^+ and H(1) or H(2) were obtained from polynomial fits by Janev, *et al.* (1987, p.65) to experimental data and theoretical claculations. The average (over statistically-populated H_2^+ vibrational levels) of the threshold for dissociation to H(1s) is 2.4 eV. Similarly, the average threshold for dissociation to H(2) is 14.0 eV. For the low (0.1 eV - 1.0 eV) electron temperatures of interest in the current plasma model, the polynomial fits given by Janev are invalid below 0.2 eV and 2.0 eV for dissociation to H(1) and H(2), respectively. Since the electron temperatures are much less than the threshold energies of 2.4 eV and 14.0 eV, it may be assumed that the cross-sections are nearly linear where they overlap with the "tails" of the electron distributions. Thus, the expression given by Zel'dovich and Raizer (1966), described at the beginning of this section, may be used to estimate these rates for "low" electron temperatures. (T_e is in eV.)

$$\begin{aligned} R_{CDS}(i=1)\left(\frac{\text{cm}^3}{\text{sec}}\right) &= (6.7 \times 10^7)\sqrt{T_e}(2.386 \times 10^{-15}) \\ &\quad (2.4 + 2T_e)e^{-2.4/T_e} \ , \ T_e < .2\text{eV} \qquad \text{(F.54)} \end{aligned}$$

$$\begin{aligned} R_{CDS}(i=2)\left(\frac{\text{cm}^3}{\text{sec}}\right) &= (6.7 \times 10^7)\sqrt{T_e}(3.23 \times 10^{-18}) \\ &\quad (14.0 + 2T_e)e^{-14/T_e} \ , \ T_e < 2.\text{eV} \qquad \text{(F.55)} \end{aligned}$$

F.3.13 Collisional Association

$$e^- + H(i) + H^+ \Longrightarrow e^- + H_2^+ \ , \ i = 1,2 \qquad \text{(F.56)}$$

The rates for the production of H_2^+ by the collisional association of H^+ and H(i), R_{CAs}, were obtained from the associated collisional dissociation rates, R_{CDs}, by invoking detailed balance.

$$n_e \cdot n_{H^+} \cdot n_{H(i)} \cdot R_{CAs}(i) = n_e \cdot n_{H_2^+} \cdot R_{CDs}(i)$$

Thus,

$$R_{CAs}(i)(\mathrm{cm}^6/\mathrm{sec}) = \left(\frac{n_{H_2^+}}{n_{H(i)} n_{H^+}}\right) R_{CDs}(i)(\mathrm{cm}^3/\mathrm{sec}) \qquad \text{(F.57)}$$

The ratio of the species concentration shown is obtained by equating the chemical potentials on each side of the reaction equation.

$$\left(\frac{n_{H_2^+}}{n_{H(i)} n_{H^+}}\right) = V \cdot \left[\frac{q_{H_2^+}}{q_{H^+} q_{H(i)}}\right]^{trans} \cdot \left[\frac{q_{H_2^+}}{q_{H^+} q_{H(i)}}\right]^{elect} \cdot q_{H_2^+}^{rot} \cdot q_{H_2^+}^{vib}$$

Using the partition functions given in Appendix H, with a common temperature, T, for all of the heavy species and another temperature for the electrons, T_e, the equilibrium concentration ratio becomes:

$$\left(\frac{n_{H_2^+}}{n_{H(i)} n_{H^+}}\right) = \left[\frac{2 \times 4.14165 \times 10^{-16}}{1836\, T_H(^\circ\mathrm{K})}\right]^{\frac{3}{2}} \left[\frac{1}{i^2} e^{\left(2\,792 + 13\,6(1 - 1/i^2)\right)/T}\right] \left[\frac{T(^\circ\mathrm{K})}{2\theta_r^{H_2^+}}\right] \left[e^{\theta_v^{H_2^+}/2T} - e^{-\theta_v^{H_2^+}/2T}\right] \qquad \text{(F.58)}$$

(θ_r and θ_v are the rotational and vibrational temperatures , given in Appendix H.) Using this expression for the equilibrium concentration ratio in the detailed balance equation, the collisional association rate is obtained from the corresponding collisional dissociation rate.

F.3.14 Collisional Detachment

$$e^- + H^- \Longrightarrow e^- + H(1s) + e^- \qquad \text{(F.59)}$$

The rate for the collisional detachment of H^- was obtained from a polynomial fit by Janev, *et al.* (1987, p.227) to experimental data. However,

for electron temperatures below .126 eV, this fit is invalid. In order to approximate this rate for electron temperatures below .126 eV, the expression given by Zel'dovich and Raizer was used (T_e is in eV):

$$R_{CDt}\left(\frac{\text{cm}^3}{\text{sec}}\right) = (6.7 \times 10^7)\sqrt{T_e}(1.2827 \times 10^{-16}) (0.7542 + 2T_e)e^{-.7542/T_e}\ ,\ T_e < .126\text{eV} \qquad \text{(F.60)}$$

F.3.15 Collisional Attachment

$$e^- + H(1s) + e^- \Longrightarrow e^- + H^- \qquad \text{(F.61)}$$

The rate for the production of H^- by collisional (three-body) attachment to H(1), R_{CAt}, was obtained from the associated collisional detachment rate, R_{CDt}, by invoking detailed balance.

$$n_e \cdot n_e \cdot n_{H(1)} \cdot R_{CAt} = n_e \cdot n_{H^-} \cdot R_{CDt}$$

Thus,

$$R_{CAt}(\text{cm}^6/\text{sec}) = \left(\frac{n_{H^-}}{n_{H(1)}n_e}\right) R_{CDt}(\text{cm}^3/\text{sec}) \qquad \text{(F.62)}$$

The ratio of the species concentration shown is obtained by equating the chemical potentials on each side of the reaction equation.

$$\left(\frac{n_{H^-}}{n_{H(1)}n_e}\right) = V \cdot \left[\frac{q_{H^-}}{q_e q_{H(1)}}\right]^{trans} \cdot \left[\frac{q_{H^-}}{q_e q_{H(1)}}\right]^{elect}$$

Using the partition functions given in Appendix H, with a common temperature, T, for all of the heavy species and another temperature for the electrons, T_e, the species concentration ratio becomes:

$$\left(\frac{n_{H^-}}{n_{H(1)}n_e}\right) = \left[\frac{4.14165 \times 10^{16}}{4}\right] \cdot \left[\frac{1}{T_e(^\circ\text{K})}\right]^{\frac{3}{2}} \cdot \left[e^{+.75416/T}\right] \qquad \text{(F.63)}$$

Using this expression for the species concentration ratio in the detailed balance equation, the collisional attachment rate is obtained from the corresponding collisional detachment rate.

F.3.16 Mutual Neutralization

$$H^- + H^+ \Longrightarrow H(1s) + H(i)\ , i = 2,3 \qquad \text{(F.64)}$$

$$H^- + H_2^+ \Longrightarrow H(1s) + H_2(v*) \qquad \text{(F.65)}$$

$$H^- + H_3^+ \Longrightarrow 2H(1s) + H_2(v*) \qquad \text{(F.66)}$$

The rate for the mutual neutralization of H^- and H^+ was obtained from two double polynomial fits by Janev, *et al.* (1987, p. 231) to recent experimental data by Szücs, *et al.* (1984) and Peart *et al.* (1985). The rates for the other two mutual neutralization processes, with H_2^+ and H_3^+, were determined from the low temperature estimate for this rate given by Bates and Boyd (1956). For plasma temperatures between 0.1 and 1.0 eV, these two rates were estimated to be approximately constant, with a value of $2.0 \times 10^{-7}(\mathrm{cm}^3/\mathrm{sec})$. (Hiskes, *et al.*, 1979)

F.3.17 Attachment and Ionization

$$H(1s) + H(i) \Longrightarrow H^- + H^+\ , i = 2,3 \qquad \text{(F.67)}$$

The rates for these attachment and ionization processes, R_{Atl}, were obtained from the corresponding mutual neutralization rates, R_{MN}, by invoking detailed balance.

$$n_{H(1)} \cdot n_{H(i)} \cdot R_{Atl}(i) = n_{H^-} \cdot n_{H^+} \cdot R_{MN}(i)$$

Thus,

$$R_{Atl}(i)(\mathrm{cm}^3/\mathrm{sec}) = \left(\frac{n_{H^-} n_{H^+}}{n_{H(1)} n_{H(i)}}\right) R_{MN}(\mathrm{cm}^3/\mathrm{sec}) \qquad \text{(F.68)}$$

The ratio of the species concentrations shown is obtained by equating the chemical potentials on each side of the reaction equation.

$$\left(\frac{n_{H^-} n_{H^+}}{n_{H(1)} n_{H(i)}}\right) = \left[\frac{q_{H^-} q_{H^+}}{q_{H(i)} q_{H(1)}}\right]^{trans} \cdot \left[\frac{q_{H^-} q_{H^+}}{q_{H(i)} q_{H(1)}}\right]^{elect}$$

Using the partition functions given in Appendix H, this ratio may be expressed as (assuming that the temperatures of all of these species are the

same):

$$\left(\frac{n_{H^-} n_{H^+}}{n_{H(1)} n_{H(i)}}\right) = \frac{e^{+(0.7542-13.605/i^2)/T_H}}{4i^2} \quad , \tag{F.69}$$

where T_H is the temperature (in eV) of these heavy species. Using this ratio of the species concentrations in the detailed balance equation, the rates for the attachment and ionization of H(1s) and H(i) may be obtained from the corresponding mutual neutralization rates.

F.3.18 Collisional Ionization of H_2

$$e^- + H_2(X) \Longrightarrow H_2^+(v) + e^- + e^- \tag{F.70}$$

The rate for the collisional ionization of H_2 in its ground electronic state was obtained from a polynomial fit by Janev *et al.* (1987, p. 59) to experimental data. However, this fit is invalid for electron temperatures below 2.0 eV. Since the 15.4 eV threshold for this process is well above temperatures at or below 2.0 eV, the rates at these low temperatures may be estimated using the expression given by Zel'dovich and Raizer (1966, p. 388). Using the rates given by Janev for temperatures above 2.0 eV, the slope of the (assumed) linear portion of the cross section is found to be $2.81 \times 10^{-18}\text{cm}^2/\text{eV}$. However, since Zel'dovich and Raizer (1966, p. 389) give a value of $5.9 \times 10^{-18}\text{cm}^2/\text{eV}$ for this slope, that figure was used for the low temperature estimates of this reaction rate. (The electron temperature, T_e, is in eV.)

$$\begin{aligned} R_{CIH2}\left(\frac{\text{cm}^3}{\text{sec}}\right) &= (6.7 \times 10^7)\sqrt{T_e}(5.9 \times 10^{-18}) \\ &\quad (15.4 + 2T_e)e^{-15.4/T_e} \ , \ T_e < 2.0\text{eV} \end{aligned} \tag{F.71}$$

F.3.19 Collisional Recombination of H_2^+

$$e^- + H_2^+(v) + e^- \longrightarrow H_2(X) + e^- \tag{F.72}$$

The rate for the collisional (three-body) recombination of H_2^+, R_{CRH2+}, was obtained from the associated collisional ionization rate, R_{CIH2}, by in-

voking detailed balance.

$$n_e \cdot n_e \cdot n_{H_2^+} \cdot R_{CRH2+} = n_e \cdot n_{H_2(X)} \cdot R_{CIH2}$$

Thus,

$$R_{CRH2+}(\mathrm{cm}^6/\mathrm{sec}) = \left(\frac{n_{H_2(X)}}{n_{H_2^+} n_e}\right) R_{CIH2}(\mathrm{cm}^3/\mathrm{sec}) \qquad \text{(F.73)}$$

The ratio of the species concentration shown is obtained by equating the chemical potentials on each side of the reaction equation.

$$\left(\frac{n_{H_2(X)}}{n_{H_2^+} n_e}\right) = V \cdot \left[\frac{q_{H_2(X)}}{q_e q_{H_2^+}}\right]^{trans} \cdot \left[\frac{q_{H_2(X)}}{q_e q_{H_2^+}}\right]^{elect} \cdot \left[\frac{q_{H_2(X)}}{q_{H_2^+}}\right]^{rot} \cdot \left[\frac{q_{H_2(X)}}{q_{H_2^+}}\right]^{vib}$$

Using the partition functions given in Appendix H, this ratio may be expressed as (the temperatures of the heavy species, T_H, are assumed to be equal and independent from the electron temperature, T_e):

$$\left(\frac{n_{H_2(X)}}{n_{H_2^+} n_e}\right) = \left[\frac{4.142 \times 10^{-16}}{T_e^{3/2}}\right] \cdot \left[\frac{e^{(4.748 - 2.792 + 13.605)/T_H}}{4}\right] \cdot \left[\frac{\theta_r^{H_2^+}}{\theta_r^{H_2}}\right] \cdot \left[\frac{e^{\theta_v^{H_2^+}/2T_H} - e^{-\theta_v^{H_2^+}/2T_H}}{e^{\theta_v^{H_2}/2T_H} - e^{-\theta_v^{H_2}/2T_H}}\right] \qquad \text{(F.74)}$$

In this expression, the electron temperature is in °K, while the heavy species temperature is in eV. Values for the vibrational and rotational temperatures are given in Appendix H. Using this ratio of the species concentrations in the detailed balance equation, the collisional recombination rate may be obtained from the collisional ionization rate.

F.3.20 Collisional Dissociation of H_2

$$e^- + H_2(X) \Longrightarrow \begin{cases} H(1s) + H(1s) + e^- \\ H(1s) + H(2s) + e^- \\ H(1s) + H(3) + e^- \\ H(2s) + H(2p) + e^- \end{cases} \qquad \text{(F.75)}$$

The rates for the collisional dissociation of molecular hydrogen in the ground electronic state was obtained from polynomial fits by Janev, *et al.*

(1987, p. 52) to experimental data and theoretical calculations. However, these fits are invalid for electron temperatures below 1.26 eV, 2.51 eV, 3.98 eV, and 5.01 eV, respectively. Since the thresholds for these processes (10.0 eV, 14.9 eV, 19.0 eV and 23.0 eV, respectively) are well above the low (0.1 to 1.0 eV) temperatures of interest in the present investigation, these low temperature rates may be estimated using the expression given by Zel'dovich and Raizer (1966, p. 388). Using the rates given by Janev, the slopes of the (assumed) linear portions of the cross-sections were calculated. The resulting analytic estimates for the reaction rates are (the electron temperature T_e, is in eV):

$$R_{CDH2}(1s,1s)(\frac{\text{cm}^3}{\text{sec}}) = (6.7\times10^7)\sqrt{T_e}(9.66\times10^{-18}) (10.0+2T_e)e^{-10.0/T_e} \ , \ T_e < 1.26\text{eV} \quad \text{(F.76)}$$

$$R_{CDH2}(1s,2s)(\frac{\text{cm}^3}{\text{sec}}) = (6.7\times10^7)\sqrt{T_e}(1.41\times10^{-18}) (14.9+2T_e)e^{-14.9/T_e} \ , \ T_e < 2.51\text{eV} \quad \text{(F.77)}$$

$$R_{CDH2}(1s,3)(\frac{\text{cm}^3}{\text{sec}}) = (6.7\times10^7)\sqrt{T_e}(2.20\times10^{-19}) (19.0+2T_e)e^{-19.0/T_e} \ , \ T_e < 3.98\text{eV} \quad \text{(F.78)}$$

$$R_{CDH2}(2s,2p)(\frac{\text{cm}^3}{\text{sec}}) = (6.7\times10^7)\sqrt{T_e}(1.40\times10^{-19}) (23.0+2T_e)e^{-23.0/T_e} \ , \ T_e < 5.01\text{eV} \quad \text{(F.79)}$$

F.3.21 Collisional Association of H(i) and H(j)

$$H(1s) + H(1s) + e^- \Longrightarrow e^- + H_2(X) \quad \text{(F.80)}$$

$$H(1s) + H(2s) + e^- \Longrightarrow e^- + H_2(X) \quad \text{(F.81)}$$

$$H(1s) + H(3) + e^- \Longrightarrow e^- + H_2(X) \quad \text{(F.82)}$$

$$H(2s) + H(2p) + e^- \Longrightarrow e^- + H_2(X) \quad \text{(F.83)}$$

The rates for the collisional association of hydrogen atoms in various electronic states, R_{CAH2}, was obtained from the associated collisional dissociation rate, R_{CDH2}, by invoking detailed balance.

$$n_e \cdot n_{H(i)} \cdot n_{H(j)} \cdot R_{CAH2}(i,j) = n_e \cdot n_{H_2(X)} \cdot R_{CDH2}(i,j)$$

Thus,

$$R_{CAH2}(i,j)(\mathrm{cm}^6/\mathrm{sec}) = \left(\frac{n_{H_2(X)}}{n_{H(i)}n_{H(j)}}\right) R_{CDH2}(\mathrm{cm}^3/\mathrm{sec}) \qquad \text{(F.84)}$$

The ratio of the species concentration shown is obtained by equating the chemical potentials on both sides of each of the reaction equations above.

$$\left(\frac{n_{H_2(X)}}{n_{H(i)}n_{H(j)}}\right) = V \cdot \left[\frac{q_{H_2(X)}}{q_{H(i)}q_{H(j)}}\right]^{trans} \cdot \left[\frac{q_{H_2(X)}}{q_{H(i)}q_{H(j)}}\right]^{elect} \cdot \left[q_{H_2(X)}\right]^{rot} \cdot \left[q_{H_2(X)}\right]^{vib}$$

Using the partition functions in Appendix H, this ratio may be expressed as:

$$\left(\frac{n_{H_2(X)}}{n_{H(i)}n_{H(j)}}\right) = \left[\left(\frac{2}{1836}\right)^{\frac{3}{2}} \frac{4.14165 \times 10^{-16}}{T_H^{3/2}}\right]\left[\frac{e^{4.748/T_H(eV)}\, e^{13.605(2-\frac{1}{i^2}-\frac{1}{j^2})/T_H(eV)}}{4i^2j^2}\right] \left[\frac{T_H}{2\theta_r^{H_2}}\right]\left[\frac{1}{e^{\theta_v^{H_2}/2T_H} - e^{-\theta_v^{H_2}/2T_H}}\right] \qquad \text{(F.85)}$$

In this expression, the temperatures of both atomic and molecular hydrogen are assumed to be equal. This temperature is in °K unless indicated otherwise. The rotational and vibrational temperatures for H_2 are listed in Appendix H. Using this ratio of the species concentrations in the detailed balance equation, the collisional association rates may be obtained from the collisional dissociation rates.

F.3.22 Associative Detachment from H^-

$$H + H^- \Longrightarrow H_2^-(^2\Sigma_u^+) \Longrightarrow H_2(X) + e^- \qquad \text{(F.86)}$$

The rate for the associative detachment from H^-, by the impact of a neutral hydrogen atom, was obtained from a double polynomial fit by Janev, /it et al. (1987, p. 239). In obtaining this rate, Janev and collaborators used theoretical cross sections normalized to experimentally-measured cross sections in the energy range from 500 eV to 40,000 eV. The validity of this technigue is shown by the close agreement between the rate calculated for this process and the rate measured by Schmeltekopf, *et al.* (1967) at 0.026 eV. Schmeltekopf, *et al.* also point out that the molecular hydrogen

produced will be highly vibrationally excited. To simplify the inclusion of this process in the current plasma model, it was assumed that the incident atomic hydrogen producing this reaction was in the 1s state. The associative detachment rate is calculated in subroutine HMADH and it is included in the rate matrix if the flag "hhmad" is set to one in the main program.

F.3.23 Dissociative Attachment of H_2(X,v*)

$$e^- + H_2(X, v \geq 4) \Longrightarrow H^- + H \qquad \text{(F.87)}$$

The rate for the dissociative attachment of vibrationally-excited hydrogen molecules, R_{DAH2}, was obtained from a polynomial fit by Janev, *et al.* (1987, p. 75) to the calculated cross sections of Wadehra and Bardsley (1978). Further work in this area, confirming and extending these cross sections, was done by Bardsley and Wadehra (1979) and Wadehra (1978). These cross sections were verified by the experimental work of Allen and Wong (1978). They found that the cross sections for dissociative attachment from the $v = 0 - 3$ vibrational levels of H_2(X) were negligible. Since the individual vibrational level populations of molecular hydrogen were not accounted for in the current plasma model, the rate given by the polynomial fit was reduced by the ratio of the appropriate vibrational partition functions.

$$R_{DAH2} = \frac{q^{vib}_{H_2(v\geq 4)}}{q^{vib}_{H_2(v\geq 0)}} R^{Janev}_{DAH2}$$

Using the partition functions given in Appendix II, this rate may be expressed as:

$$R_{DAH2}(\mathrm{cm}^3/\mathrm{sec}) = \frac{\sum_{j=4}^{\infty} e^{-\epsilon_j/k_B T_{H_2}}}{e^{\theta_v^{H_2}/2T_{H_2}} - e^{-\theta_v^{H_2}/2T_{H_2}}} R^{Janev}_{DAH2}\,, \qquad \text{(F.88)}$$

where

$$\epsilon_j = \left(j + \frac{1}{2}\right) h\nu = \left(j + \frac{1}{2}\right) \theta_v^{H_2} k_B$$

The molecular hydrogen temperature in this equation is in units of °K and the vibrational temperature, θ_v, is given in Appendix H.

F.3.24 H Impact Detachment from H^-

$$H + H^- \Longrightarrow H_2^-(^2\Sigma_g^+) \Longrightarrow H + H + e^- \qquad \text{(F.89)}$$

The rate for the detachment of an electron from H^- by the impact of a neutral H atom was obtained from a double polynomial fit by Janev, *etal.* (1987, p. 241). In obtaining this rate, Janev and his collaborators used theoretical cross sections normalized to experimentally-measured cross sections. To simplify the inclusion of this rate in the current plasma model, it was assumed that the atomic hydrogen involved was predominantly in the ground electronic state. It was further assumed that the H^- and H had identical temperatures.

F.3.25 Collisional Attachment to H

$$e^- + H + H \Longrightarrow H + H^- \qquad \text{(F.90)}$$

The rate for the collisional (three-body) attachment of an electron to atomic hydrogen, R_{AeHH}, was obtained from the associated H impact detachment from H^- rate, R_{CDHM}, by invoking detailed balance. (To simplify the inclusion of this rate in the model, the atomic hydrogen involved was assumed to be in the ground electronic state.)

$$n_H \cdot n_H \cdot n_e \cdot R_{AeHH} = n_{H^-} \cdot n_H \cdot R_{CDHM}$$

Thus,

$$R_{AeHH}(\mathrm{cm}^6/\mathrm{sec}) = \left(\frac{n_{H^-}}{n_H n_e}\right) R_{CDHM}(\mathrm{cm}^3/\mathrm{sec}) \qquad \text{(F.91)}$$

The ratio of the species concentrations shown is obtained by equating the chemical potentials on each side of the reaction equation.

$$\left(\frac{n_{H^-}}{n_{H(1)} n_e}\right) = V \left[\frac{q_{H^-}}{q_{H(1)} q_e}\right]^{trans} \cdot \left[\frac{q_{H^-}}{q_{H(1)} q_e}\right]^{elect}$$

Using the partition functions given in Appendix H, this ratio may be expressed as (the temperatures of H and H^- are considered equal and distinct from the electron temperature):

$$\left(\frac{n_{H^-}}{n_{H(1)} n_e}\right) = \left[\frac{4.14165 \times 10^{-16}}{T_e^{3/2}(^\circ K)}\right] \left[\frac{e^{+.7542/T_H(eV)}}{4}\right], \qquad \text{(F.92)}$$

Using this expression for the species concentration ratio in the detailed balance equation, the attachment rate may be obtained from the associated detachment from H^- rate.

F.3.26 Dissociative Recombination of H_3^+

$$e^- + H_3^+ \Longrightarrow H + H + H \quad \text{(a)} \tag{F.93}$$

$$e^- + H_3^+ \Longrightarrow H(n=2) + H_2(v \geq 6) \quad \text{(b)} \tag{F.94}$$

The rates for the dissociative recombination of H_3^+ to three hydrogen atoms, in one case, or to vibrationally-excited molecular hydrogen and electronically-excited hydrogen, in the other, were obtained from a polynomial fit by Janev, *et al.* (1987, p. 71) to theoretical calculations normalized to experimental data. These rates are valid only for a plasma with a Boltzmann distribution of vibrationally-excited H_3^+ molecules: Michels and Hobbs (1984) theoretically estimated that the dissociative recombination of H_3^+ in the $v = 0$ vibrational state is less than that for H_3^+ in vibrationally-excited ($v \geq 3$) states by two orders of magnitude.

The rates for the individual reaction channels (a) and (b) were determined using the branching ratios measured by Mitchell *et al.* (1983) and the theoretical calculations by Kulander and Guest (1979). For temperatures between 0.1 and 1.0 eV, Mitchell and his collaborators reported that the formation of H + H + H is favored by approximately 2.5 : 1.0. Above 1.0 eV, Kulander and Guest indicated that the reverse is true. To simplify the inclusion of the 3H branch of the reaction in the model, it was assumed that these atoms were formed in the ground electronic state.

F.3.27 Associative Ionization of 3H and H + $H_2(v^*)$

$$H + H + H \Longrightarrow e^- + H_3^+ \quad \text{(a)} \tag{F.95}$$

$$H_2(v \geq 6) + H(n=2) \Longrightarrow e^- + H_3^+ \quad \text{(b)} \tag{F.96}$$

The rates for these associative ionization reactions were obtained from the associated dissociative recombination rates by invoking detailed balance and assuming that equilibrium prevails. For reactions (a) and (b),

respectively,

$$(n_H)^3 \cdot R_{AI3H} = n_e \cdot n_{H_3^+} \cdot R_{DRH3P} \cdot BR(3H)$$

$$n_{H_2(v\geq 6)} \cdot n_{H(2)} \cdot R_{AIH2H} = n_e \cdot n_{H_3^+} \cdot R_{DRH3P} \cdot BR(H2H) \ ,$$

where $BR(3H)$ and BR(H2H) are the branching ratios for the two dissociative recombination channels. (Refer to the previous section for a description of these channels.) Thus, the associative ionization rates for the two processes are:

$$R_{AI3H}\left(\frac{\text{cm}^6}{\text{sec}}\right) = \left(\frac{n_e n_{H_3^+}}{(n_H)^3}\right) BR(3H) R_{DRH3P}\left(\frac{\text{cm}^3}{\text{sec}}\right) \qquad \text{(F.97)}$$

$$R_{AIH2H}\left(\frac{\text{cm}^3}{\text{sec}}\right) = \left(\frac{n_e n_{H_3^+}}{n_{H(2)} n_{H_2(v\geq 6)}}\right) BR(H2H) R_{DRH3P}\left(\frac{\text{cm}^3}{\text{sec}}\right) \qquad \text{(F.98)}$$

To simplify the inclusion of reaction (a) in the model, the atomic hydrogen was assumed to be in the ground electronic state. The ratios of the species concentrations in the previous equations are obtained by equating the chemical potentials of the species on each side of the two reaction equations.

$$\left(\frac{n_e n_{H_3^+}}{n_H^3}\right) = V \cdot \left[\frac{q_e q_{H_3^+}}{(q_H)^3}\right]^{trans} \cdot \left[\frac{q_e q_{H_3^+}}{(q_H)^3}\right]^{elect} \cdot \left[q_{H_3^+}\right]^{rot} \cdot \left[q_{H_3^+}\right]^{vib}$$

$$\left(\frac{n_e n_{H_3^+}}{n_{H(2)} n_{H_2(v\geq 6)}}\right) = \left[\frac{q_e q_{H_3^+}}{q_H q_{H_2}}\right]^{trans} \cdot \left[\frac{q_e q_{H_3^+}}{q_H q_{H_2}}\right]^{elect} \cdot \left[\frac{q_{H_3^+}}{q_{H_2}(v\geq 6)}\right]^{rot} \cdot \left[\frac{q_{H_3^+}}{q_{H_2}(v\geq 6)}\right]^{vib}$$

Using the partition functions given in Appendix II, these ratios may be expressed as (the temperatures of the heavy species, T_H, are assumed to be equal and independent from the electron temperature, T_e):

$$\begin{aligned}\left(\frac{n_e n_{H_3^+}}{n_H^3}\right) \;=\; & \left[\left(\frac{\sqrt{3}}{.836}\right)^3 4.14165 \times 10^{-16} \frac{\left(\frac{T_e}{T_H}\right)^3}{(T_e(^\circ K))^{3/2}}\right]\left[\frac{2e^{+36.5675/T_H}}{\left(2e^{+13.605/T_H}\right)^3}\right] \\ & \left[\frac{\sqrt{\pi}}{6}\left(\frac{T_H}{\theta_{RC}^{H_3^+}}\right)^{3/2}\right]\left[\frac{1}{e^{\theta_{v1}^{H_3^+}/2T_H} - e^{-\theta_{v1}^{H_3^+}/2T_H}}\right. \\ & \left.\frac{1}{\left(e^{\theta_{v2}^{H_3^+}/2T_H} - e^{-\theta_{v2}^{H_3^+}/2T_H}\right)^2}\right] , \end{aligned} \qquad \text{(F.99)}$$

where the rotational and vibrational temperatures of H_3^+ are given in Appendix H. Similarly, for the second reaction:

$$\left(\frac{n_e n_{H_3^+}}{n_{H(2)} n_{H_2(v\geq 6)}}\right) = \left[\left(\frac{3 \cdot T_e}{2 \cdot 1836 \cdot T_H}\right)^{3/2}\right]\left[.25 e^{+(36.5675-31.9432-13.605/4)/T_H}\right] \left[\frac{\sqrt{\pi}}{6}\left(\frac{T_H}{\theta_{RC}^{H_3^+}}\right)^{3/2}\left(\frac{2\theta_r^{H_2(v\geq 6)}}{T_H}\right)\right]\left[\frac{1}{e^{\theta_{v1}^{H_3^+}/2T_H} - e^{-\theta_{v1}^{H_3^+}/2T_H}}\right. \left.\frac{1}{\left(e^{\theta_{v2}^{H_3^+}/2T_H} - e^{-\theta_{v2}^{H_3^+}/2T_H}\right)^2} \frac{1}{\sum_{j=6}^{\infty} e^{-\epsilon_j/T_H}}\right], \quad \text{(F.100)}$$

where the rotational and vibrational temperatures of H_3^+ are the same as those in the previous equation and $\epsilon_j = (j+\frac{1}{2})\theta_v^{H_2}$. Using these two expressions for the species concentration ratios in the detailed balance equations, the two associative ionization rates may be obtained from the total dissociative recombination rate and the branching ratios for the two inverse processes. (Refer to the previous section, on the dissociative recombination of H_3^+, for more information on these branching ratios.) For temperatures between 0.1 and 1.0 eV,

$$\begin{aligned} BR(3H) &\approx 2.5/3.5 \\ BR(H2H) &\approx 1.0/3.5 \end{aligned}$$

while for temperatures above 1.0 eV,

$$\begin{aligned} BR(3H) &\approx 1.0/3.5 \\ BR(H2H) &\approx 2.5/3.5 \end{aligned}$$

F.3.28 Proton Exchange from H_2 to H_2^+

$$H_2 + H_2^+ \Longrightarrow H + H_3^+(v+) \quad \text{(F.101)}$$

The rate for this process was obtained from a double polynomial fit by Janev, *et al.* (1987, p. 189) to experimental cross section measurements integrated over Maxwellian electron distributions. The efficiency of this exothermic reaction and the large dissociation energy of the H_3^+ formed make H_3^+ the most abundant ion in many hydrogen plasmas. In addition,

a substantial fraction of these H_3^+ ions have been found to have internal energies in excess of 2 eV. (Bacal, *et al.*, 1981) As a result, the H_3^+ ions in these plasmas are often in high vibrational levels.

F.3.29 Proton Exchange from H_3^+ to H

$$H_3^+ + H \Longrightarrow H_2^+ + H_2 \qquad \text{(F.102)}$$

The rate for this process was obtained from the associated process of proton exchange from H_2 to H_2^+ by invoking detailed balance and assuming that equilibrium prevails. (In order to simplify the inclusion of this process in the model, it was assumed that the atomic hydrogen was in the ground state.)

$$n_{H_3^+} \cdot n_H \cdot R_{H3PXH} = n_{H_2^+} \cdot n_{H_2} \cdot R_{H2XH2P}$$

Thus,

$$R_{H3PXH}(\text{cm}^3/\text{sec}) = \left(\frac{n_{H_2^+} n_{H_2}}{n_{H_3^+} n_H}\right) R_{H2XH2P}(\text{cm}^3/\text{sec}) \qquad \text{(F.103)}$$

The ratio of the species concentrations in this equation is obtained by equating the chemical potentials of the species on each side of the reaction equation.

$$\left(\frac{n_{H_2^+} n_{H_2}}{n_{H_3^+} n_H}\right) = \left[\frac{q_{H_2^+} q_{H_2}}{q_{H_3^+} q_H}\right]^{trans} \cdot \left[\frac{q_{H_2^+} q_{H_2}}{q_{H_3^+} q_H}\right]^{elect} \cdot \left[\frac{q_{H_2^+} q_{H_2}}{q_{H_3^+}}\right]^{rot} \cdot \left[\frac{q_{H_2^+} q_{H_2}}{q_{H_3^+}}\right]^{vib}$$

Using the partition functions given in Appendix H, this ratio may be expressed as:

$$\left(\frac{n_{H_2^+} n_{H_2}}{n_{H_3^+} n_H}\right) = \left[\left(\frac{4}{3}\right)^{\frac{3}{2}}\right]\left[\frac{2e^{+16.3897/T_H} e^{+31.9432/T_H}}{e^{+36.5675/T_H} 2e^{+13.605/T_H}}\right]\left[\frac{\frac{T_H}{2\theta_r^{H_2^+}} \frac{T_H}{2\theta_r^{H_2}}}{\frac{\sqrt{\pi}}{6} \frac{T_H}{\theta_{rr}^{H_3^+}}}\right] \qquad \text{(F.104)}$$

$$\left[\frac{\left(e^{\theta_{v1}^{H_3^+}/2T_H} - e^{-\theta_{v1}^{H_3^+}/2T_H}\right)\left(e^{\theta_{v2}^{H_3^+}/2T_H} - e^{-\theta_{v2}^{H_3^+}/2T_H}\right)^2}{\left(e^{\theta_v^{H_2^+}/2T_H} - e^{-\theta_v^{H_2^+}/2T_H}\right)\left(e^{\theta_v^{H_2}/2T_H} - e^{-\theta_v^{H_2}/2T_H}\right)}\right],$$

where the rotational and vibrational temperatures are given in Appendix H and the temperatures of all of the hydrogen species are assumed to be equal. Using this species concentration ratio in the detailed balance equation, the rate for the process of proton exchange from H_3^+ to H may be obtained.

Bibliography

Allen M and Wong S F 1978 *Physical Review Letters* **41** 1795

Bacal M, Bruneteau A M, Graham W G, Hamilton G W, and Nachman M 1981 *Journal of Applied Physics* **52**(3) 1247-54

Bardsley J N and Wadehra J M 1979 *Physical Review A* **20**(4) 1398-1405

Bates D R and Boyd R L F 1956 *Proceeding of the Physical Society of London, A* **69** 910

Hiskes J R, Bacal M, and Hamilton G W 1979 *Atomic Reaction Rates in H^- and D^- Plasmas* **UCID-18031** (Lawrence Livermore National Laboratory)

Janev R K, Langer W D, Evans K Jr, and Post D E 1987 *Elementary Processes in Hydrogen-Helium Plasmas* (New York: Springer-Verlag)

Johnson L C 1972 *The Astrophysical Journal* **174** 227-36

Kulander K C and Guest M F 1979 *Journal of Physics B: Atomic and Molecular Physics* **12**(16) L501-4

Michels H H and Hobbs R H 1984 *The Astrophysical Journal* **286** L27-29

Mihalas D 1978 *Stellar Atmospheres* (San Francisco: Freeman and Company)

Mitchell J B A, Forand J L, Ng C T, Levac D P Mitchell R E, Mul P M, Claeys W, Sen A, and McGowan J W 1983 *Physical Review Letters* **51**(10) 885-8

Peart B, Bennett M A, and Dolder K 1985 *Journal of Physics B: Atomic and Molecular Physics* **18** L439-44

Rybicki G B and Lightman A P 1979 *Radiative Processes in Astrophysics* (New York: John Wiley and Sons)

Schmeltekopf A L, Fehsenfeld F C and Ferguson E E 1967 *The Astrophysical Journal* **148** L155-6

Seaton M J 1959 *Monthly Notes of the Royal Astronomical Society* **119** 81

Szücs S, Karema M, Terao M, and Brouillard F 1984 *Journal of Physics B: Atomic and Molecular Physics* **17** 1613-22

Takayanagi K and Suzuki H (eds) 1978 *Cross Sections for Atomic Processes, Volume 1* (Nagoya, Japan: Institute of Plasma Physics)

Vriens L and Smeets A H M 1980 *Physical Review A* **22**(3) 940-51

Wadehra J M and Bardsley J N 1978 *Physical Review Letters* **41** 1795

Wiese W L, Smith M W, and Glennon B M 1966 *Atomic Transition Probabilities, Vol 1* (Washington,DC: National Bureau of Standards)

Zel'dovich Ya B and Raizer Yu P 1966 *Physics of Shock Waves and High-Temperature Hydrodynamic Phenomena, Vol 1* (New York: Academic Press)

Appendix G

Laser Interactions with a Hydrogen Plasma

G.1 Laser Reaction Rates

For particles within the volume illuminated by a laser, the reaction rate, per reacting particle, is given by:

$$\text{Reaction Rate (1/sec)} = \frac{\sigma(\text{cm}^2) \cdot \text{laser power density}(\text{W/cm}^2)}{\text{photon energy}(\text{J})}$$

where σ is the cross-section for the laser-induced reaction. The (illuminated) volume reaction rate ($1/\text{cm}^3/\text{sec}$) for this process is then the product of this reaction rate with the number density of the reacting species in the illuminated volume. It is assumed that the laser power will not be significantly attenuated in passing through the plasma. Thus, the laser power density is assumed to be spatially constant throughout the illuminated volume.

G.2 Effects of Small Illumination Volume

In most experiments involving laser-induced effects in plasmas, the illuminated volume comprises only a small fraction of the total plasma volume. For example in the LIF experiment by Burgess, *et al.* (1980), the illuminated volume made up less than 9% of the discharge tube's volume.

Such small illuminated volumes, in conjunction with the short laser pulse lengths often used, guarantee that the laser illumination will have no long-term, macroscopic effects on the plasma. (In the Burgess LIF experiment, the laser pulse length was approximately 200 nsec.)

Although the small relative size of the illuminated region precludes any long-term or macroscopic laser-induced effects, the small size of the region does accentuate any effects due to diffusion. In a random walk diffusion of a particle a distance d from its initial position, the time for this diffusion is the product of the mean time between collisions and the square of the number of mean free paths, l, in the distance d:

$$T_D = (\frac{l}{v_{th}}) \cdot (\frac{d}{l})^2 = \frac{d^2}{l v_{th}}$$

where v_{th} is the thermal speed of the particle and the collision mean free path, l, is approximately given by

$$l \approx \frac{1}{\sqrt{2} n \sigma}$$

For example, consider a .8 eV hydrogen plasma with a neutral atomic hydrogen density of 2.8×10^{16} $1/cm^3$, as in the LIF experiments of Burgess, *et al.* (1980). Assuming a hard sphere collision cross-section, with a sphere diameter of one Angstrom, the collision mean free path is approximately 8.4×10^{-2} cm. Thus, with a thermal speed, v_{th}, of 1.4×10^6 cm/sec, in a diffusion time, T_D, of 200 nsec, the diffusion distance is approximately .15 cm. With a cylindrical illuminated volume of radius .7 cm, as in the Burgess experiments, this diffusion would produce about a 50% increase in the volume affected by a 200 ns laser pulse. Alternatively, laser-induced level population changes would be reduced in magnitude by a factor of 1/3, to 2/3 of their total possible change, during a 200 ns laser pulse.

Obviously, then, the smaller the illuminated region and the longer the time interval involved, the greater this diffusive effect would be. In addition, the rate of diffusion out of the illuminated volume would also be increased by a reduction in the neutral number density. Such reductions, by factors of at least 40%, have been suggested by some experimentalists (Jones, 1982; Long and Newton, 1971; and Newton and Sexton, 1969) to be due to recombination and subsequent long-term attachment at the plasma's confining walls.

Since it is the level populations in the illuminated region which are deduced from experimental observations, the diffusion of particles into and out of this volume must be accounted for in a numerical model. Thus, each species energy level in the model must include both losses due to diffusion out of the illuminated volume and gains due to diffusion into this region from the remainder of the plasma. With no laser illumination, the species within the "plasma core" volume (*i.e.* the illuminated region) will diffuse to the walls, where the ions will be neutralized, atoms may join to form molecules, and all species will be cooled to the wall temperature. These particles will then diffuse back into the plasma core, colliding with other particles and thereby lowering the overall plasma temperature. This diffusive energy loss, combined with radiative losses, are empirically accounted for in the model by assuming that all species in the plasma have the same, experimentally-measured temperature. The diffusion rate back into the plasma core is based on this time-dependent temperature. With laser illumination, the number densities of certain species and energy levels will be altered within the iluminated region. These species will, as with no laser illumination, diffuse to the walls and later return to the plasma core.

G.3 Photoexcitation and Stimulated Emission

A pump laser tuned to a particular transition in hydrogen will produce both photoexcitation (stimulated absorption) and stimulated emission. The laser photoexcitation rate, R_{ij}^{L}, from level i to level j, is the product of the Einstein B_{ij} coefficient and average spectral intensity of the laser, $\langle J_\nu \rangle$:

$$R_{ij}^{L}(1/\text{sec}) = B_{ij}\left(\frac{\text{cm}^2}{\text{erg}\cdot\text{sec}}\right)\cdot\langle J_\nu\rangle\left(\frac{\text{erg}}{\text{sec}\cdot\text{cm}^2\cdot\text{Hz}}\right)$$

Similarly, the stimulated emission rate is:

$$R_{ji}^{L} = B_{ji}\cdot\langle J_\nu\rangle$$

where B_{ji} may be obtained directly from B_{ij} by using the degeneracies of the upper and lower states:

$$B_{ji} = \left(\frac{g_i}{g_j}\right)\cdot B_{ij} = \left(\frac{i}{j}\right)^2\cdot B_{ij}$$

Thus, the stimulated emission rate due to the laser may be obtained directly from the photoexcitation rate:

$$B_{ji} = B_{ij} \cdot \left(\frac{i}{j}\right)^2$$

The Einstein B_{ij} coefficient is:

$$B_{ij} = \left(\frac{\pi e^2}{mc}\right) \cdot \frac{fos(i,j)}{\Delta E}$$

where

$$\left(\frac{\pi e^2}{mc}\right)(\mathrm{cm}^2/\mathrm{sec}) = .0265 \qquad \text{(G.1)}$$

$$fos(i,j) = \text{absorption oscillator strength} \qquad \text{(G.2)}$$

$$\Delta E\ (\mathrm{ergs}) = (13.6 \times 1.602 \times 10^{-12})(1/i^2 - 1/j^2) \qquad \text{(G.3)}$$

The average spectral intensity of the laser may be approximated by assuming that the laser has a square spectral profile with a width of $\Delta\lambda$ (in Angstroms) or $\Delta\nu$ (in Hertz):

$$\langle J_\nu \rangle \left(\frac{\mathrm{erg}}{\mathrm{sec} \cdot \mathrm{cm}^2 \cdot \mathrm{Hz}}\right) = flxlsr \times \left(\frac{10^7 \cdot 10^3}{\Delta\nu}\right) \qquad \text{(G.4)}$$

$$\Delta\nu(\mathrm{Hz}) = \frac{\Delta E^2 \cdot \Delta\lambda \cdot 10^{-8}}{h^2 \cdot c} \qquad \text{(G.5)}$$

$$flxlsr(\mathrm{kW/cm}^2) = \text{laser energy flux} \qquad \text{(G.6)}$$

For the H_α transition in atomic hydrogen, $B_{23} \approx 5.6 \times 10^9$. If the laser flux is 50 $\mathrm{kW/cm}^2$ and the width of the laser line is 5Å, the average spectral intensity of the laser is

$$\langle\ J_\nu\ \rangle \approx 1.44\ \left(\frac{\mathrm{erg}}{\mathrm{sec} \cdot \mathrm{cm}^2 \cdot \mathrm{Hz}}\right).$$

Thus, the photoexcitation rate from the $i = 2$ to the $i = 3$ state is approximately

$$R_{23}^L \approx 8.0 \times 10^9 (1/\mathrm{sec})\ .$$

Since the laser flux will vary with time, the laser's average spectral intensity, $\langle J_\nu \rangle$ will also vary. Consequently, both the laser photoexcitation

and laser stimulated emission rates used in the model are time dependent. The rise and fall of the pump laser pulse were modeled after the pulse described by Burgess and Skinner (1974). It was assumed that the laser exponentially reached its peak power in 2.5 time constants (*trise*), after which it decreased linearly to zero in a time *toff*. With the inclusion of this time dependence of the laser pump pulse, the laser photoexcitation and stimulated emission rates are time dependent. These rates are designated simply as *up* and *down* in the current model.

$$up = \begin{cases} R_{ij}^{L}(1 - e^{-t/trise}) , & t \leq 2.5 \cdot trise \\ R_{ij}^{L}(1 - e^{-2.5}) \cdot (1 - \frac{t - 2.5 \cdot trise}{toff}) , & t > 2.5 \cdot trise \end{cases} \tag{G.7}$$

$$down = up \cdot \left(\frac{i}{j}\right)^2 \tag{G.8}$$

G.4 Photoionization of Atomic Hydrogen

A photon with an energy greater than or equal to the ionization potential for a hydrogen atom in a given electronic level, n, has a finite probability for ionizing the hydrogen atom. That is, for the single-photon ionization of hydrogen,

$$h\nu + H(i) \Longrightarrow H^+ + e^-,$$

the cross-section is given by Mihalas (1978, p99):

$$\begin{aligned} \alpha_\nu(i)(\mathrm{cm}^2) &= \left(\frac{64\pi^4 m e^{10}}{3\sqrt{3} c h^6}\right) \frac{g_{II}(i,\nu)}{i^5 \nu^3} \\ &= (2.815 \times 10^{29}) \frac{g_{II}(i,\nu)}{i^5 \nu^3} \end{aligned} \tag{G.9}$$

where $g_{II}(i,\nu)$ is the bound-free Gaunt factor. The Gaunt factor is a number of order unity at the ionization threshold, rising slowly to about 1.10 (in the limit as $n \rightarrow \infty$ for photon energies about a Rydberg (13.6 eV) above the ionization threshold. (In the experiment by Burgess, *et al.* (1980), the pump laser was tuned to the H_α transition ($\lambda = 6563$Å and $\Delta\epsilon = 1.89$ eV, so that the Gaunt factor was assumed to be one in the model.) Thus, the cross-section for ionization of the $n = 3$ state of hydrogen by the H_α pump laser is approximately

$$\alpha_\nu(3) \approx 1.21 \times 10^{-17} \mathrm{cm}^2$$

The photoionization rate out of $H(i)$ is the product of this cross-section and the flux of those photons with energies greater than or equal to $13.6/i^2$ eV, the ionization threshold for $H(i)$. This product represents the number of photoionizations, per second, per $H(i)$ atom in the volume illuminated by the laser. That is,

$$R^{L}_{phion}(i)(1/\text{sec}) = \alpha_{\nu}\frac{10^{10} flxlsr}{\Delta E} \qquad \text{(G.10)}$$

Using the previously given photoionization cross-section, the photoionization rate for a pump laser tuned to the H_{α} transition in atomic hydrogen is:

$$R^{L}_{phion}(i) \approx 9.767 \times 10^{6}\frac{flxlsr}{i^5} \; . \qquad \text{(G.11)}$$

For example, at a laser flux of 50 kW/cm^2, the photoionization rate out of the $i = 3$ state is:

$$R^{L}_{phion}(3) \approx 2.0 \times 10^{6}(1/\text{sec}) \; .$$

(Note that this rate is over three orders of magnitude less than the rate for photexcitation from the $i = 2$ to the $i = 3$ state.)

G.5 Photodetachment of H^-

The H_{α} pump laser used in the Burgess and Skinner experiment (1980) can also cause electron detachment from the H^- ions in the plasma.

$$h\nu + H^- \Longrightarrow H(1s) + e^-$$

The reaction rate for such a process, per H^- ion, may be approximated as:

$$R^{L}_{pdhm}(1/\text{sec}) \approx \sigma^{L}_{pdhm}(\text{cm}^2)\frac{flxlsr(\text{kW/cm}^2) \times 10^{10}}{\Delta E(\text{ergs})}$$

The cross-section for this process, which is given by Takayanagi and Suzuki (1978), is approximately 3.57×10^{-17} cm^2 for H_{α} ($\lambda = 6565$Å) radiation. Thus, the H^- photodetachment rate, per H^- ion, due to H_{α} laser radiation is:

$$R^{L}_{pdhm}(1/\text{sec}) \approx (1.18 \times 10^{5}) \times flxlsr(\text{kW/cm}^2) \; . \qquad \text{(G.12)}$$

For example, at a laser flux of 50 kW/cm^2, the photdetachment rate is

$$R^{L}_{pdhm} \approx 5.88 \times 10^{6}\ (1/\text{sec})\ .$$

(Note that this rate is nearly three times the photionization rate from the $i = 3$ state, but over three orders of magnitude less than the photoexcitation rate from $i = 2$ to $i = 3$.)

Bibliography

Burgess D D, Myerscough V P, Skinner C H, and Ward J M 1980 *Journal of Physics B: Atomic and Molecular Physics* **13** 1675-1701

Newton A A and Sexton M C 1968 *Journal of Physics B: Atomic and Molecular Physics* **1** 669-80

Newton A A and Sexton M C 1969 *Journal of Physics B: Atomic and Molecular Physics* **2** 1069-74

Long J W and Newton A A 1971 *Numerical Simulation of Hydrogen Afterglow* Proceedings of 10th International Conference on Phenomena in Ionized Gases, Oxford (ed R N Franklin)

Jones W M 1982 *Plasma Physics* **24**(4) 361-68

Mihalas D 1978 *Stellar Atmospheres* (San Francisco: W H Freeman and Company)

Takayanagi K and Suzuki H (editors) 1978 *Cross Sections for Atomic Processes, Volume 1* (Nagoya,Japan: Institute of Plasma Physics)

Appendix H

Partition Functions for Hydrogen Species

H.1 Total Partition Functions

If the Hamiltonian of a system is separable, the total partition function of the system may be simply related to its individual partition functions. For example, for a gas of N_A indistinguishable atoms, the total partition function is approximately given by

$$Q_A = \frac{1}{N_A!}[q_A^{trans} q_A^{elect} q_A^{nuclear}]^{N_A}, \tag{H.1}$$

since the translational Hamiltonian, q_A^{trans}, is separable from the electronic and nuclear Hamiltonians, q_A^{elect} and $q_A^{nuclear}$, respectively. Similarly, the total partition function for a molecular gas may be approximated as

$$Q_M = \frac{1}{N_M!}[q_M^{trans} q_M^{elect} q_M^{nuc} q_M^{rot} q_M^{vib}]^{N_M}, \tag{H.2}$$

if the total Hamiltonian is separable. (McQuarrie, 1976, pp. 93-95) Each of the individual partition functions shown in these two equations are described in detail in the following sections.

H.2 Translational Partition Functions

For an electron, atom, or molecule of mass m and temperature T, the translational partition function is (McQuarrie, 1976, p. 82):

$$q^{trans} = V\left(\frac{2\pi m k_B T}{h^2}\right)^{\frac{3}{2}}, \tag{H.3}$$

where V is the volume to which the particle is confined. The translational partition functions for each of the species in a hydrogen plasma are:

$$q_e^{trans} = \frac{T_e(^\circ K)^{\frac{3}{2}} V(\mathrm{cm}^3)}{4.14165 \times 10^{-16}} \tag{H.4}$$

$$q_H^{trans} = (1836)^{\frac{3}{2}} q_e^{trans}\left(\frac{T_H}{T_e}\right)^{\frac{3}{2}} \tag{H.5}$$

$$q_{H_2}^{trans} = (2 \cdot 1836)^{\frac{3}{2}} q_e^{trans}\left(\frac{T_{H_2}}{T_e}\right)^{\frac{3}{2}} \tag{H.6}$$

$$q_{H_3^+}^{trans} = (3 \cdot 1836)^{\frac{3}{2}} q_e^{trans}\left(\frac{T_{H_3^+}}{T_e}\right)^{\frac{3}{2}} \tag{H.7}$$

Note that the heavy species' translational partition functions are simply related to the electrons' translational partition function if their temperatures are equal.

H.3 Electronic Partition Functions

The electronic partition function for a certain species of particles at temperature T may be represented as a sum over all possible electronic energy levels i:

$$q_e^{elect} = \sum_i \omega_i^e e^{-\epsilon_i/k_B T} \tag{H.8}$$

In this expression, ω_i^e is the degeneracy and ϵ_i is the energy of the ith electronic energy level. Although the zero of energy for a single species is arbitrary, the same electronic energy "zero" must be used for all species in a given reaction in order for their electronic partition functions to be consistent. For those reactions which involved only atomic hydrogen, the energy "zero" was arbitrarily chosen to correspond to the ground state of

the hydrogen atom. Reactions involving diatomic hydrogen species used an energy zero corresponding to completely dissociated H_2, *i.e.* $H(1s)+H(1s)$. For reactions involving the triatomic hydrogen species H_3^+, the energy zero corresponded to the completely dissociated and ionized system $3H^+ + 3e^-$.

The electronic partition functions of the atomic hydrogen species are (20 electronic levels were considered):

$$q_e^{elect} = 2 \tag{H.9}$$

$$q_H^{elect} = \sum_{i=1}^{20} 2i^2 e^{-13.6(1-1/i^2)/T_H(\mathrm{eV})} \tag{H.10}$$

$$q_{H(i)}^{elect} = 2i^2 e^{-13.6(1-1/i^2)/T_H(\mathrm{eV})} \tag{H.11}$$

$$q_{H^+}^{elect} = e^{-13.6/T_H(\mathrm{eV})} \tag{H.12}$$

$$q_{H^-}^{elect} = e^{+.7542/T_H(\mathrm{eV})} \tag{H.13}$$

(The H^- binding energy of .7542 eV was calculated by Pekeris (1958).)

The electronic partition functions of the diatomic hydrogen species were determined using the energy levels given by Sharp (1971). The molecular energies used correspond to the energy differences between the bottom of each potential well and the reference energy of the $H(1s)+H(1s)$ system. Because the next higher electronic state of H_2 has an energy significantly greater than the ground state energy, only the first term in its partition function was considered.

$$q_{H_2}^{elect} \approx 1e^{+4.7481/T_{H_2}(\mathrm{eV})} \tag{H.14}$$

$$q_{H_2^+}^{elect} = 2e^{+2.792/T_{H_2^+}(\mathrm{eV})} e^{-13.6/T_{H_2^+}(eV)} \tag{H.15}$$

$$q_{H_2^-}^{elect} = 2e^{+1.7737/T_{H_2^-}(\mathrm{eV})} e^{+.7542/T_{H_2^-}(\mathrm{eV})} \tag{H.16}$$

The partition functions for reactions involving H_3^+ were determined using an energy zero corresponding to the completely dissociated and ionized system $3H^+ + 3e^-$. The energy minimum of the H_3^+ potential well (-1.3439 Hartree) was calculated by Mentch and Anderson (1981). In terms of this energy zero, the electronic partition functions of the hydrogen species are:

$$q_H^{elect} = \sum_{i=1}^{20} 2i^2 e^{-(13.6/i^2)/T_H(eV)} \tag{H.17}$$

$$q_{H_2}^{elect} \approx 1e^{+31.94318/T_{H_2}(eV)} \quad \text{(H.18)}$$

$$q_{H_2^+}^{elect} = 2e^{+16.38967/T_{H_2^+}(eV)} \quad \text{(H.19)}$$

$$q_{H_3^+}^{elect} = 1e^{+36.56752/T_{H_3^+}(eV)} \quad \text{(H.20)}$$

H.4 Nuclear Partition Functions

The nuclear partition function has a form similar to that of the electronic partition function, but with energy levels separated by millions of electron volts rather than tens of electron volts. As a result, at the temperatures of interest here, this partition function contributes to Q only a multiplicative constant, the degeneracy of the ground nuclear state, ω_1^n. Since the nuclear state is rarely altered in chemical processes, such as those occuring in a 1 eV hydrogen plasma, its effect was neglected by arbitrarily setting the value of its partition function to one.

$$q^{nuclear} = 1 \quad \text{(H.21)}$$

H.5 Vibrational Partition Function

The vibrational energy levels of a molecule, with respect to the bottom of its internuclear potential well, are given by:

$$\epsilon_j = (j + \frac{1}{2})\, h\nu \;,\; j = 0, 1, 2, \ldots \quad \text{(H.22)}$$

where $\nu = \sqrt{\kappa/\mu}/2\pi$, the force constant for the molecule is κ, and μ is its reduced mass. With these energy levels, the vibrational partition function,

$$q^{vib} = \sum_j e^{-\epsilon_j/k_B T} \quad \text{(H.23)}$$

becomes

$$q^{vib} = \frac{1}{e^{\theta_v/2T} - e^{-\theta_v/2T}} \quad \text{(H.24)}$$

where θ_v is termed the vibrational temperature and T is the temperature of the particular molecular species.

$$\theta_v = \frac{h\nu}{k_B} \quad \text{(H.25)}$$

The vibrational partition function for each molecular species has the same form as shown above, but with a unique value for its vibrational temperature, θ_v. For the diatomic hydrogen species that were considered, the vibrational temperatures are:

$$\begin{aligned} \theta_v^{H_2} &= 6270°\text{K} \\ \theta_v^{H_2^+} &= 3288°\text{K} \\ \theta_v^{H_2^-} &= 2054°\text{K} \end{aligned} \tag{H.26}$$

The vibrational temperature for H_2 was obtained from McQuarrie (1976, p. 98), while that for H_2^+ was calculated using the definition of the vibrational temperature and the energies given by Sharp (1971) for the lowest vibrational level and the potential well minimum. The temperature for H_2^- was determined similarly using an estimated value for the energy of the lowest vibrational level ($h\nu/2 \approx .05 \cdot D_e^{H_2^-}$, where D_e is the dissociation energy of H_2^-).

The triatomic hydrogen speices H_3^+ has three vibrational modes, a symmetric stretch and two degenerate asymmetric stretches. In its ground electronic state, H_3^+ has an equilateral configuration which gives it vibrational fundamental frequencies of 3186 cm^{-1} and 2521 cm^{-1} for the symmetric and asymmetric modes, respecitvely. (Kulander, 1986) Using the definition of vibrational temperature and these fundamental frequencies, the vibrational temperatures of the symmetric ($v1$) mode and the two asymmetric ($v2$ and $v3$) modes are:

$$\begin{aligned} \theta_{v1}^{H_3^+} &= 4583°\text{K} \\ \theta_{v2}^{H_3^+} &= 3614°\text{K} \\ \theta_{v3}^{H_3^+} &= 3614°\text{K} \end{aligned} \tag{H.27}$$

The total vibrational partition function for H_3^+ is the product of all three vibrational mode partition functions.

$$q_{H_3^+}^{vib} = \left[\frac{1}{e^{\theta_{v1}^{H_3^+}/2T} - e^{-\theta_{v1}^{H_3^+}/2T}} \right] \cdot \left[\frac{1}{e^{\theta_{v2}^{H_3^+}/2T} - e^{-\theta_{v2}^{H_3^+}/2T}} \right]^2 \tag{H.28}$$

H.6 Rotational Partition Function

The rotational energy levels and degeneracies for a rigid diatomic molecule are

$$\epsilon_J = \frac{\hbar^2}{2I} J(J+1) \ , \ J = 0, 1, 2, \ldots \tag{H.29}$$

$$\omega_J^r = 2J + 1 \ , \tag{H.30}$$

where I is the moment of inertia, μr_e^2, of the molecule. With these energy levels and degeneracies, the rotational partition function,

$$q^{elect} = \sum_{J=0}^{\infty} (2J+1) e^{-\epsilon_J / kT} \ , \tag{II.31}$$

may be approximated (for heteronuclear molecules) as:

$$q^{rot}_{heteronuclear} \approx \frac{T}{\theta_r} \ , \ \theta_r \ll T \tag{H.32}$$

In this expression, the constant θ_r (in degrees Kelvin) is termed the "characteristic temperature" of rotation. In terms of fundamental quantities, this rotational temperature is defined to be

$$\theta_r = \frac{\hbar^2}{2\kappa I} \ , \tag{H.33}$$

where $I = \mu r_e^2$ is the moment of inertia in a rigid-rotor model of a diatomic molecule and κ is the force constant for the (assumed) Hooke's Law force holding the two atoms together. However, for homonuclear diatomic molecules there are two indistinguishable orientations of each molecule. That is, there is a two-fold axis of symmetry perpendicular to the internuclear axis which doubles the degeneracy of each rotational energy level. Thus, for homonuclear diatomic molecules, the rotational partition function is approximately given by:

$$q^{rot}_{homonuclear} \approx \frac{T}{2\theta_r} \ , \ \theta_r \ll T \tag{H.34}$$

The rotational partition functions for the diatomic species in a hydrogen plasma are given by this equation, but with unique values for the rotational

temperatures.

$$\begin{aligned} \theta_r^{H_2} &= 87.7°\text{K} \\ \theta_r^{H_2^+} &= 42.9°\text{K} \\ \theta_r^{H_2^-} &= 87.7°\text{K} \end{aligned} \tag{H.35}$$

The rotational temperature for H_2 was obtained from McQuarrie (1976, p. xx), while that for H_2^+ was calculated using the definition for θ_r and spectroscopic values for I and κ from Herzberg. (197X, p. xx) The rotational temperature for H_2^- was assumed to be approximately the same as that of H_2 since their internuclear separations are nearly identical. (Sharp, 1971)

The rotational partition function for the triatomic molecule H_3^+ is similar in form to those for the diatomic molecules. However, in its equilateral ground-state configuration, H_3^+ has three distinct modes of rotation, as shown in Figure H.1. The bond lengths in this configuration are considered

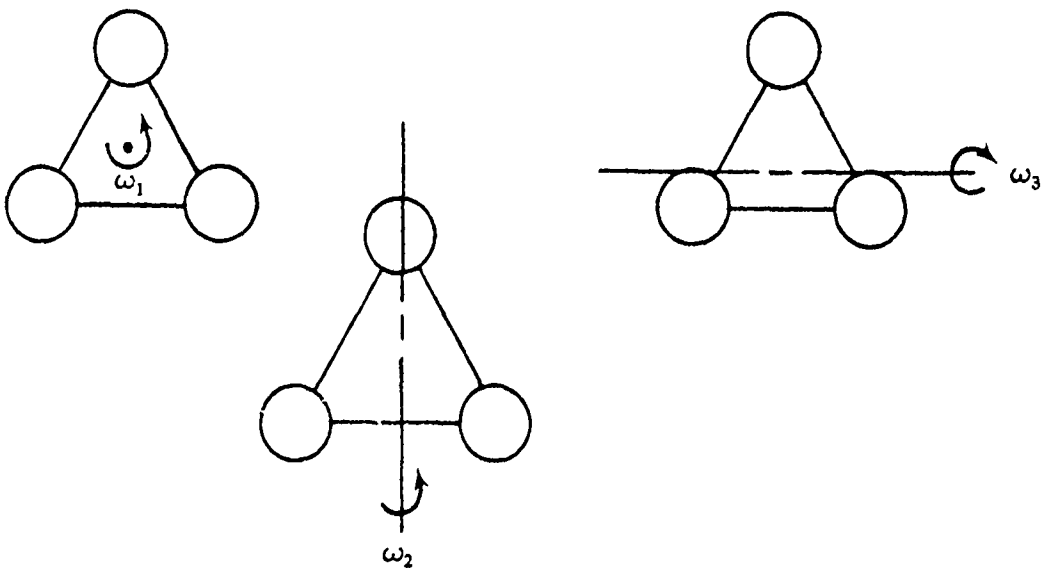

Figure H.1: Rotational Modes of H_3^+

to be .8734 Å. (Carrington and Kennedy, 1984) Although there are three

distinct modes of rotation, the moments of inertia associated with ω_2 and ω_3 are identical and, by the perpendicular axis theorem, their moments of inertia must sum to equal the moment of inertia for the ω_1 rotation. ($I_2 = I_3 = I_1/2$) Using the momemts of inertia and force consatants obtained experimentally by Oka (1980) for H_3^+, rotational temperatures were obtained using the definition of the rotational temperature.

$$\begin{aligned} \theta_{r1}^{H_3^+} &= 31.59°\text{K} \\ \theta_{r2}^{H_3^+} &= 63.18°\text{K} \\ \theta_{r3}^{H_3^+} &= 63.18°\text{K} \end{aligned} \tag{II.36}$$

With these rotational temperatures, the rotational partition function for H_3^+ was obtained using the expression given by McQuarrie (1976, p. xx)

$$q_{H_3^+}^{rot} = \frac{\sqrt{\pi}}{3}\sqrt{\frac{T^3}{\theta_{r1}\theta_{r2}\theta_{r3}}} \tag{H.37}$$

(The factor of 3 is due to the three-fold symmetry of this triatomic system.) Since $\theta_{r1}^{H_3^+} = 2 \cdot \theta_{r2}^{H_3^+} = 2 \cdot \theta_{r3}^{H_3^+}$, the rotational partition function may be simplified

$$q_{H_3^+}^{rot} = \frac{\sqrt{\pi}}{6}\left(\frac{T(°\text{K})}{\theta_{r1}^{H_3^+}}\right)^{\frac{3}{2}}. \tag{H.38}$$

Bibliography

Carrington A and Kennedy R A 1984 *Journal of Chemical Physics* **81**(1) 91-112

Kulander K C 1986 *Journal of Chemical Physics* **85**(4) 1938-49

McQuarrie D M 1976 *Statistical Mechanics* (New York: Harper and Row)

Mentch F and Anderson J B 1981 *Journal of Chemical Physics* **74**(11) 6307-11

Pekeris C L 1958 *Physical Review* **112** 1649

Sharp T E 1971 *Atomic Data* **2** 119-69

Appendix I

Ambipolar Diffusion Coefficients

I.1 Diffusion in a Mixture of Gases

The ambipolar diffusion coefficients for H^+, H^-, H_2^+, and H_3^+ in a mixture of atomic and molecular hydrogen may be obtained using Dalgarno's (1958) theoretical mobilities for hydrogen ions in atomic hydrogen and the experimentally measured mobilities for hydrogen ions in molecular hydrogen, as presented in the compilation by Ellis, *et al.* (1976). Since mobility is a function of gas temperature and pressure, these mobilities are given at a pressure of one atmosphere and for a temperature of 273.16 °K. In this form, the mobility is termed the "reduced" mobility, K_0. Since these reduced mobilities are usually given for a certain species in a single species background gas, the mobility of the species in a mixture of gases must be approximated using Blanc's Law (Ellis, *et al.*, 1976):

$$\frac{1}{K_0} = \sum_j \frac{X_j}{K_{0j}} C$$

where K_{0j} is the reduced mobility measured in the pure gas j and X_j is the mole fraction of species j in the mixture. The ambipolar diffusion coefficient in a gas at temperature $T(^\circ\mathrm{K})$ and pressure p (Torr) may be obtained from the total reduced mobility using the relationship given by

McDaniel and Mason (1973, p. 27),

$$D_a = \frac{K_0 T^2}{2.086 \times 10^3 \times p} .$$

Equivalently, the ambipolar diffusion coefficient may be expressed as

$$D_a(\mathrm{cm}^2/\mathrm{sec}) = K_0(\mathrm{cm}^2/\mathrm{volt}\cdot\mathrm{sec}) \times 5.37 \times 10^{19} \times T(\mathrm{eV})/n(1/\mathrm{cm}^3) \quad \text{(I.1)}$$

where n is the number density of the background gas. Since the plasma being modeled in the present analysis has only a minimal radial electric field, formed by the ambipolar diffusion itself, the "zero-field" reduced mobility is used to calculate the ambipolar diffusion coefficient.

I.2 Ionic Mobilities in Atomic Hydrogen

The zero-field reduced mobilities of the ionic species in atomic hydrogen were obtained from theoretical calculations. Dalgarno, *et al.* (1958) give theoretical values for the zero-field reduced mobility of H^+ in H. These values were fit to an analytic expression in order to simplify their use in the present computational model.

$$K_{0H}^{H^+} \approx \begin{cases} -2.4525816 \ln(T(^\circ\mathrm{K})) & +24.3418333,\ 1000^\circ\mathrm{K} \le T < 2000^\circ\mathrm{K} \\ -1.8553063 \ln(T(^\circ\mathrm{K})) & +19.8020025,\ 2000^\circ\mathrm{K} \le T < 5000^\circ\mathrm{K} \\ -1.0098865 \ln(T(^\circ\mathrm{K})) & +12.6013987,\ 5000^\circ\mathrm{K} \le T \end{cases} \quad \text{(I.2)}$$

In addition, since the mobility of a species is inversely proportional to the square root of the reduced mass of the species and background gas particles (Dalgarno, *et al.*, 1958), the mobilities of H_2^+ and H_3^+ in H could be determined directly from the mobility of H^+ in H. That is,

$$K_{0H}^{H_2^+} \approx \frac{\sqrt{1/2}}{\sqrt{2/3}} K_{0H}^{H^+} \approx .8660 \times K_{0H}^{H^+} \quad \text{(I.3)}$$

$$K_{0H}^{H_3^+} \approx \frac{\sqrt{1/2}}{\sqrt{3/4}} K_{0H}^{H^+} \approx .8165 \times K_{0H}^{H^+} \quad \text{(I.4)}$$

The zero-field reduced mobility of H^- in H was determined theoretically by Dalgarno and McDowell (1956). At temperatures between 0.1 eV and 1.0 eV this mobility asymptotically approaches a value of

$$K_{0H}^{H^-} \approx 1.5 \tag{I.5}$$

The zero-field reduced mobilities of H^+, H_2^+, H_3^+, and H^- in H, which were used in the present model, are shown in Figure I.1.

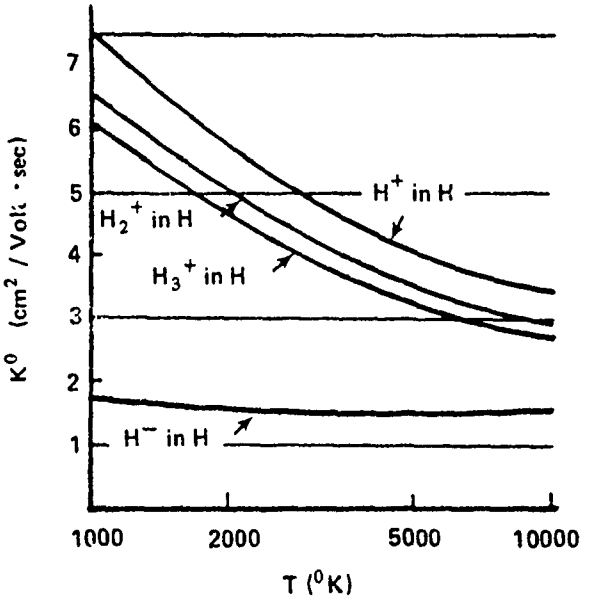

Figure I.1: Ion Mobilities in Atomic Hydrogen

I.3 Ionic Mobilities in Molecular Hydrogen

The mobilities of hydrogen ions in molecular hydrogen were obtained from the compilation of experimental results given by Ellis, *et al.* (1976). Using the concept of an "effective" temperature, Ellis and his collaborators were able to show that a wide range of experimental mobility measurements could be concisely presented as a function of such an "effective" temperature. The effective temperature corresponds to the kinetic energy of an

ion swarm and the neutral gas in their center-of-mass frame. To a first approximation, this effective temperature is given by

$$\frac{3}{2}k_B T_{eff} = \frac{3}{2}k_B T + \frac{1}{2}M v_d^2 ,$$

where k_B is Boltzmann's constant, M is the mass of the neutral molecules, v_d is the drift velocity of the ions in the electric field within the plasma, T is the gas temperature, and T_{eff} is the effective temperature of the diffusing ions. In the present context, however, the internal electric fields created by the ambipolar diffusion of electrons and positive ions are not large enough to produce an ion drift velocity which would produce a significant difference between the gas and effective temperatures. Thus, zero-field reduced mobilities were obtained from the data given by Ellis, *et al.* by replacing T_{eff} with the gas temperature, T.

Analytic expressions were used to represent these zero-field reduced mobilities in molecular hydrogen for temperatures between 0.1 eV and 1.0 eV. The expressions used for the H^+, H^-, and H_3^+ mobilities were:

$$K_{0H_2}^{H^+} \approx -0.9320 \ln(T(^\circ\mathrm{K})) + 21.0841 \quad \text{(I.6)}$$

$$K_{0H_2}^{H^-} \approx -2.8854 \ln(T(^\circ\mathrm{K})) + 61.1317 \quad \text{(I.7)}$$

$$K_{0H_2}^{H_3^+} \approx -1.9883 \ln(T(^\circ\mathrm{K})) + 21.5127 \quad \text{(I.8)}$$

Although Ellis, *et al.* did not give values for the mobility of H_2^+ in H_2, this mobility was estimated from the mobility of H^+ in H_2 by relating the theoretical expressions for their mobilities and comparing the result to a directly-calculated theoretical mobility. As mentioned previously, the mobility of an ion in a neutral gas is inversely proportional to the square root of the reduced mass of the ion and neutral particle. Consequently, the zero-field reduced mobility of H_2^+ in H_2 is approximately given by

$$K_{0H_2}^{H_2^+} \approx \frac{\sqrt{2/3}}{\sqrt{1}} K_{0H_2}^{H^+} \approx .8165 \times K_{0H_2}^{H^+} .$$

However, although the theoretical mobility calculated by Mason and Vanderslice (1959) agree with this estimate in the limit as $T \rightarrow 0^\circ\mathrm{K}$, their theoretical mobility decreases slightly from this estimate at higher temperatures. Thus, in the present model the reduced mobility of H_2^+ in H_2 was

assumed to be approximately 76% of the mobility of H^+ in H_2. The lack of experimental data on the mobility of H_2^+ is not too surprising since the cross-section for the reaction $H_2^+ + H_2 \Rightarrow H_3^+ + H$ is, in the words of R. N. Varney (1960), simply "enormous." Thus, as asserted by Barnes, *et al.* (1961), "the H_2^+ ion is never observed in hydrogen mobility experiments" and the ions which do appear are H_3^+ and H^+.

The ionic mobilities in molecular hydrogen which were used in the current model are shown in Figure I.2. The dramatic rise in the H_3^+ mobility

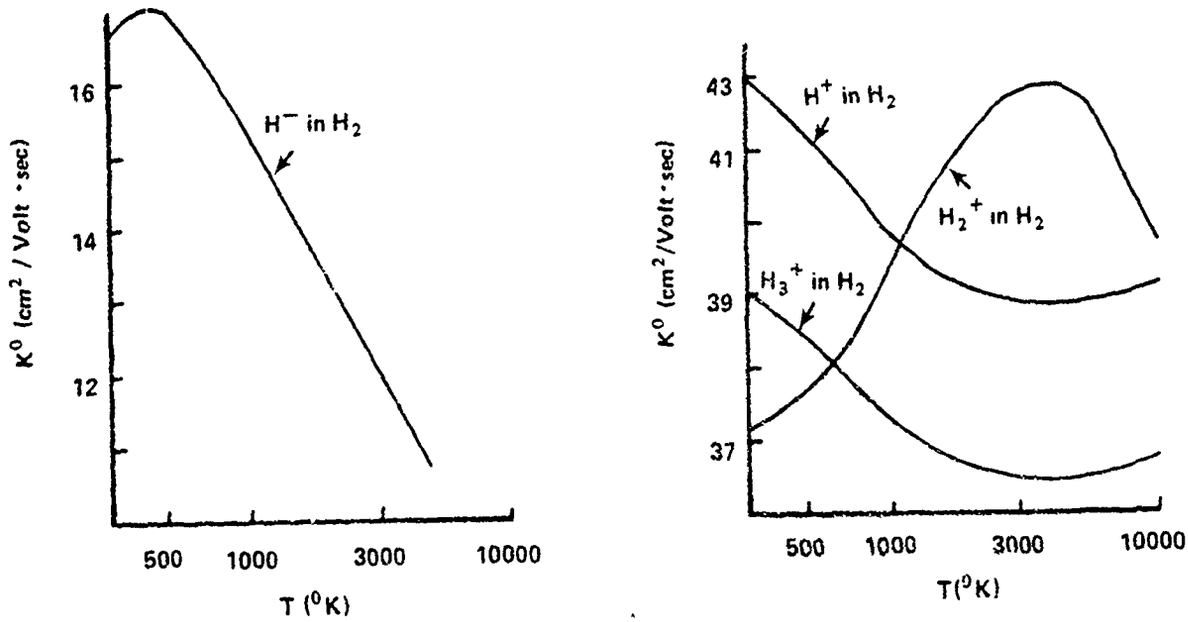

Figure I.2: Ionic Mobilities in Molecular Hydrogen

appears to be a consequence of the fact that the binding energies of H_2 and H_3^+, 4.48 eV and 4.18 eV, respectively, are nearly the same. Thus, if the H_3^+ has a temperature of a few tenths of an eV, the proton (charge) exchange process is "virtually a resonance phenomenon" and the mobility of the H_3^+ is greatly increased. (Varney, 1960)

Bibliography

Barnes W S, Martin D W, and McDaniel E W 1961 *Physical Review Letters* **6**(3) 110-11

Dalgarno A and McDowell M R C 1956 *Proceedings of the Physical Society A* **69** 615

Dalgarno A 1958 *Philosophical Transactions A* **250** 426-39

Ellis H W, Pai R Y, McDaniel E W, Mason E A, and Viehland L A 1976 *Atomic Data and Nuclear Data Tables* **17** 177-210

Mason E A and Vanderslice J T 1959 *Physical Review* **114**(2) 497-502

McDaniel E W and Mason E A 1973 *The Mobility and Diffusion of Ions in Gases* (New York: Wiley)

Varney R N 1960 *Physical Review Letters* **5**(12) 559-60

Appendix J

Neutral H and H_2 Diffusion Coefficients

The mutual diffusion coefficients of H and H_2 in their mixture were obtained from calculations based on experimental data (Weissman and Mason, 1962) and from a theoretical extension of those calculations to higher temperatures (Vanderslice, *et al.*, 1962). (The theoretical extension covers the temperature range from 1000°K to 15000°K.) These calculations assumed that both atomic and molecular hydrogen remained in their ground electronic states even though it is known that hydrogen is appreciably ionized for temperatures above 5000°K. However, since the plasma being modeled is at a pressure of less than .45 Torr, the excitation and ionization rates are much lower and this assumption may not be a serious limitation. Vanderslice, *et al.* (1962) calculated the diffusion coefficients for a range of temperatures at a pressure of one atmosphere. The coefficients obtained for H_2 in H_2 and H in H were, for each temperature, lower than the coefficient for diffusion of H in H_2 (or H_2 in H). Although this coefficient is actually a function of the relative atomic and molecular composition of the mixture, to the level of approximation used by Vanderslice, *et al.*, the diffusion coefficient is independent of composition. In fact, an earlier theoretical investigation by Amdur (1936) actually determined the effect of mixture composition by varying the composition from a gas of van der Walls molecules to a gas of elastic spheres without attractive forces. Amdur found that the diffusion coefficient varied by less than four percent over the entire range of compositions.

Thus, the mutual diffusion coefficients given by Weissman and Mason (1962) and Vanderslice, *et al.*, (1962), for an arbitrary mixture composition, were fit to an analytic expression and then adjusted to correspond to a lower pressure. At a pressure of one atmosphere the coefficient for the diffusion of atomic hydrogen in a mixture of atomic and molecular hydrogen at temperature T is:

$$D_H^0 \approx \exp[+1.9215 \ln(T(^\circ\mathrm{K})) - 10.4602] . \qquad \text{(J.1)}$$

At the reduced pressure in the current model the diffusion coefficient becomes:

$$D_H(\mathrm{cm}^2/\mathrm{sec}) = D_H^0 \frac{(2.69 \times 10^{19})\ (1/\mathrm{cm}^3)(273^\circ\mathrm{K})}{(n_H + n_{H_2})\ T} . \qquad \text{(J.2)}$$

In addition, since diffusion coefficients are, in general, given as

$$D = v_{avg} \cdot (mean\ free\ path)/3 ,$$

they are thus proportional to $1/\sqrt{mass}$. Consequently, the diffusion coefficient for H_2 in a mixture of atomic and molecular hydrogen is simply:

$$D_{H_2} = D_H/\sqrt{2} \qquad \text{(J.3)}$$

Bibliography

Amdur I 1936 *Journal of Chemical Physics* 4 339-43

Vanderslice J T, Weissman S, Mason E A, and Fallon R J 1962 *Physics of Fluids* 5(2) 155-64

Weissman S and Mason E A 1962 *Journal of Chemical Physics* 36(3) 794-97

Appendix K

Neutral H and H_2 Diffusion

The rates of neutral H and H_2 diffusion from the plasma chamber walls back into the plasma core were determined only approximately, using a combination of theoretical models and experimental observations. In order to determine the neutral diffusion rates, diffusion coefficients must be supplemented with a knowledge of the radial concentration gradients of the species and their temperatures. The concentrations of H and H_2 near the walls are a result of several competing processes: recombination of adsorbed hydrogen within the walls and desorption of H_2, surface recombination of incident atomic hydrogen with adsorbed hydrogen, and diffusive losses of both H and H_2 back into the plasma core. The complexity of these interactions and the limited experimental data did not allow for an accurate model of this diffusion.

K.1 Adsorbed Hydrogen

Hydrogen is readily adsorbed by many materials, including pyrex. In the aftermath of the z-pinch which formed the plasma being investigated, it was assumed that the pyrex was "saturated" to a depth on the order of 10 μm. Thus, it was assumed that, of the hydrogen "missing" from the plasma, the fraction adsorbed in the walls decreased exponentially with time, in a manner given by

$$f_{wall} \approx .45e^{-t/100\mu s} + .05 \qquad \text{(K.1)}$$

The remainder of this "missing" hydrogen was assumed to reside in a layer near the walls.

K.2 Wall Sheath

The existence of a wall sheath of hydrogen in plasmas similar to those being investigated was described by Jones (1980), who claimed that up to 40% of the hydrogen was "trapped" near the walls of the discharge chamber for several hundred microseconds. Numerical simulations of cylindrical plasmas by Long and Newton (1971) indicated that such a wall sheath is quickly formed after the plasma is produced and that it decreases in thickness as the plasma cools. In an attempt to model the z-pinch plasma being investigated, the predictions of Long and Newton were used to model the sheath thickness as:

$$\Delta r(\text{cm}) = 1.238e^{-t/46.9\mu s} + .05 \qquad \text{(K.2)}$$

This wall sheath is composed of both atomic and molecular hydrogen. In order to determine the concentration of each species, measured surface recombination coefficients for incident H atoms were used, along with estimated volume recombination coefficients, and a steady state was assumed to exist. That is, assuming that a steady state exists in the wall sheath, the H_2 production rate by surface and volume recombination was required to equal the H_2 loss rate by diffusion back into the plasma. As shown later in this appendix, this assumption allows the H and H_2 concentrations in the sheath to be determined.

K.3 "Missing" Hydrogen

In order to obtain these concentrations, it is first necessary to estimate how much of the hydrogen is actually "missing" from the plasma at each instant in time. In the current model, values for the species concentrations in the plasma core were determined using a rate equation formalism. Assuming that these concentrations were approximately constant within the entire cylindrical container (of length l and radius a), the total number of hydrogen atoms which could be formed from this plasma (at each time step

taken by the model) was computed,

$$N_H = \pi \cdot a^2 \cdot l \cdot fill \ ,$$

where $fill$ is the sum of the concentrations of all hydrogenic species, weighted by the number of H atoms that each could form. By comparison, the total number of hydrogen atoms which could be formed from the molecular hydrogen used to initially fill the cylindrical container is given by

$$N_H^0 = \pi \cdot a^2 \cdot l \cdot fillmax \ ,$$

where $fillmax$ is twice the concentration of molecular hydrogen used to fill the container initially. Thus, the total number of H atoms "missing" from the plasma is

$$N_{missing}^{total} = N_H^0 - N_H = \pi \cdot a^2 \cdot l \cdot (fillmax - fill)$$

K.4 Sheath Concentration of "Missing" Hydrogen

Assuming that a certain fraction of these atoms are adsorbed in the walls, the total concentration of H atoms in the sheath is:

$$\Delta n^{sheath} = \frac{(1 - f_{wall}) N_{missing}^{total}}{V^{sheath}} \ ,$$

where the cylindrical sheath volume, of thickness Δr and outside radius a, is given by

$$V^{sheath} = \pi a^2 l - \pi (a - \Delta r)^2 l = \pi l (2a\Delta r - (\Delta r)^2) \ .$$

Thus, the increase in the hydrogen concentration in the sheath due to this missing hydrogen is:

$$\Delta n^{sheath} = \frac{a^2 (fillmax - fill)}{2a\Delta r - (\Delta r)^2} (1 - f_{wall}) \ .$$

Thus, the total concentration of atomic hydrogen "available" in the sheath is:

$$n^{sheath} = fill + \Delta n^{sheath} = fill + \frac{a^2 (fillmax - fill)}{2a\Delta r - (\Delta r)^2} (1 - f_{wall}) \ .$$

This available hydrogen concentration is divided between atomic and molecular forms by the previously-mentioned production and loss processes.

K.5 Sheath Concentrations of H and H_2

The H atoms in this wall sheath collide with the wall and recombine with adsorbed H atoms to form molecular hydrogen with an experimentally measured probability, γ_{sr}, the surface recombination coefficient. In addition, adsorbed hydrogen recombines spontaneously and molecular hydrogen is desorbed from the wall. Assuming that equilibrium prevails in this wall sheath, the H_2 production rate by surface and volume recombination must equal the H_2 loss rate by diffusion back into the plasma core. Within a mean free path of the wall ($\sim$ 100 Å), the flux of H atoms striking the wall and the flux of H_2 molecules leaving the sheath may be approximated as "beams" of particles. Thus, in equilibrium,

$$\text{production rate of } H_2 = \text{loss rate of } H_2 \ ,$$

then

$$\frac{1}{2}\left[\frac{1}{4}\cdot n_H^{sheath}\cdot \bar{v_H}\cdot\gamma_{sr}\cdot(2\pi al)\right]+\frac{1}{2}\left[(n_H^{wall})^2\cdot\gamma_{vr}\cdot(2\pi al)\right] \approx \frac{1}{4}\cdot n_{H_2}^{sheath}\cdot\bar{v_{H_2}}\cdot(2\pi(a-\Delta r)l) \ , \tag{K.3}$$

where γ_{sr} and γ_{vr} are the surface and volume recombination coefficients, respectively, and $\bar{v_H}$ and $\bar{v_{H_2}}$ are the average atomic and molecular hydrogen speeds, respectively. In addition, the atomic and molecular sheath concentrations must be related to the total sheath concentration :

$$n_H^{sheath} + 2n_{H_2}^{sheath} = n^{sheath} \tag{K.4}$$

Using this relation in the previous equation, it is found that the sheath concentrations of H and H_2 may be determined if the thermal speeds, recombination coefficients, total sheath concentration, and hydrogen wall concentration can be estimated.

$$n_{H_2}^{sheath} \approx \frac{\frac{1}{2}n^{sheath}\bar{v_H}a\gamma_{sr} + 2(n_H^{wall})^2 a\gamma_{vr}}{\bar{v_H}a\gamma_{sr} + \bar{v_{H_2}}(a-\Delta r)} \tag{K.5}$$

K.5.1 Volume Recombination Coefficient

The volume recombination coefficient for hydrogen adsorbed in pyrex was estimated by using experimental measurements for other materials. (Baskes, 1980) The value obtained was:

$$\gamma_{vr} \approx 1.0 \times 10^{-19} \ .$$

K.5.2 Wall Concentration of Atomic Hydrogen

The concentration of atomic hydrogen adsorbed in the pyrex walls of the discharge tube was estimated using the empirically determined value for the saturation depth in the pyrex ($r_g \approx 10\mu m$) and the time-dependent expression for the fraction of hydrogen in the wall ($f_{wall} \approx .45\ exp(-t/100\mu s) + .05$). Assuming that this hydrogen is uniformly distributed within the pyrex to a depth of r_g, the concentration of adsorbed hydrogen is:

$$n_H^{wall} \approx \frac{f_{wall}(fillmax - fill)a^2}{2ar_g + r_g^2} .$$

K.5.3 Surface Recombination Coefficient

In order to determine the wall sheath concentrations of atomic and molecular hydrogen it is also necessary to have a value for the surface recombination coefficient, γ_{sr}, the probability that an incident hydrogen atom will recombine with an adsorbed hydrogen atom and be released from the surface. The recombination coefficient for atomic hydrogen incident on pyrex at room temperature was measured by Wood and Wise (1961) to be

$$\gamma_{sr} = 5.8 \pm 1.8 \times 10^{-3} .$$

Although they did not indicate what the temperature of the hydrogen was, it was probably not much above the wall temperature of 300 °K since, in their experiment, the atoms simply diffused into the pyrex test cylinder from an rf discharge. The recombination coefficient they reported was used in the present model without any temperature scaling. However, reflectivity differences have been observed for other materials as a result of differing incident particle energies. (Baskes,1984)

It should also be noted that surface imperfections and contaminants can greatly alter such recombination coefficients. (McNeil and Kim, 1982) Although the pyrex cylinders used by Wood and Wise (1961) were initially washed with chromic or nitric acid and rinsed with distilled water, there was no mention of any such pre-treatment in the laser-induced fluorescence experiments of Burgess, *et al.* (1980).

K.5.4 Wall Sheath Temperatures of H and H_2

Calculation of the wall sheath concentrations of atomic and molecular hydrogen also requires a knowledge of these species' average thermal speeds, and thus their temperatures. In addition as described previously, Baskes (1984) has shown that the reflectivity of a surface, and hence its recombination coefficient, is a strong function of the atomic hydrogen's temperature. However, the temperatue dependence of the surface and volume recombination coefficients was neglected in the current model of the plasma.

The experimental measurements and theoretical calculations presented by Baskes (1984) show that the reflectivity for H atoms incident on nickel surfaces increases rapidly with the atoms' kinetic energy. In particular, the reflectivity increases from nearly zero at 0.1 eV, to approximately 50% at 1.0 eV, and to a maximum of over 90% at approximately 4.0 eV. Although nickel and pyrex are obviously very different materials, they do have some similarities: they both have surface energy barriers (Baskes, 1980 and Kubiak, 1987) and Baskes (1984) observed only a weak effect due to nickel crystal orientation. Thus, the reflectivity of crystalline nickel surface may be an acceptable approximation to the reflectivity of an amorphous pyrex surface. Because of the assumed temperature dependence of the reflectivity, the initially hot hydrogen atoms probably strike the walls many times before they are cool enough to have a reasonable probability of recombining. Once the atomic hydrogen in the wall sheath reaches this temperature, their more rapid loss by wall recombination greatly slows further temperature reductions. Thus, the atomic hydrogen in the wall sheath probably has a temperature somewhat above the wall temperature.

Considering only thermal diffusion effects, Long and Newton's (1971) cylindrical plasma simulations showed that the atomic temperature in the wall sheath was a factor of two lower than the temperature on axis.

In an attempt to include both of these observations, the atomic hydrogen temperature in the wall sheath was estimated to be:

$$T_H \approx T_{wall} + \frac{T_{plasma} - T_{wall}}{3} , \qquad \text{(K.6)}$$

where T_{plasma} is the plasma (heavy species) temperature on axis and $T_{wall} \approx 0.025\ eV$. For example, for a plasma temperature of 1 eV, the atomic hydrogen temperature given by this equation agrees with the value (0.35 eV)

used by Chan, *et al.* (1983), which was obtained from spectroscopic data on a 1 eV positive ion source.

The wall sheath would also (presumbably) contain molecular hydrogen, assumed to be formed primarily by the recombination of atomic hydrogen with hydrogen adsorbed in the walls. As a consequence of pyrex's large surface energy barrier, the molecular hydrogen coming off the walls would have an excess of energy to distribute between its kinetic motion and its internal degrees of freedom. (Kubiak, 1987) Thus, the molecular hydrogen in the wall sheath would probably have a temperature somewhat above the wall temperature and, in addition, a significant level of vibrational excitation. (Such vibrational excitation, followed by dissociative attachment, has been proposed as the process responsible for the anomalously high concentrations of H^- in certain gas discharges. (Hiskes, 1987) In such negative ion discharges, however, it is usually presumed that the vibrational excitation is primarily due to collisions with energetic electrons. (Hiskes, 1987)) In an attempt to model this "warm" molecular hydrogen, its sheath temperature was assumed to be given by:

$$T_{H_2} \approx 2T_{wall} + \frac{T_{plasma} - T_{wall}}{10} . \qquad \text{(K.7)}$$

For example, for a plasma temperature of 1 eV, this formula yields a temperature for the molecular hydrogen which is only slightly larger than .12 eV, the temperature observed by Chan, *et al.* (1983) for the molecular hydrogen in a 1 eV plasma.

K.6 Solution of the Diffusion Equation

With the atomic and molecular hydrogen concentrations known in both the plasma core and in the wall sheath, the diffusion equation (in cylindrical geometry) may be solved to obtain the time-dependent radial concentration of either species.

$$n(r,t) = e^{t/\tau} I_0\left(\frac{r}{\sqrt{D\tau}}\right) n^{core} , \qquad \text{(K.8)}$$

where D is the diffusion coefficient, n^{core} is the concentration of either H or H_2, τ is the time constant for the diffusive decay, and I_0 is the modified Bessel function. (A very similar radial dependence was produced in the

simulations done by Long and Newton (1971).) Applying the boundary conditions at the plasma core and wall sheath (for H and H_2 separately), the time constant for the diffusion, τ, may be obtained by numerically taking the inverse of the Bessel Function.

$$\frac{1}{\tau}(1/\text{sec}) = D\left[\frac{J_0^{-1}(n_{H,H_2}^{sheath}/n_{H,H_2}^{core})}{a-\Delta r}\right]^2 \qquad \text{(K.9)}$$

The diffusion rates ($1/cm^3/sec$) for atomic and molecular hydrogen, then, are obtained by multiplying the inverse of the time constant by the "excess" sheath concentration for atomic hydrogen, $(n_H^{sheath} - n_H^{core})$, and similarly for molecular hydrogen. If there is no "excess", the diffusion rate is set to zero.

K.7 Empirical Adjustments

Using this approach, the diffusion rates of H and H_2 into the plasma were obtained. However, these rates were modified in order to incorporate the suggestion by Jones (1982), that the atomic and molecular hydrogen in the wall sheath remained there for several hundred microseconds before diffusively returning to the plasma "core". That is, the diffusion coefficients of H and H_2 were "adjusted" so that approximately 90% of the "missing" atomic and molecular hydrogen was returned to the plasma by 300 μs. In order to achieve such a result, the diffusion rate for hydrogen was reduced by a factor of 20, while the diffusion rate for molecular hydrogen was increased by a factor of 1.8. Although these changes had a long term effect on the neutral densities, there was no short term impact on the behavior of the plasma during the modeling of the laser-induced fluorescence.

Bibliography

Baskes M I 1980 *Journal of Nuclear Materials* **92** 318-24

Baskes M I 1984 *Dynamical Calculation of Low Energy Hydrogen Reflection* SAND84-8729 Sandia National Laboratories

Burgess D D, Myerscough V P, Skinner C H, and Ward J M 1980 *Journal of Physics B: Atomic and Molecular Physics* **13** 1675-1701

Chan C F, Burrell C F, and Cooper W S 1983 *Journal of Applied Physics* **54**(11) 6119-37

Hiskes J R, Lietzke A F, and Hauck C 1986 *Proceedings of the Fourth International Symposium on the Production and Neutralization of Negative Ions and Beams* (New York: Brookhaven National Laboratory)

Hiskes J R 1987 *Comments on Atomic and Molecular Physics* **19**(2)

Jones W M 1982 *Plasma Physics* **24**(4) 361-68

Kubiak G 1987 *private communication* (Livermore, California: Sandia National Laboratory)

Long J W and Newton A A 1971 *Proceedings of the Tenth International Conference on Phenomena in Ionized Gases* (Oxford, ed R N Franklin) 19

McNeill D H and Kim J 1982 *Physical Review A* **25**(4) 2152-63

Newton A A and Sexton M C 1969 *Journal of Physics B: Atomic and Molecular Physics* **2**(2) 1069-74

Wood B J and Wise H 1962 *Journal of Physical Chemistry* **66** 1049-53